AIR LEAKAGE MEASUREMENT OF BUILDINGS BY AN INFRASONIC METHOD

by

W. Howard Card
Ahsan Sallman
Richard W. Graham
Eugene E. Drucker

Technical Report TR-78-1

Final Report

NSF Grant ENG-75-23416

Department of Electrical and Computer Engineering
Syracuse University
Syracuse, NY 13210

31 January 1978

ABSTRACT

One property of a building that is of great importance in determining the infiltration performance is the size of the leakage passages (cracks) through the building envelope. The composite effective size of the leakage passages can be determined by using a blower to pressurize (or evacuate) the building while at the same time measuring both flow (m^3 per sec or cfm) and inside-outside pressure difference. As an alternative to the blower method we have been experimenting with an infrasonic method whereby a very low frequency (about one cycle per second) alternating air flow of known magnitude is applied to the building, and the alternating component of inside pressure that results is measured. Thus, the object of the research is to compare the efficacy of the new infrasonic method with that of the blower method. It is hoped that a portable easy-to-use measuring instrument for testing small buildings, mainly houses and apartments, will eventually be developed as a consequence of our research.

Our apparatus comprises a portable pump and pressure sensor which are set up inside the building to be tested. All inside doors are opened and all windows and outside doors are closed. No through-the-wall ducts or pressure probes are required. The present experimental pump employs an air-tight diaphragm sealed over the open end of a 50-gallon drum; the diaphragm is deflected in and out by a motor-driven crank mechanism to produce the sinusoidal flow. The sensor is somewhat like an ultra-sensitive barometer or microphone. Electronic filters, however, suppress barometric fluctuations and other unwanted interference.

This paper reports on the system design and test results obtained to date. One house, five apartment, and three interior rooms have been tested. Results of the infrasonic tests up to now usually agree with the results of blower tests within a factor of three but improvements in the apparatus are expected to improve the agreement.

PREFACE

This document is the final report for a research project sponsored by the National Science Foundation on Grant No. ENG-75-23416, entitled "Acoustic Impedance Determination of the Air Leakage Characteristics of Housing Units." The authors of this report gratefully acknowledge the financial support received on this grant.

In addition it is appropriate to acknowledge the support received from other sources, and the work done by other researchers over the past three years. During the summer of 1974 preliminary work was carried out by Douglas Morrison, Mario Bricetti and Catherine Girard using a vented pump; Morrison and Bricetti were supported by an NSF Undergraduate Research Participation grant GY-11216. During the 1975-76 academic year Richard Graham constructed a first version of the final infrasonic source; he was supported during that period by Syracuse University. During the summer of 1976 Dennis Flanagan was supported by NSF URP grant SMI-76-03527, and during the summer of 1977 Patrick Kelly and Linda Zaleon were supported by the same grant. Kelly designed and built the synchronous detector, Zaleon worked on a system to suppress manometer fluctuations during blower tests, and Flanagan improved the source and carried out some infrasonic measurements.

CONTENTS

SYMBOLS AND UNITS

Symbol	Description and SI Unit
A	Leakage passage area, m^2
A_d	Pressure sensor diaphragm area, m^2
C	Acoustic capacitance, m^5/N
C_d	Acoustic capacitance of pressure sensor, m^5/N
G	Electrical conductance, $ohms^{-1}$
K	Empirical constant relating flow to pressure
K_l	Conductance of leakage passage, $m^5/N\text{-}sec$
L	Total acoustical inertance, $N\text{-}sec^2/m^5$
L	Electrical inductance, H
L_ℓ	Inertance of leakage passage, $N\text{-}sec^2/m^5$
L_r	Radiation inertance, $N\text{-}sec^2/m^5$
N_R	Reynolds number
P	Atmospheric pressure, N/m^2 (Pascals)
Q	Volumetric flow rate, m^3/sec
Q_o	Quality factor (ω_o L/R)
Q_s	Volumetric source amplitude, m^3/sec
R	Leakage resistance, $N\text{-}sec/m^5$
R	Electrical resistance, ohms
S	Radiation resistance parameter, $N\text{-}sec^3/m^5$
V	Volume, m^3
V_d	Pressure sensor chamber volume, m^3
V_o	Total enclosure volume, m^3
V_s	Half of source displacement, m^3

Symbol	Description and SI Unit
X	Inertive reactance, N-sec/m^5
X_ℓ	Inertive reactance of leakage passage, N-sec/m^5
X_r	Inertive reactance due to radiation, N-sec/m^5
Z	Total impedance, N-sec/m^5
Z_ℓ	Impedance of leakage passage, N-sec/m^5
Z_r	Radiation impedance, N-sec/m^5
a	Radius of piston, m
b	Width of flow or crack length across flow, m
c	Velocity of sound, m/sec
d	Diameter, m
e_d	Fotonic Sensor output voltage, V
f	Frequency, Hz
h	Half of leak thickness across flow, m
i_d	Capacitance current, A
i_g	Conductance current, A
i_s	Source current, A
k	Dimensionless frequency parameter
k_1	Dimensionless impedance parameter
ℓ	Length of leak along the flow, m
m	Mass flow rate kg_m/sec
n	Air leakage exponent
p	Pressure, N/m^2 (Pascals)
p_o	Atmospheric pressure, N/m^2 (Pascals)
$q(t)$	Total volumetric current, m^3/sec
$q_c(t)$	Volumetric capacitance current, m^3/sec
$q_g(t)$	Volumetric leakage current, m^3/sec

Symbol	Description and SI Unit
q_o	Volumetric flow at one Pascal from infrasonic measurement
q_1	Capacitance volumetric current, m^3/sec
q_2	Leakage impedance current, m^3/sec
q_3	Leakage resistance current, m^3/sec
t	Time variable, sec
u	Velocity, m/sec
$v_s(t)$	Source volume time function, m^3
w	Separation between parallel plates, m
y	Coordinate perpendicular to flow direction
y_d	Pressure sensor diaphragm displacement, m
ΔP	Incremental change in total pressure, N/m^2 (Pascals)
ΔV	Incremental change in volume, m^3
ΔV_o	Half of source displacement, m^3
Δp	Static pressure difference, N/m^2 (Pascals)
Δp_m	Amplitude of pressure response for sinusoidal example, N/m^2
$\Delta p(t)$	Time-varying component of pressure, N/m^2
γ	Ratio of specific heats of air
μ	Absolute viscosity of air, $N\text{-}sec/m^2$
ν	Kinematic viscosity of air, m^2/sec
ρ	Density of air, kg_m/m^2
ϕ	Angle that pressure lags flow, rad
ω	Angular frequency, rad/sec
ω_o	Resonant frequency, rad/sec
ω_1	Break-point frequency (linear example), rad/sec
ω_2	Break-point frequency (nonlinear example), rad/sec

Chapter 1

INTRODUCTION

1.1 Motivation

The present and anticipated future shortages of energy make it desirable to find ways to reduce energy waste. One sector where significant reductions in energy consumption can be achieved is residential heating and cooling. Studies have shown that 11 per cent of the energy used in the United States in 1968 was for heating houses [Ref. 1].

For representative conventional houses [Ref. 2] and apartments [Ref. 3] from 15 to 30 per cent of the heat loss is accounted for by the replacement of warm inside air by cold outside air due to air leakage. Houses designed for electrical heating, and especially houses designed for solar heating, have much better than average insulation with the result that, while the total heating energy required will be less, the proportion of that total attributable to air leakage will be increased. The present proposal relates to the air-leakage problem for the most numerous kinds of housing units, including single-family houses, multiple-unit buildings, mobile homes, and other self-contained living units.

The occupants of a building require fresh air for health and comfort; moreover, some fresh air is desirable to keep down the humidity when large quantities of moisture are released, e.g., by cooking and washing. But in most present-day construction the amount of fresh air entering a residential unit depends more on the outside wind speed and the indoor-outdoor temperature difference than on the needs of the occupants [Ref. 4, 5, 6, 7, 8]. This results because, for any given wind velocity and air temperature, the fresh air supply depends largely on the tightness of construction of the building, and

on window and door clearances. Of course, if there were no accidental air-leakage paths, then some positive means of ventilation would have to be provided; but these could be subject to automatic or manual control; moreover, some form of heat recovery means could be installed.

At the present time almost the only method of control over new building thermal performance that is available to the designer of the building is to specify the details of construction. It is difficult and time-consuming to measure the thermal performance of a completed building. Specifying the construction details may achieve an acceptable level of control over the conduction heat loss. However, since air leakage depends strongly on the quality of workmanship, control over air leakage is more difficult to achieve. What is needed are accurate methods for determining if the designer's objectives and specifications have been met.

The problem of improving the thermal performance of existing buildings is even more difficult. What is usually wanted is an accurate estimate of the energy saving that can be achieved by making proposed improvements, such as adding insulation, storm windows, or weather stripping. Good methods for measuring the air-leakage properties of an existing building would be quite useful for helping to make such extimates.

In order to help meet these and other needs we have investigated the performance of a new method, called the infrasonic impedance method, for measuring the flow-versus-pressure difference characteristics of various laboratory enclosures and actual housing units.

1.2 Relationship of the Present Research to the State of the Art

Some work on air leakage has been done using portable infiltration meters that employ helium [Ref. 9] or sulphur hexaflouride [Ref. 10, 11, 12] tracer

gas techniques; but the methods are awkward and the results weather-dependent. It is believed that, at their present stage of development, the tracer-gas methods are not very suitable for routine tests by a builder or buyer to determine if a building meets specification, or for a building owner contemplating making improvements to reduce energy consumption.

A tracer gas infiltration meter measures the air infiltration rate of a building that is subjected to inside-outside pressure differences resulting from outside wind and inside-outside temperature differences. Thus, the results of an infiltration test depend not only on the flow-versus-Δp characteristic of the building, but also on the driving forces of wind and temperature. Because of this the infiltration test results on a building using the tracer gas method will change from day to day; it is therefore difficult to interpret test results in a general way, or to compare tests on different buildings made at times when weather conditions are not identical.

Individual building components, such as window and door assemblies and wall sections, can be tested in the laboratory for air leakage. The ASHRAE Handbook of Fundamentals reports some of these results for use in air-leakage predictions. Various manufacturers' associations have also developed standards including air-leakage limits for newer windows having steel or aluminum frames. Tests such as these are made with the window or door frame carefully sealed into a wall section in a laboratory test enclosure, whereas in actual buildings the joints between window or door frames and walls may have large gaps. Thus, laboratory tests on building components are not an adequate substitute for tests on complete buildings. Considerable work has been done and is in progress using a blower method (pressurization/evacuation method)[Ref. 13, 14, 15, 16, 17] whereby a blower, usually having an adjustable output, is connected to an opening in the envelope of a building to pump air into or out

of the building. The blower flow and also the resulting inside-outside pressure difference Δp are measured. Ideally the flow-versus-Δp characteristic that can be measured this way is independent of weather conditions, but in practice manometer fluctuations on windy days make accurate results difficult to obtain. In principle there are no limits on the size of buildings that may be tested by the blower method, but a large leaky building will require a very large blower. Sometimes existing blowers are employed. The infrasonic impedance method reported on here is also intended to measure the flow-versus-Δp characteristics of buildings.

Of course, the infiltration performance of a building is not determined uniquely by the flow-versus-Δp property: the actual infiltration performance depends to a considerable degree on the location of the openings (whether or not all are on one side, or all at the same elevation, etc.). But for typical residential units, we believe that the flow-versus-Δp characteristic of the whole unit would provide an unambiguous indicator closely related to infiltration performance. For example, a building designer could specify that a building is to have no worse than a certain maximum flow-versus-Δp characteristic, which the builder would then undertake to achieve.

The infrasonic method reported on here basically provides an alternative procedure for measuring the flow-versus-Δp characteristic of a building. It operates by applying a sinusoidally varying volumetric air flow of known amplitude and frequency to the enclosure (building) under test; the resulting pressure variation is measured by means of a highly sensitive transducer. Usually a frequency response curve is measured over a frequency range from about 0.1 Hertz to about 5 Hertz. Leakage properties of the enclosure equivalent to a flow-versus-Δp curve can, under ideal conditions, be obtained from the frequency response curve.

The main advantages expected of the infrasonic impedance method are that the measuring equipment can be compact, portable, self-contained, and easy to use. Of great importance is the fact that the method would not require an air inlet or exhaust blower connection to the outside of the residential unit nor outside pressure taps for pressure difference measurement. In apartments and small houses, measurements can be made at pressure differences reasonably close to those experienced by a building in normal operation.

1.3 Research Methodology

The main theme of the research is a comparison of results obtainable using the new infrasonic method with the results obtainable using the blower method.

Figure 1-1 shows a schematic diagram of the infrasonic impedance measuring equipment, and photographs are shown in Figs. 1.2 and 1.3. The system comprises a special pressure sensor. More details are given in Chapter 3 and Appendix A.

The pump employs a reciprocating piston driven by an electric motor which, on its upper side, alternately compresses and rarefies the air inside a 55-gallon rigid air-tight container. It is, of course, the lower or underneath side of the piston that performs the useful function: it alternately rarefies and compresses the air in the enclosure (e.g., apartment or house) under test, at the pump rate of about one cycle per second. The average pressure in the enclosure (house under test) remains equal to the atmospheric pressure; the pump causes the instantaneous pressure to vary cyclically above and below the atmospheric pressure. The pump employs no through-the-wall connections and is portable.

The pressure sensor employs a closed container (about five litres) having

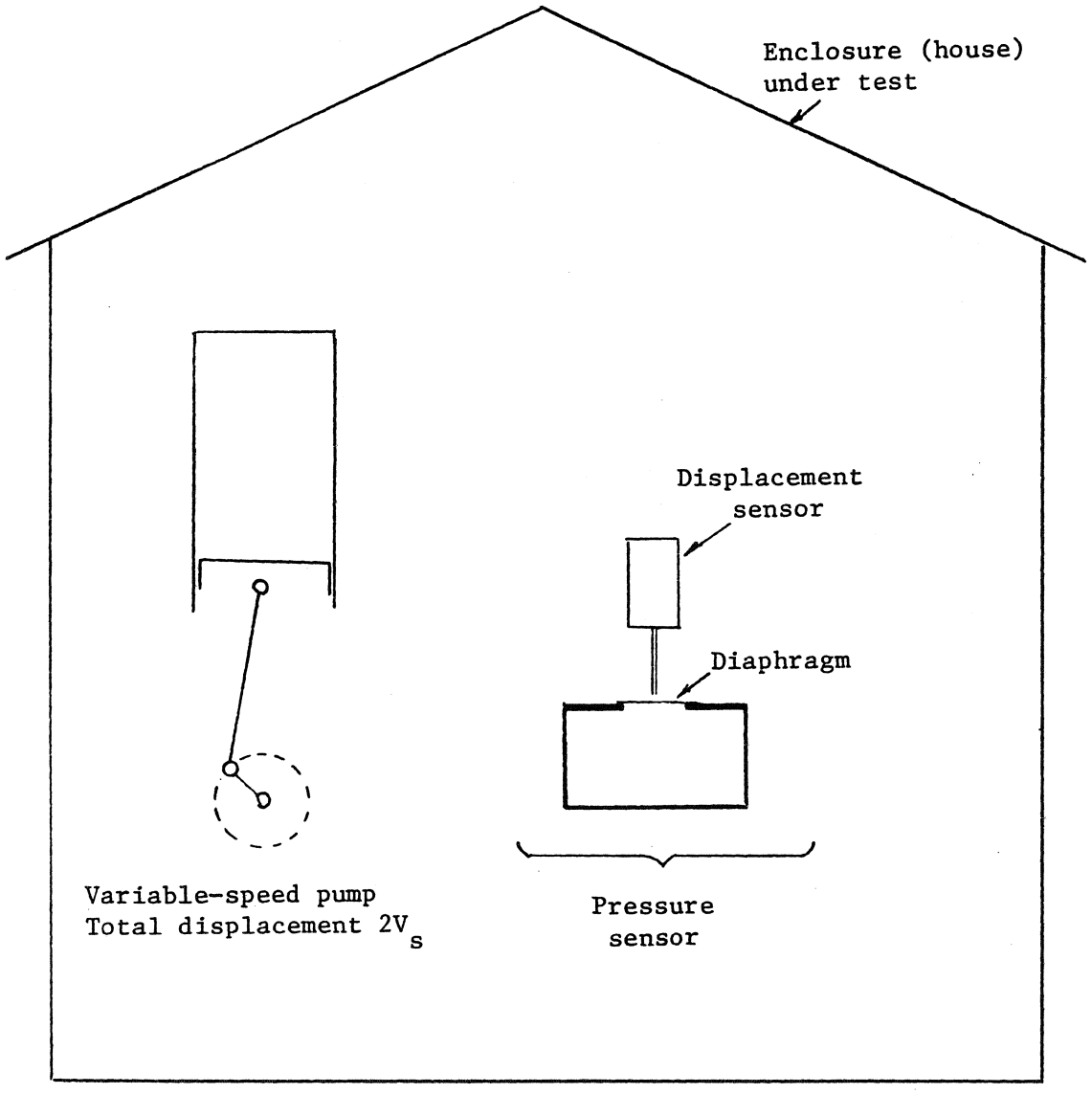

Fig. 1-1 Simplified schematic diagram of a system for measuring the infrasonic impedance of a house.

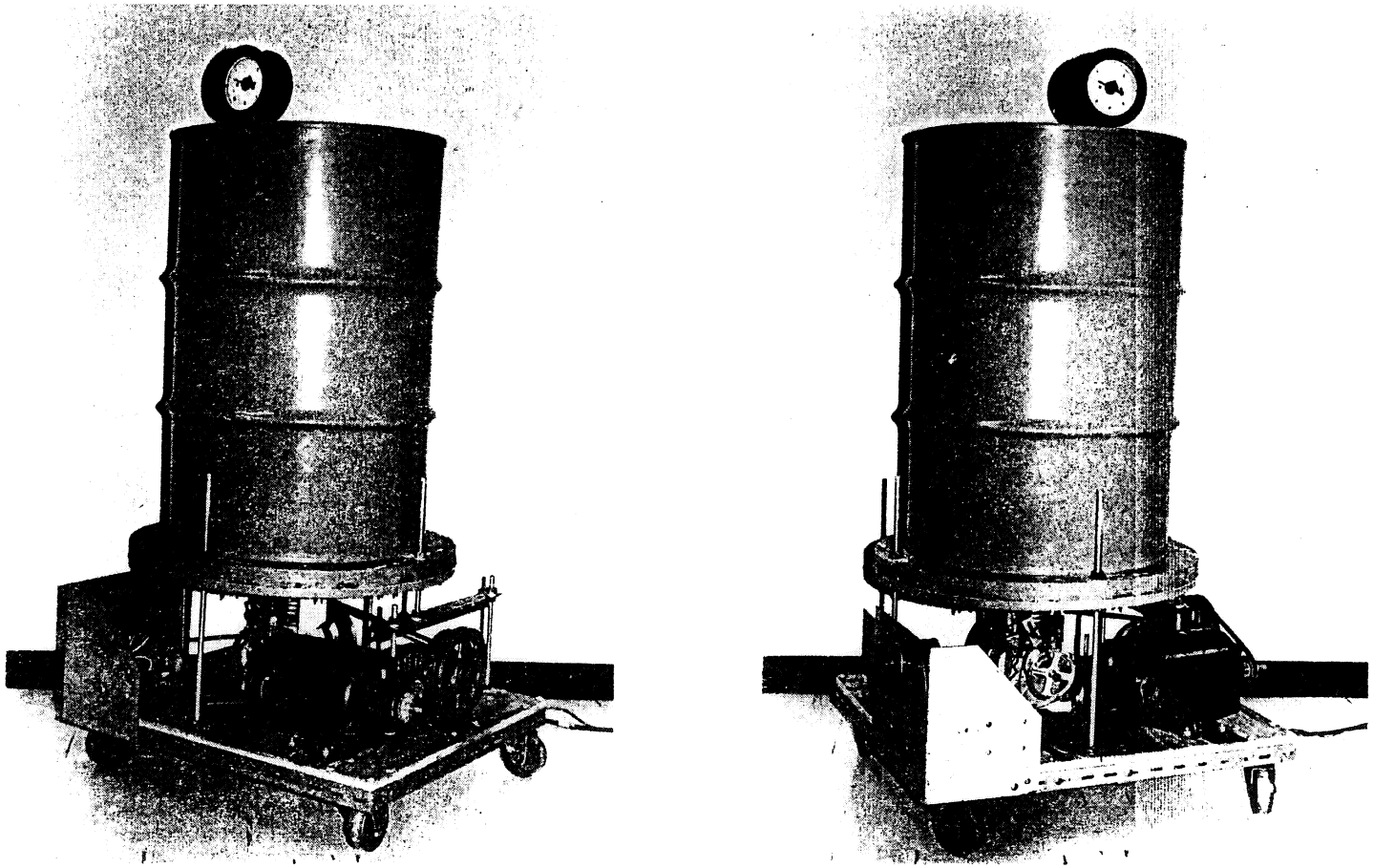

(a) (b)

Figure 1.2. (a) and (b). Photographs showing two views of infrasonic source equipment.

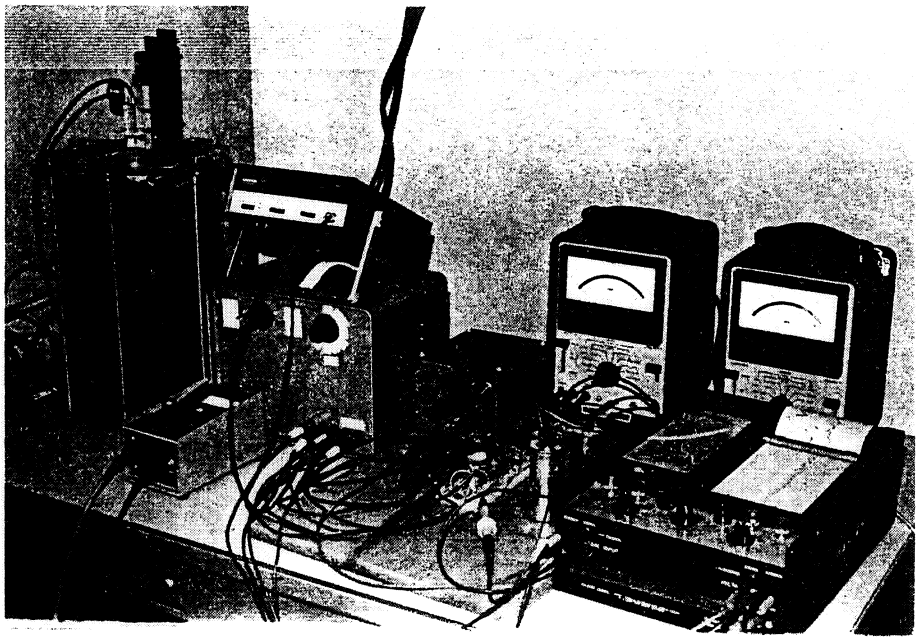

Figure 1.3. Photograph showing the pressure sensing equipment. From the left hand side: pressure pickup chamber, fotonic sensor in the front, filter-amplifier unit, electronic time period counter-on the top of amplifier box, synchronous detector, meters for measuring output voltage and strip chart recorder.

a limp film of Saran wrap over a 10.16 cm opening. This diaphragm deflects in step with the compressions and rarefactions in the enclosure caused by the pump. The output signal is displayed on voltmeters and fed to a strip chart recorder.

It is apparent that a tightly sealed enclosure (house) will yield a relatively large pressure signal, whereas a leaky enclosure will yield a relatively small pressure signal. Detailed expressions showing how the magnitude and phase of the pressure signals depend on the volume and leaks of the enclosure and on the test conditions are contained in Chapter 2.

Turning attention now to the blower method, Figs. 1-4 and 1-5 show the basic system. A one-horsepower blower is mounted in a two-foot by two-foot by four-foot-high air-tight blower box. An ASME nozzle in the top of the blower box permits blower flow to be measured. The output of the blower is connected by a 6-inch-diameter air-tight hose pipe through the enclosure envelope. This blower box is located either inside or outside the enclosure under test, whichever location is most convenient.

1.4 Limitations of the Infrasonic Impedance Method

Several complications arise, however, in using the infrasonic method. First, for a small pump and a large building, the resulting pressure signal using the infrasonic system is generally smaller than the pressure difference used for the blower tests. Thus an expression for flow-versus-Δp applicable over a range of Δp, wide enough to encompass both methods is required. Our research indicates that the generally-used empirical expression according to which the flow varies as Δp^n is adequately accurate in view of the other limitations on the accuracy of our results.

Second, the dimensions of a building have to be small compared to the

acoustic wavelength at the frequencies of interest. Thus frequencies under a few Hertz are generally required. The pressure is assumed to vary approximately uniformly throughout the enclosure in response to the pump volumetric flow.

Third, wide cracks and open chimneys or ventilator flues may have an appreciable inertance effect. Consequently, the whole housing unit may act as an acoustic resonator having a natural frequency of a few Hertz. Thus, again, test frequencies under a few Hertz are generally required if the inertance effect is to be neglected.

The following chapters explore these issues in more detail.

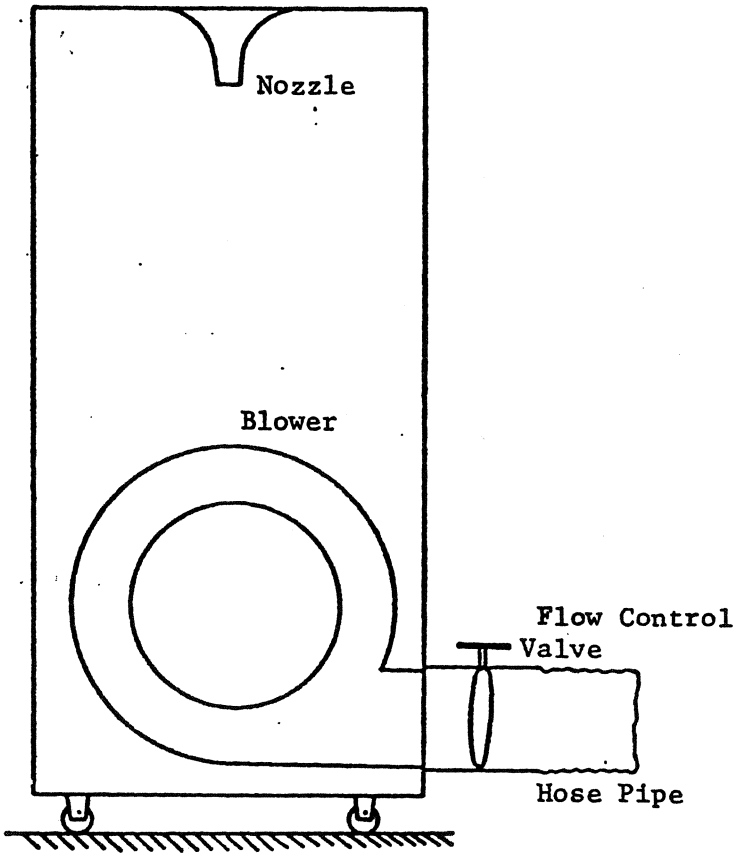

Fig. 1-4. Blower box.

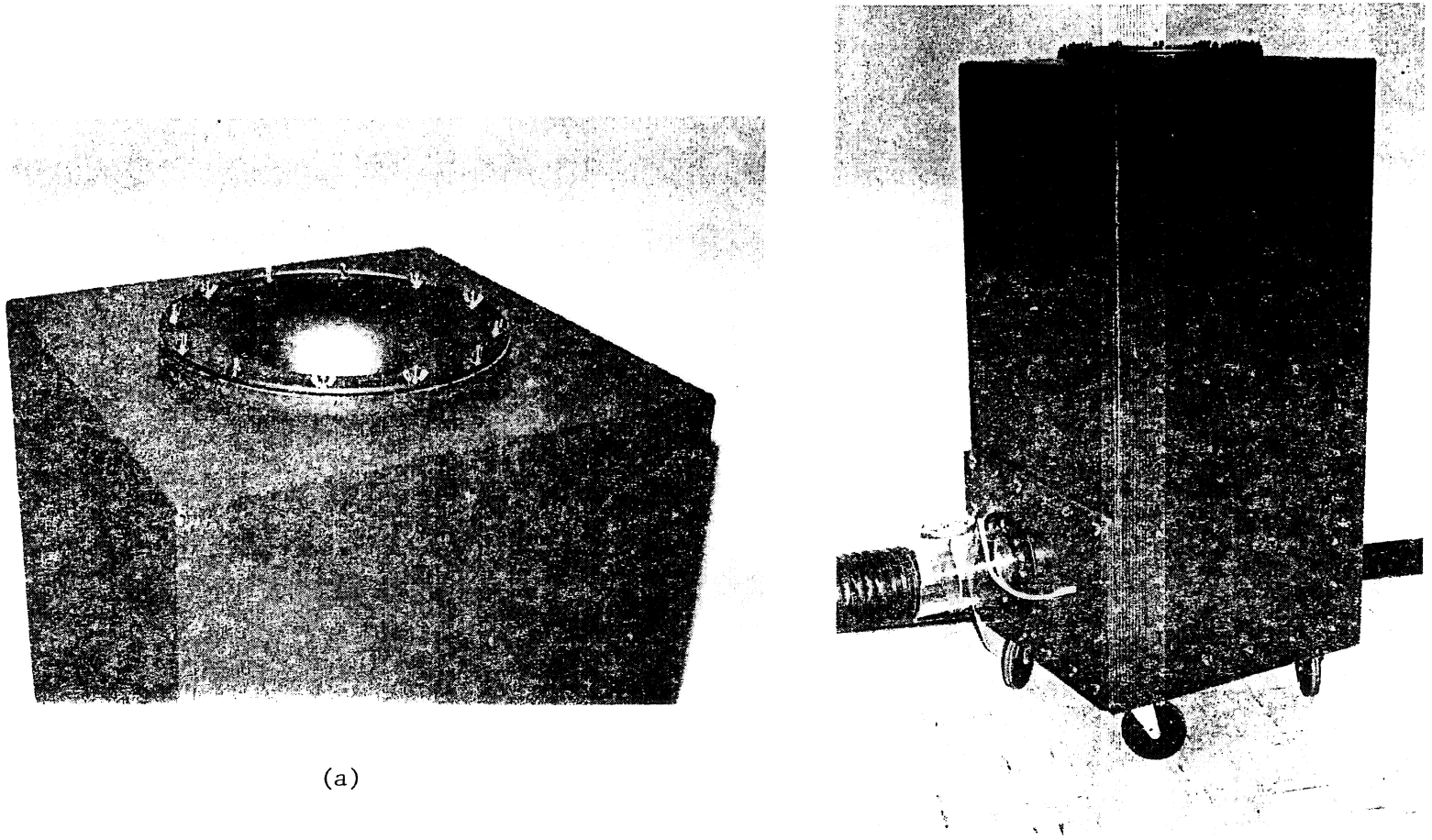

(a)

(b)

Figure 1.5. (a) Photograph showing the top view of the blower box.
(b) Photograph of the blower box.

Chapter 2

THEORETICAL ANALYSIS

This chapter provides a theoretical analysis of the infrasonic impedance method for measuring the air-leakage properties of buildings, and relates the infrasonic method to the blower method. Also included are discussions of how to interpret experimental results, and the limits on the applicability of the theory.

2.1 Pressure Ranges of Interest

The air leakage of practical buildings results both from buoyancy effects due to inside-outside temperature differences, and also from the velocity head due to outside wind.

As an example, for a two-story building such as a house about 6 m (20 feet) high having equal-sized small openings at the top and bottom, the pressure difference across each opening due to an inside-outside temperature difference of 39 Celsius degrees (70 Fahrenheit degrees) would be about 5 Pascals (0.02 inches of water)[Ref. 18]. For milder days the temperature difference and resulting pressure difference would be less. For energy-use problems, as opposed to design peak-load problems, probably a pressure difference of 2.5 Pascals (0.01 inches of water) would be representative of typical conditions.

For a 5 m/sec (11.2 mph) wind, which is close to the average wind for most of the U.S., the excess pressure on the windward side of a house might be as much as 90 per cent of the velocity head, or about 13.5 Pascals (or 0.056 inches of water)[Ref. 19]. In a 10 m/sec (22.4 mph) wind this would increase to about 54 Pascals (0.22 inches of water). However for energy-use problems a pressure difference of 10 Pascals (0.04 inches of water) might be representative.

For cold windy days the buoyancy and velocity-head effects can be additive. Consequently, it appears that static pressure in the range 2.5 to 15 Pascals (0.01 to 0.06 inches of water) is of most interest for energy-use studies of typical U.S. houses. Results for higher and lower pressures are also of interest.

2.2 Static Pressure Leakage Tests

One way to test a building for air leakage is to use a blower either to pump air into the building or out of it, while measuring both the flow and the resulting inside-to-outside pressure difference. All interior dooors would be open and all windows and exterior doors would be closed.

In general air leakage would take place through numerous passages around window sash, doors, and elsewhere. The geometry of each of these passages would, in general, be quite complicated yielding a complicated flow-versus-pressure difference characteristic. Thus, the total flow through all of the passages will also be complicated so that a simple and accurate theoretically-derived expression for the total flow-versus-pressure difference characteristic of a building does not exist.

As an example to illustrate the limitations of an analytical approach, consider flow through the cracks beside a wood window sash. Let us attempt to model this flow by fully-developed steady-state laminar flow between infinite parallel flat plates. For this geometry the flow-versus-pressure characteristic is given by

$$Q = \frac{w^3 b}{12 \mu \ell} \Delta p \qquad (2\text{-}1)$$

where Q is the volumetric flow rate in a width b for plates separated by a distance w. The pressure drop is Δp in a length ℓ. The absolute viscosity

of the fluid is μ. The symbols and their units are listed on page vi. For any Δp the predicted flow rate can be calculated, then the Reynolds number, N_R (based on plate separation) can be computed from

$$N_R = \frac{u\ w\ \rho}{\mu} \tag{2-2}$$

where u is the average velocity, ($u = Q/wb$), ρ is the mass density, and μ is the absolute viscosity of the fluid.

For the wood-sash window assume ℓ is 2.54 cm (1.0 inch), w is 0.16 cm (1/16 inch), and Δp is 25 Pascals (0.1 inch of water). When the calculations are carried out the predicted Reynolds number is about 1230 which is low enough to suggest laminar flow, as initially assumed. Using the listed values of volumetric flow from the ASHRAE Handbook [Ref. 20] for wood-sash windows, and assuming the same crack dimensions, yields an even lower Reynolds number. Experimental results [Ref. 20], however, do not exhibit the linear Q-versus-Δp characteristic predicted by Eq. (2-1). Similarly, the measured Q-versus-Δp characteristics for doors and other types of windows generally do not exhibit linearity. Thus, it is apparent that fully-developed laminar flow is not obtained. Because the length-to-width ratios of flow passages are generally fairly small it appears that transitional conditions are prevalent.

In view of the difficulties with employing a purely theoretical analysis, most work on the air-leakage properties of buildings employs an empirical approach. Laboratory measurements on complete windows [Ref. 13] shows that an equation of the form

$$Q = K(\Delta p)^n \tag{2-3}$$

characterizes the flow-versus-pressure difference behavior in most cases. Here K and n are experimental constants, with n usually in the range 1/2 to 2/3.

Other work on several sizes of capilliary tubes [Ref. 21] shows that Eq. (2-3) characterizes the results within experimental error for the pressure ranges 7.5 to 370 Pascals (0.03 to 1.5 inches of water) and length-to-diameter ratios (0.45 to 18) that were employed. Furthermore, the results of our own experiments (Chapter 4) are consistent with Eq. (2-3).

In view of these results we expect that Eq. (2-3) will provide a reasonable empirical expression for the air leakage of complete houses within and somewhat beyond the pressure ranges of primary interest 2.5 to 15 Pascals (0.01 to 0.06 inches of water) indicated in Section 2-1 (above). Some of the analysis in the following sections is based on this assumption.

Static pressure tests on tall buildings [Ref. 14] and on electrically heated houses [Ref. 17] have been reported. However, static-pressure tests seem not to have been widely adopted as a routine test procedure for houses, possibly because the apparatus would take considerable time to set up and considerable skill to use.

2.3 Dynamic Leakage Tests

Figure 2-1 shows apparatus for conducting a dynamic air-leakage test on an enclosure such as a building. Ideally, the variable-speed reciprocating piston source provides an almost-sinusoidal volumetric drive on the building given by

$$v_s(t) = V_s \sin \omega t \qquad (2\text{-}4)$$

where V_s is one half of the total piston displacement and ω is the angular speed of the shaft. There are no valves associated with the piston or cylinder so that the source is more akin to an acoustic source (e.g. a loudspeaker) than to a conventional pump or blower.

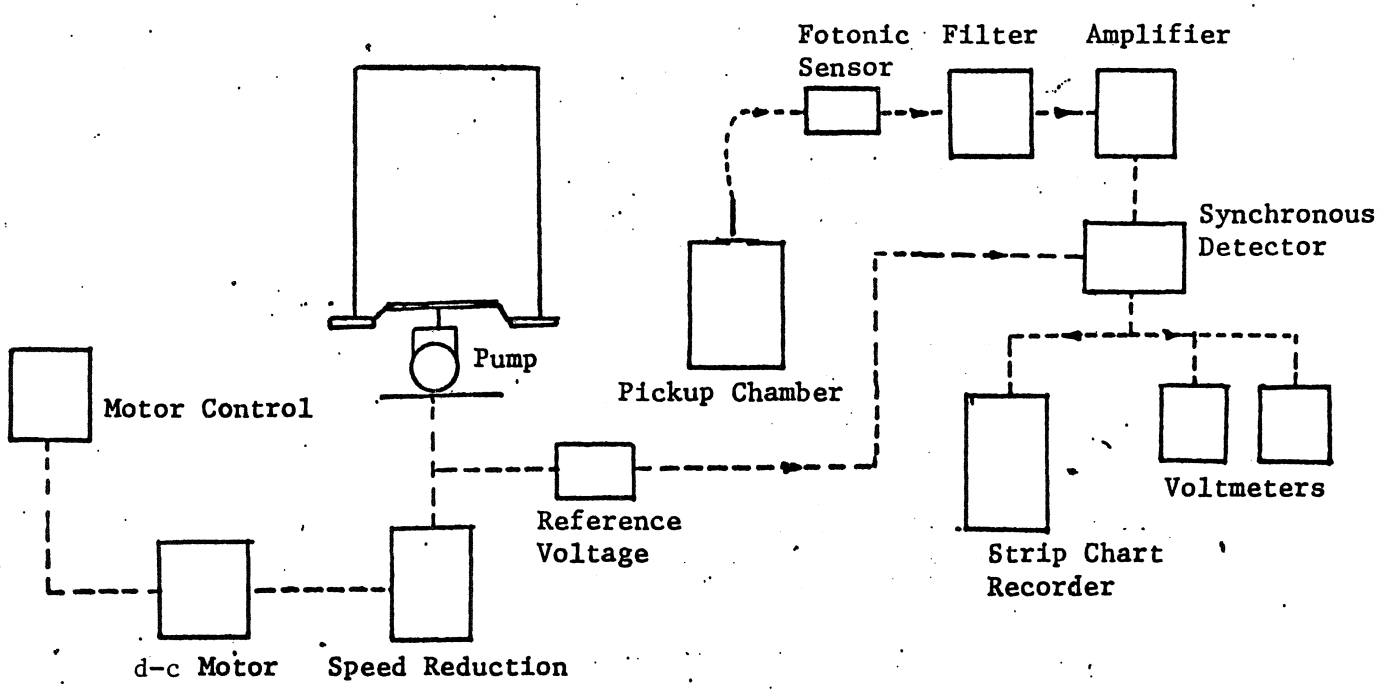

Fig. 2-1. Schematic diagram of infrasonic impedance measuring equipment.

Differentiating Eq. (2-4) yields the volumetric flow rate of the source

$$q_s(t) = \frac{d\, v_s}{dt} = V_s\, \omega \cos \omega t = Q_s \cos \omega t \qquad (2\text{-}5)$$

where

$$Q_s = V_s\, \omega \qquad (2\text{-}6)$$

is the amplitude of the volumetric flow source.

In any given building some of the sinusoidally varying $q_s(t)$ from the source will result in an alternating compression and rarefaction of the air within the building (a capacitance effect), and the remainder of the $q_s(t)$ will result in a back-and-forth flow of air through the cracks (leakage effect).

Consider first the capacitance effect of an enclosure such as a building having negligible air leakage. For low frequencies such that the dimensions of the building are small compared to an acoustic wavelength, the (acoustic) capacitance of the enclosure can be defined as

$$C = \frac{\Delta V}{\Delta P} \qquad (2\text{-}7)$$

where ΔP is the small increase in pressure that would result if the size of the enclosure were decreased by ΔV. Assuming isentropic conditions so that

$$PV^{\gamma} = \text{constant} \qquad (2\text{-}8)$$

where P is the pressure, V is the volume, and γ is the ratio of specific heats for air (1.401) analysis using Eq. (2-7) yields

$$C = \frac{V}{\gamma P} = \frac{V_o}{\gamma P} \qquad (2\text{-}9)$$

Here V_o is the volume of the enclosure such as a house.

Since for our problem P is atmospheric pressure, which is nearly constant, the capacitances of various enclosures, such as a building, mainly differ only if their volumes, V_o, differ.

The concept that we are using of a lumped capacitance is valid provided that several conditions are fulfilled. It is necessary that $\Delta P << P$; that the walls of the enclosure be rigid; and (as already mentioned) that the acoustic wavelength for frequencies of interest be large compared to the dimensions of the enclosure. A piston displacement of $0.003\ m^3$ (one tenth cubic foot), a building volume of the order of $300\ m^3$ (10^4 cubic feet) building linear dimensions not exceeding 30 m (100 feet) and frequencies up to one Hertz satisfy these conditions adequately. For higher frequencies or larger buildings the lumped-parameter approximation is not valid.

For small sinusoidal changes in volume, as provided by Eq. (2-4), we can express the resulting time-varying pressure by $\Delta p(t)$, and use Eq. (2-7) to write

$$\Delta p(t) = \frac{1}{C} v_s(t) \tag{2-10}$$

Differentiation and using Eq. (2-5) yields

$$\frac{d}{dt} \Delta p(t) = \frac{1}{C} \frac{d}{dt} v_s(t) = \frac{1}{C} q_s(t) \tag{2-11}$$

But since there is no leakage, so that $q_s(t)$ is all accounted for by flow into the capacitance, $q_s(t) = q_c(t)$, Eq. (2-11) can be written as

$$q_c(t) = C \frac{d}{dt} \Delta p(t) \tag{2-12}$$

which is the usual form of the flow-versus-pressure relationship for an acoustic capacitance

Next, consider the air-leakage effect alone of an enclosure having negligible volume so that now the capacitance can be neglected. For the present assume that pressure and flow change value slowly enough so that Eq. (2-3) applies for time-varying quantities as well as for static quantities, so that we can write (for $\Delta p(t)$ positive)

$$q_g(t) = K[\Delta p(t)]^n \tag{2-13}$$

where $q_g(t)$ is the time-varying leakage flow rate. In order to accommodate negative values of $\Delta p(t)$ and $q_g(t)$, however, it is necessary to write

$$q_g(t) = K \frac{\Delta p(t)}{|\Delta p(t)|} |\Delta p(t)|^n$$

or alternatively

$$q_g(t) = K \, [\text{sgn } \Delta p(t)] \, |\Delta p(t)|^n \tag{2-14}$$

Since very low frequencies (one Hertz or less) are of greatest interest, using the static pressure analysis for dynamic conditions will be valid for narrow-leakage passages. The more general case is discussed below in Section 2-7.

The next step is to consider an enclosure having both appreciable capacitance and appreciable leakage. Then

$$q_c(t) + q_g(t) = q_s(t) \tag{2-15}$$

Upon substitution of Eqs. (2-12) and (2-14) into (2-15) we get

$$C \frac{d}{dt} \Delta p(t) + K \, [\text{sgn } \Delta p(t)] \, |\Delta p(t)|^n = q_s(t) \tag{2-16}$$

which is, in general, a nonlinear differential equation.

One case of mathematical interest occurs when $n = 1$, for then Eq. (2-16) is linear. Using Eq. (2-5) for $q_s(t)$ and also designating K as K_1 for this

special case yields

$$C \frac{d}{dt} \Delta p(t) + K_1 \Delta p(t) = V_s \omega \cos \omega t \qquad (2\text{-}17)$$

Section (2-4), below, treats this linear case.

Figure 2-2 shows the analogous electric circuit for the infrasonic measuring system of Fig. 2-1. Also shown on the figure are the analogous electrical and mechanical quantities. The drive is provided by the variable-frequency current source; this source is unusual from an electrical point of view because its amplitude increases linearly with frequency as a consequence of Eq. (2-6). The capacitance is essentially constant for a fixed building, but the conductance varies (unless n = 1) as shown in Fig. 2-2(b). The analogous electric circuit helps to clarify the analysis presented in the next four sections.

2.4 Frequency Response -- Linear Analysis

Consider the case where n = 1 in Eq. (2-3) so that Eq. (2-17) applies. This condition would obtain, for example, if the air leakage were essentially fully-developed laminar flow. Analysis of this case will indicate the general kind of experimental frequency response that often occurs and will also indicate the frequency range suitable for testing. We consider only the sinusoidal steady-state behavior.

From electric circuit analysis, the steady-state solution of Eq. (2-17) is

$$\Delta p(t) = \Delta p_m \cos (\omega t - \phi) \qquad (2\text{-}18)$$

where Δp_m is half the peak-to-peak variation in $\Delta p(t)$, and is given by

$$\Delta p_m = \frac{Q_s}{[K_1^2 + (\omega C)^2]^{1/2}} = \frac{V_s \omega}{[K_1^2 + (\omega C)^2]^{1/2}} \qquad (2\text{-}19)$$

Also

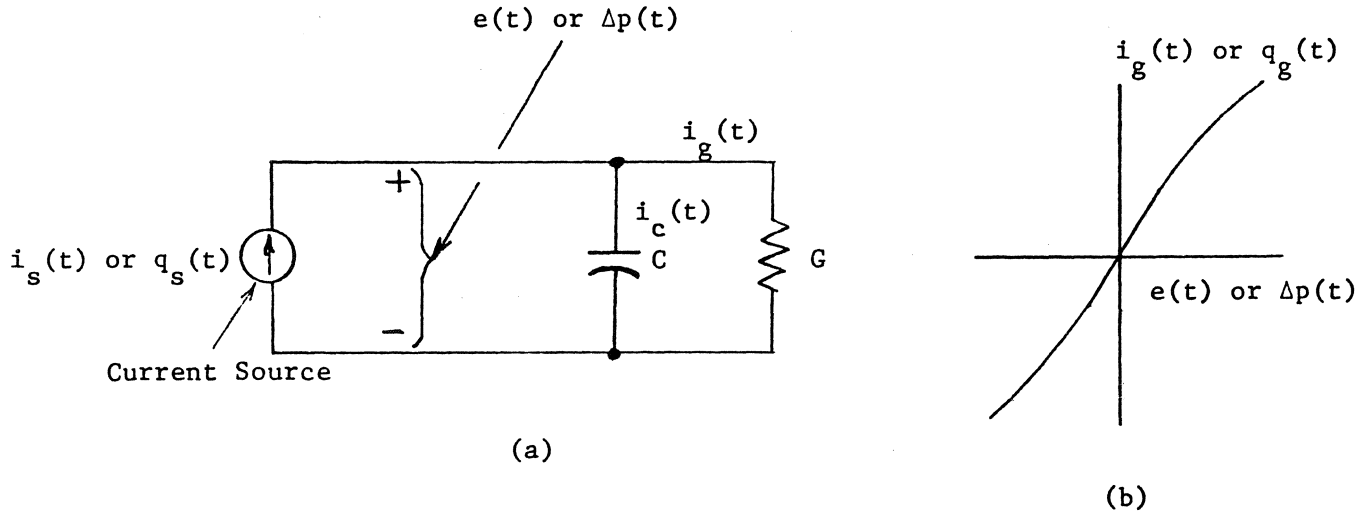

Analogous Quantities

Electrical	Mechanical
$i_s(t)$	$q_s(t)$
$i_c(t)$	$q_c(t)$
$i_g(t)$	$q_g(t)$
C	C
G	K or K_1
e(t)	Δp(t)

Fig. 2-2(a). Analogous electric circuit for enclosure having capacitance and leakage (b) nonlinear conductance or leakage characteristics.

$$\phi = \tan^{-1} \frac{\omega C}{K_1} \tag{2-20}$$

Equation (2-18) shows the expected result that, for a linear system, a sinusoidal drive results in a sinusoidal steady-state response. Moreover K_1 is the real part of the acoustic admittance. Since K_1 is the parameter that determines the air leakage, it is the unknown that is to be determined.

It is convenient to plot the frequency response, Δp_m versus ω, on log-log scales, as shown in Fig. 2-3(a), in order to show the frequency range of interest. For high frequencies, Eq. (2-19) shows that the asymptote is

$$\Delta p_m = \frac{Q_s}{\omega C} = \frac{V_s}{C} \tag{2-21}$$

indicating that the capacitance dominates behavior at high frequencies, or, in other words, at high shaft speeds of the source the air inside the building is alternately compressed and rarefied, but very little air leaks in or out during each cycle. Since Eq. (2-21) does not include K_1, the high-frequency behavior, alone, can not be employed to determine K_1.

For low frequencies, Eq. (2-19) yields an asymptote

$$\Delta p_m = \frac{Q_s}{K_1} = \frac{V_s}{K_1} \omega \tag{2-22}$$

indicating that leakage dominates behavior, and that the compressibility of the air within the house is relatively unimportant at very low frequencies. Dynamic pressure measurements at low frequencies, where Eq. (2-22) applies, can be used to determine K_1, provided V_s and ω are known.

The two asymptotes given by Eqs. (2-21) and (2-22) intersect at the so-called break-point frequency

$$\omega_1 = \frac{K_1}{C} \tag{2-23}$$

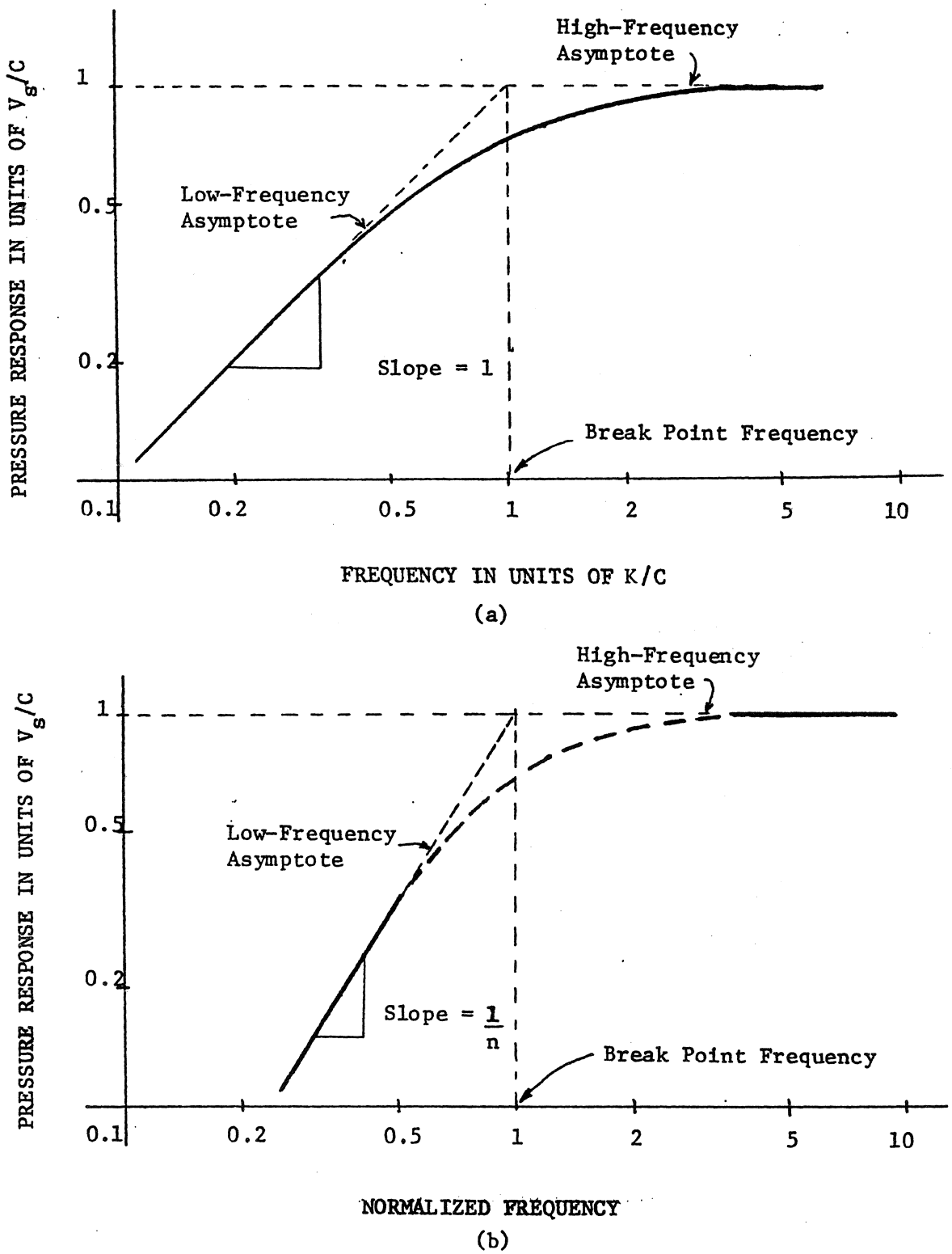

Fig. 2-3. Theoretical normalized log-log response curves of pressure versus frequency: (a) for a linear system, i.e. n = 1 and K = K_1; (b) for a nonlinear system, i.e., n ≠ 1.

which indicates approximately the upper frequency limit at which dynamic measurements designed to determine K_1 can be made. Our experimental results show typical values of ω_1 of 10 to 50 radians per second.

One feature of the dynamic system becomes apparent: as the source speed is increased, the pressure, Δp_m, increases, but a sort of saturation effect is exhibited at high speeds due to the compressibility of the air within the building.

A second factor also is apparent: the ratio of the source displacement to the volume of the enclosure determines the maximum pressure that can be achieved. From Eqs. (2-21) and (2-9) the maximum of Δp_m is

$$\frac{V_s}{C} = \frac{V_s \gamma P}{V_o} \tag{2-24}$$

For a source displacement of 0.006 m^3 so that V_s = 0.003 m^3 (approximately the size of source actually used), for a building (typical small house) of volume 300 m^3, and for P = 101325 Pascals, the result from Eq. (2-24) for maximum pressure is 1.4 Pascals (0.0057 inches of water), which is somewhat lower than the 2.5 to 15 Pascals range shown to be of interest in Section 2.1 (above). The implications of this result are included in the next section.

2.5 Frequency Response -- Nonlinear Analysis

The complete steady-state frequency-response analysis for the nonlinear model ($n \neq 1$) is more complicated than for the linear model ($n = 1$). However, the high-frequency and low-frequency asymptotes are readily found.

For low frequencies we can neglect the capacitance term by omitting the first term in Eq. (2-16) to leave

$$K[\text{sgn } \Delta p(t)] \; |\Delta p(t)|^n = q_s(t) = Q_s \cos \omega t \tag{2-25}$$

Consequently, when cos ωt is unity, $\Delta p(t)$ takes on its maximum positive magnitude so that

$$K \left|\Delta p(t)\right|^{n}_{max} = Q_s = V_s \omega \tag{2-26}$$

or

$$\left|\Delta p(t)\right|_{max} = \left[\frac{V_s \omega}{K}\right]^{1/n} \tag{2-27}$$

Taking logarithms, and separating the right-hand side into two terms yields

$$\ell n \left|\Delta p(t)\right|_{max} = \ell n \left[\frac{V_s}{K}\right]^{1/n} + \frac{1}{n} \ell n \, \omega \tag{2-28}$$

The low-frequency asymptote given by Eq. (2-28) shows that $\ell n \left|\Delta p(t)\right|_{max}$ plotted against ℓn will be a straight line having slope 1/n. Experimentally, n ω can be determined from the measured slope.

We distinguish $\left|\Delta p(t)\right|_{max}$ from Δp_m because Δp_m is the magnitude of a sinusoidal pressure variation, whereas $\left|\Delta p(t)\right|_{max}$ is the maximum of a generally nonsinusoidal alternating pressure variation.

At high frequencies the capacitance dominates the behavior, just as it does for the linear system. Thus, in Eq. (2-17) we can neglect the second term so that

$$C \frac{d}{dt} \Delta p(t) = V_s \omega \cos \omega t \tag{2-29}$$

from which can be found

$$\left|\Delta p(t)\right|_{max} = \frac{V_s}{C} \tag{2-30}$$

This results in substantially the same as Eq. (2-21).

Figure 2-3(b) shows the two asymptotes represented by Eqs. (2-28) and (2-30). The asymptote intersect at

$$\omega_2 = \frac{K}{C^n V_s^{1-n}} \tag{2-31}$$

which reduces to ω_1 given by Eq. (2-23) when n = 1, and K = K_1, as it should.

The details of the shape of the frequency response curve in the vicinity of ω_2 are not given by a simple closed-form solution, but can be worked out numerically. For the purposes of interpreting experiments, however, a simple approximate expression was employed, namely

$$|\Delta p(t)|_{max} = \frac{V_s}{C} \frac{\left(\frac{\omega}{\omega_2}\right)^{1/n}}{\sqrt{1 + \left(\frac{\omega}{\omega_2}\right)^{2/n}}} \tag{2-32}$$

It is observed that Eq. (2-32) has correct low-frequency and high-frequency asymptotes, and also reverts to the correct expression for n = 1, i.e. for the linear case. Numerical solution of Eq. (2-16) yields results that agree with the approximation of Eq. (2-32) within five per cent for all values tested [Ref. 22] as illustrated in Fig. 2-4. Figure 2-5 shows computer calculated frequency response curves using Eq. (2-32) for several values of n [Ref. 22].

2.6 Frequency Range for Measurements

Using the preceding analysis the frequency range at which experiments should be conducted can now be deduced.

Clearly, the high-frequency range does not give information about the leakage properties of the building. As shown by Eqs. (2-30) and (2-9)

$$|\Delta p(t)|_{max} = \frac{V_s}{C} = \frac{V_s}{V_o} \gamma P \tag{2-33}$$

the maximum amplitude of the cyclic pressure fluctuation depends on the ratio

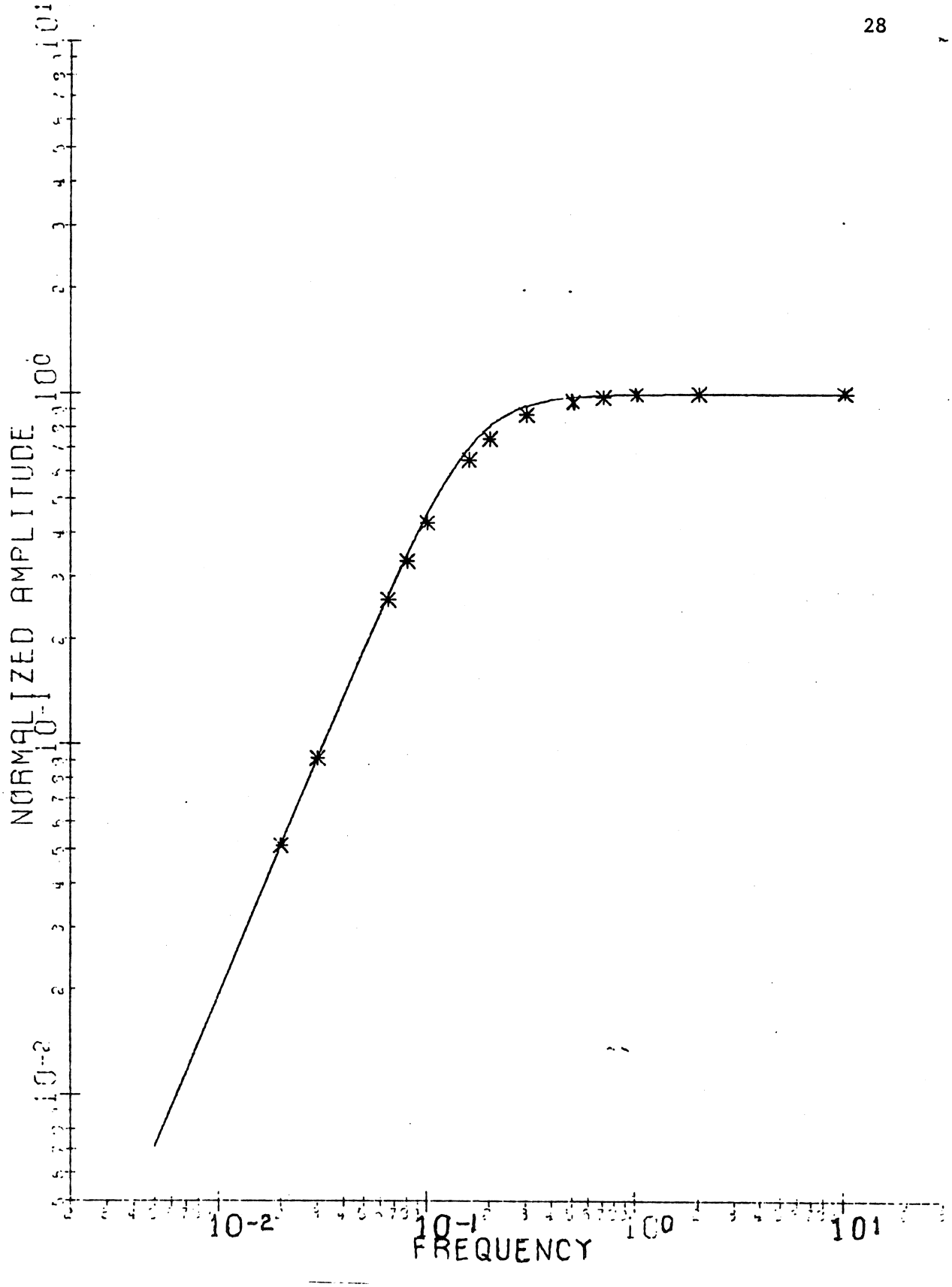

Fig. 2-4. Approximate nonlinear solution (solid line) shown with points from numerical solution.

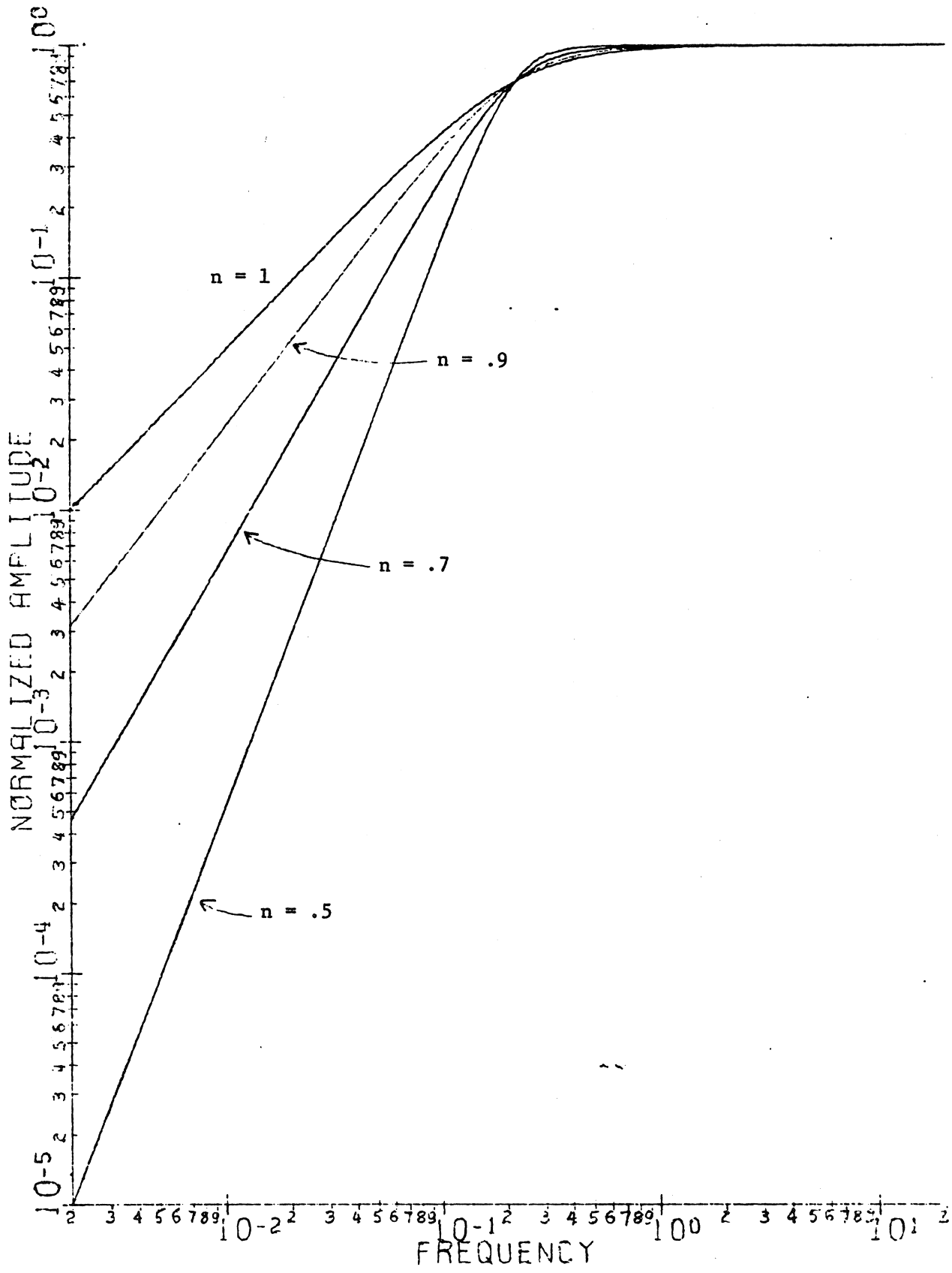

Fig. 2-5. Change in slope of low frequency asymptote as n decreases, approximate solution, Eq. (2-32).

V_s/V_o, but not on K. In the laboratory the response at high frequency (typically 3 to 7 Hz is high enough) can sometimes be used to check the calibration of the measuring system.

The low-frequency range, well below the break-point frequency, can in principle be used to determine the flow-versus-pressure difference characteristics. Thus, for example, using Eq. (2-6)

$$Q_s = V_s \omega \tag{2.6}$$

for any pump speed ω, and knowing V_s, the peak flow Q_s is calculated. If the measuring system gives the corresponding $|\Delta p(t)|_{max}$ then the corresponding pressure is determined. A plot of Q_s thus calculated versus the $|\Delta p(t)|_{max}$ thus measured should be the same as the Q versus Δp curve implied by Eq. (2-3).

The range of values over which the Q_s versus $|\Delta p(t)|_{max}$ can be measured by the infrasonic method is limited at both ends. At the high end the capacitance effect (and the inertance effect to be discussed below in Section 2-7) cause the response to deviate from the low-frequency asymptote shown in Fig. 2-3(b). At the low end man-made and natural interference make accurate readings difficult to obtain.

Thus, instead of limiting measurements to the range where the low-frequency asymptote applies it is more usual to measure the complete frequency response curve over the full range that the equipment is capable of handling. As reported in Chapter 4 the typical range is about 0.1 to 5 Hz for the investigation reported on here. In principle, the measured results are compared with the normalized curve of Fig. 2-3(b). The exponent n is determined from the reciprocal of the slope of the low-frequency asymptote. The capacitance is determined from the high-frequency asymptote using

$$C = \frac{V_s}{|\Delta p_m(t)|_{max}} \tag{2-34}$$

The parameter K is determined from the break-point frequency ω_2 using Eq. (2-31)

$$K = \omega_2 \, C^n \, V_s^{1-n} \tag{2-35}$$

Thus, in Chapter 4, most measured results are presented as frequency response curves.

2-7 Inertance Effects

All the preceding analysis has neglected any inertial effects of the flow, and originally it was hoped that inertial effects could be neglected in the measurements. It turns out, however, that for wide cracks at high frequencies inertial effects must be taken into account. Unfortunately only the linear case, n = 1, can be analyzed accurately.

Consider first the incompressible flow of air having density ρ between parallel plates of width b, separated by w ($w \ll b$), and having length ℓ along the flow. Neglect end effects, and friction so that the velocity is uniform. Using f = ma yields

$$\Delta p(t) = \frac{\rho \ell}{wb} \frac{dq(t)}{dt} \tag{2-36}$$

where $\Delta p(t)$ is the pressure drop in the length ℓ, and q(t) is the flow through the area wb. The coefficient $\rho\ell/wb$ is called the inertance and is analogous to electrical inductance.

An accurate analysis of the inertial effects of viscous flow between parallel plates [Appendix B and Ref. 23] shows that the first term of the infinite series solution differs from Eq. (2-36) only by a factor 6/5. Thus, a better approximate solution for the inertial effect is

$$\Delta p(t) = \frac{6}{5} \frac{\rho \ell}{wb} \frac{dq(t)}{dt} \tag{2-37}$$

We shall use Eq. (2-37).

Equation (2-1) shows the relation of flow to pressure difference for steady flow, and an accurate solution for the dynamic case [Appendix B and Ref. 23] shows that Eq. (2-1) provides the first term of the infinite series solution for the dynamic case. Thus, we shall use

$$\Delta p(t) = \frac{12\mu\ell}{w^3 b} q(t) \tag{2-38}$$

to describe the friction effect.

Clearly, when inertance effects are considered, the model of Fig. 2-2 must now be replaced by the model of Fig. 2.6. For leakage passages that can be modeled by narrow slots

$$R = \frac{12\mu\ell}{w^3 b} \tag{2-39}$$

$$L = \frac{6}{5}\frac{\rho\ell}{wb} \tag{2-40}$$

Similarly, for a leakage passage that can be modeled by a circular pipe [see Appendix B and Ref. 23]

$$R = \frac{128\mu\ell}{\pi d^4} \tag{2-41}$$

and

$$L = \frac{16\rho\ell}{3\pi d^2} \tag{2-42}$$

where d is the pipe diameter. Unfortunately any practical enclosure such as houses are likely to have numerous leakage passages, each one of which has R and an L.

It is of interest to compute the largest size of leakage passage for which the inertance can be neglected. Unfortunately this depends on the size of the building which determines C. However, since typical break-point frequencies

are about 1 to 3 Hertz we can make a useful estimate at $\omega = 10$ rad/sec ($f = 1.6$ Hz). Assume that $\omega L \leq 0.1\ R$ is acceptable, at $\omega = 10$ rad/sec. Then for a slit using Eqs. (2-39) and (2-40)

$$\omega \frac{6}{5} \frac{\rho \ell}{wb} \leq 0.1 \frac{12\mu\ell}{w^3 b} \tag{2-43}$$

with $\rho = 1.226$ kg/m^3 (0.0765 lb/ft^3) and $\mu = 1.780 \times 10^{-5}$ N-sec/m^2 (3.719×10^{-7} lb-sec/ft^2) we get

$$w \leq 1.334 \text{ mm}$$

or about 1/20 of an inch. Since wood sash windows frequently have wider cracks than 1/20 inch, especially in older buildings, inertial effects, hence overshoots in the frequency response curves, are to be expected, and indeed are frequently observed.

Figure 2-7 shows computed frequency response curves for the circuit of Fig. 2-6 for the case where the current source amplitude increases linearly with frequency. The results have also been multiplied by Eq. (2-32) with $n = 0.7$ so as to include the effect of the nonlinear leakage resistance. As reported in Chapter 4, experimental results sometimes have the general shape of Fig. 2-7.

2.8 Wall Movements

Early in the research it was observed that the walls of rooms under test moved back and forth perceptibly due to the cyclic pressure variation caused by the infrasonic source. It was also (incorrectly) conjectured that the overshoots observed in the frequency response curves might be due in part or entirely to wall mechanical resonances.

Analysis was carried out to compare the resilience of a column of air with the resilience of a wood-frame wall consisting of 2 by 4's on 16-inch centers, with the wall facing material (plywood, sheetrock, etc) contributing negligibly

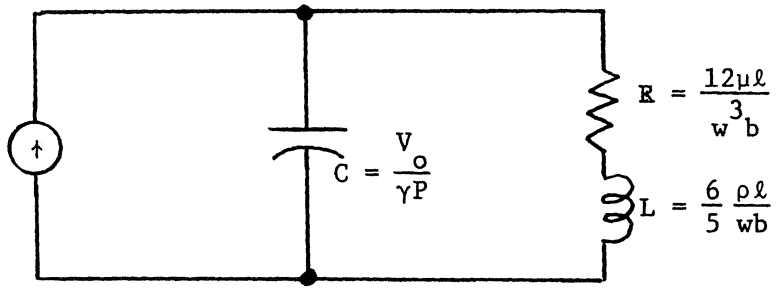

Fig. 2-6. Analogous electric circuit including the inertance effects of leakage passages.

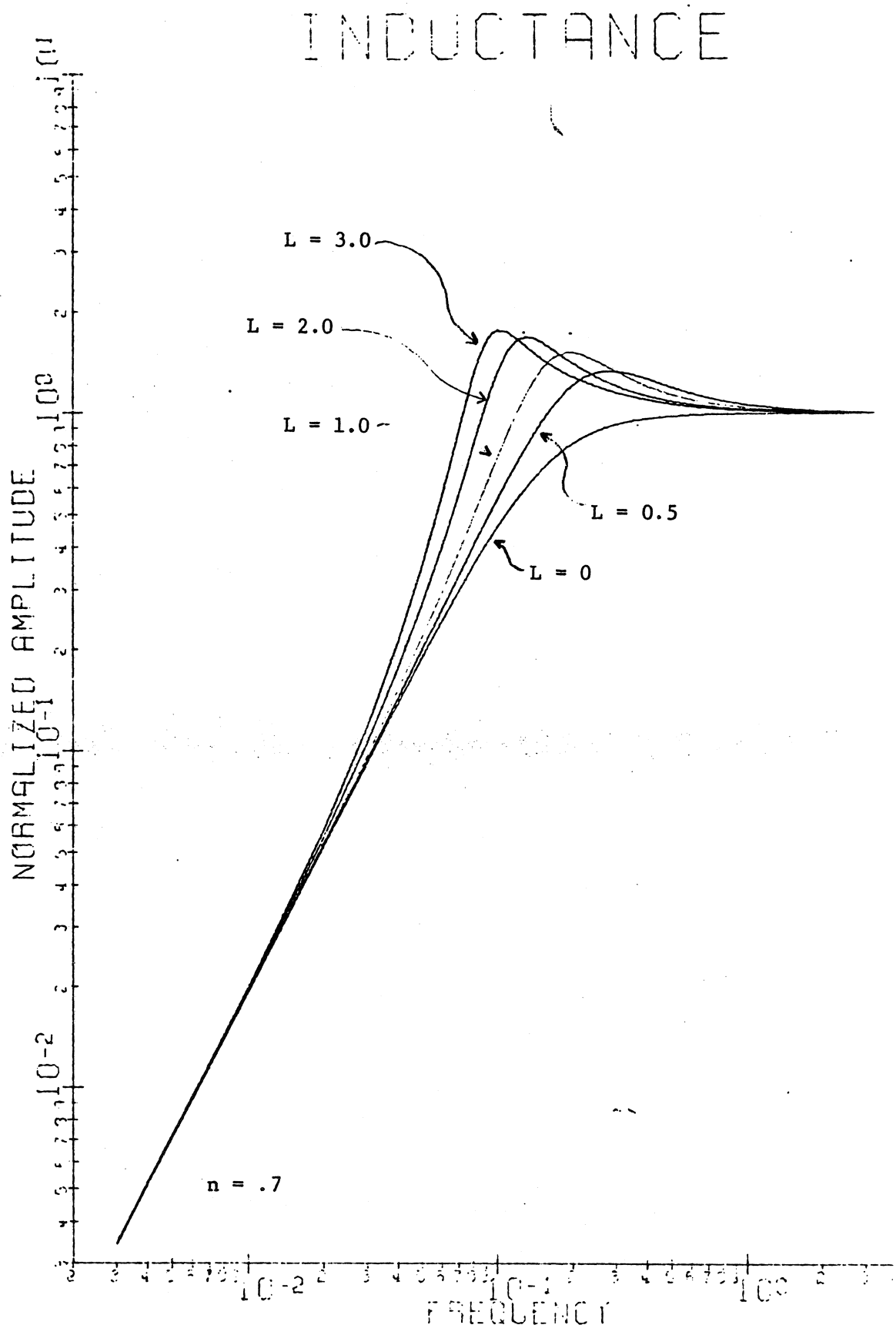

Fig. 2-7. **Frequency response with different inductances.**

to the stiffness (an excessively conservative assumption). It was found that one meter or more of air was more resilient than such a wall. Thus, in typical buildings, the resilience of the walls makes a negligible addition to the resilience due to the air within the building.

When wall resonance is taken into account (considering both the resilience and mass of the wall) analysis indicates that a series RLC branch is added to the circuit model of Fig. 2-6 or Fig. 2-2. Such a branch can be shown to contribute a valley to the frequency-response curve at the self-resonant frequency of the wall. Since no valleys were observed that could be attributed to wall resonance it was concluded that wall movement was not important in any enclosure tested.

Chapter 3

EQUIPMENT DESIGN

3.1 Infrasonic Source

As already mentioned in Section 1-3, and shown in Figs. 1-1 and 1-2 the infrasonic source employs a motor-driven piston that alternately compresses and rarefies the air in a 55-gallon drum. The piston is driven by the crank mechanism from a 3-hp lawn-mower engine having a 3.81 cm (1.5 inch) stoke. The shaft of the lawn-mower engine is driven by way of V-belts and a 31-to-6 speed-reducing gear box from a separately-excited d-c motor. See Appendix E for an equipment list, and Fig. E-1 for the motor control circuit. In spite of the cyclically-varying mechanical load imposed by the air in the drum on the piston, the mechanical speed is kept almost constant by the inertia of the motor. Also, the separately-excited motor connection tends to keep the speed constant independent of load.

Actually, the source is more like a bellows than a conventional piston in a cyclinder. Instead of using a sliding seal between piston and cyclinder the system uses a piston consisting of plywood discs that are centered in and sealed to the open bottom of the 55-gallon drum by means of a sheet of gum rubber 1.6 or 0.8 mm (1/16 or 1/32 inch) thick. In this way the leakage is made essentially negligible, which is necessary for such a low-speed system.

In view of the engine stroke (3.81 cm) and piston diameter (45.7 cm) the displacement is approximately 0.00626 m^3, hence V_s is 0.00313 m^3. The infrasonic source weighs about 90 kg. A more powerful but lighter-weight source would be desirable.

3.2 Pressure Sensor

Exceedingly small pressure variations need to be detected, of the order of one Pascal, so that a pressure sensor having a resolution of 0.1 or 0.01 Pascals is desirable. This implies a resolution about a thousand times smaller than that of a typical household barometer. At such low operating signal levels man-made and natural interference may (and often does) mask the signal unless special filters are employed as described below.

Some very sensitive pressure sensors for use in somewhat similar applications (microbarographs) employ a very thin metal diaphragm separating two air chambers, each chamber being connected to the atmosphere by a specially-chosen leakage passage [Ref. 28]. By properly proportioning the two chamber volumes and the two leak resistances such a system can be designed to have band-pass properties. That is, pressure variations in some desired frequency range (the pass band) deflect the diaphragm back and forth, whereas pressure variations at frequencies outside the pass band are attenuated and cause relatively less diaphragm deflection. Diaphragm deflection is detected electrically, for example, by a capacitance pickup. Such a system is relatively expensive and has to be calibrated by subjecting it to known pressures, but otherwise it should have desirable characteristics.

We use, instead, a one-chamber pressure sensor employing a rigid container of volume 0.005663 m^3, and having a 10.16 cm diameter opening, as shown in the photograph of Fig. 1-3. A thin (0.01 mm) plastic film (SARAN wrap) covers the opening and is sealed in place with lubricating grease. Deflection of the center of the diaphragm is measured using a probe employing fibre optics (FOTONIC Sensor). For the frequency range of present interest such a film has a negligible mass. Also the stiffness due to the diaphragm material is negligible compared to the stiffness due to the air in the chamber.

The scale factor for the pressure sensor is derived assuming that the deflected diaphragm has a paraboloid shape, and that the air in the sensor chamber, like the air in the enclosure (house) under test, expands and contracts isentropically.

The volume ΔV_d of a paraboloid having a base area A_d and a height y_d is

$$\Delta V_d = \frac{1}{2} A_d \, y_d \tag{3-1}$$

But the volume ΔV_d of the deflected diaphragm is related to the sensor chamber volume V_d and the pressure signal $\Delta p(t)$ by the capacitance of the pickup chamber

$$\Delta V_d = C_d \, \Delta p(t) \tag{3-2}$$

Using Eq. (2-9) for the capacitance of the sensor chamber

$$C_d = \frac{V_d}{\gamma P} \tag{3-3}$$

then combining Eqs. (3-1), (3-2) and (3-3) yields

$$y_d = \frac{2}{A_d} \frac{V_d}{\gamma P} \Delta p(t) \tag{3-4}$$

For $A_d = 0.00811 \ m^2$, $V_d = 0.005663 \ m^3$, and P = 101325 Pascals, y_d in meters given by

$$y_d = 9.84 \times 10^{-6} \, \Delta p(t) \tag{3-5}$$

Thus, for example, a pressure of 25 Pascals (0.1 inches of water) would give a diaphragm center deflection of about 0.25 mm. For most of the measurements even smaller diaphragm deflections are obtained.

Turning now to the Fotonic Sensor, employed to measure diaphragm deflection, the instrument used has a response curve shown in Fig. 3-1. For the

linear range where the broken line and actual characteristic essentially coincide the Fotonic Sensor has a sensitivity of 340 V/m. Using this factor with Eq. (3-5) yields an expression for the Fotonic Sensor output voltage e_d in volts in terms of pressure

$$e_d = 340 \times 9.84 \times 10^{-6} \Delta p(t) \qquad (3\text{-}6)$$
$$= 3.35 \times 10^{-3} \Delta p(t)$$

Thus, for example, a pressure of 25 Pascals would yield a 83.6 mV. Such a signal is small enough so that the Fotonic Sensor is effectively linear, but too small for some strip-chart recorders. Hence further amplification is needed.

It should be noted that the sensor chamber needs a slow leak to equalize the inside and outside pressures, since the naturally-occurring slow variations in barometric pressure would otherwise cause the diaphragm to take on a quasi-static deflection. For this purpose a 1.27 cm length of tubing having an inside diameter of 0.28 mm was employed, and found to be satisfactory. To show that the slow leak did not affect the sensitivity in the frequency range of interest, the leak was plugged briefly; no change in response amplitude was detected. Such a slow leak gives the sensor a high-pass filter characteristic: it passes (does not attenuate) signals above approximately 0.01 Hz.

3-3 Electronic Amplifier and Filter

The pressure sensor, as described up to this point, behaves as a broad-band microphone responding to signals at frequencies from about 0.01 Hz, as limited by the slow leak of the sensor chamber, up to about 40 kHz, as limited by the high-frequency limit of the Fotonic Sensor. However, only signals in the range 0.1 to 10 Hz are of interest so that a band-pass filter having this smaller frequency range can be used. In fact a band-pass filter must be used

in order to cut out the unwanted audio frequency signals which otherwise interfere with the operation of the strip-chart recorder and electronic circuits.

Appendix F describes the electronic amplifier and band-pass filter that were employed. Two different band-pass characteristics were available, and a choice of pass-band gains of 1, 2, 4, 10, 15, 20, 30 and 50 were provided. Because the Fotonic Sensor has a large d-c component in its output the electronic filter employs a-c coupling; however, the response is essentially flat down to 0.1 Hz.

The output signal from the electronic filter is fed directly into a fast-responding strip-chart recorder which therefore plots the instantaneous value of the cyclically-varying pressure in the enclosure (house) under test. Ideally, therefore, the strip chart shows a sinusoid having a frequency that is the pump frequency, and having an amplitude proportional to the instantaneous pressure.

3 .4 Synchronous Detector

All of the early experimental work was done using a strip-chart recorder as the output indicator. It was found, however, that on large enclosures at low frequencies the interfering signals due to barometric pressure fluctuations, wind noise, and other causes made it difficult and tedious to determine the signal size from the strip chart. In view of this problem a synchronous detector system was developed.

Figure 2-1 shows the complete measuring system including the synchronous detector. Here two square-wave signals from the source shaft are used to multiply the pressure signal from the Fotonic Sensor; the two resulting product signals are then fed into separate low-pass filters. The output signals E_a and E_b from the low-pass filters are indicated on two electronic voltmeters visible in the photograph of Fig. 1-3.

Provided the slightly nonsinusoidal nature of the pressure waveform (due to the nonlinear flow-versus-pressure characteristics of leaks) is ignored it can be shown that

$$\Delta p_m = K_s \left[E_a^2 + E_b^2 \right]^{1/2} \tag{3-7}$$

where K_s is a scale factor that can be calculated. In addition

$$\phi = \tan^{-1} \frac{E_a}{E_b} \tag{3-8}$$

is the angle by which the pressure signal is shifted from the source shaft angle used as reference. Appendix A describes the synchronous detector in more detail.

3.5 Blower and Manometers

The major equipment items are listed in Appendix E.

For most of the static pressure tests a blower driven by a one-horsepower 3450-rpm direct-connected motor was employed. (See Fig. 1-5) This blower has a capacity of about 0.4 m^3/sec (850 CFM) at zero head, and a maximum head of about 1800 Pascals (7.2 inches of water). Such a high-head blower was required to provide adequate pressure drop -- up to 750 Pascals (3 inches of water)-- across the nozzle used to measure flow.

The volumetric flow rate was measured using various nozzles, as listed in Appendix E ranging from 11.43 cm (4.5 inch) diameter to 1.905 cm (0.75 inch) diameter. The calibration curves supplied with the nozzles showed that

$$Q = K_n (\Delta p)^{1/2}$$

applied over the useable pressure ranges.

Pressure drop across the nozzle was measured with an inclined manometer having a range 0 to 3 inches of water and 0.02 inch divisions. Inside-outside pressure drop was measured using an inclined manometer having a range (-0.05)-0-(+0.25) inches of water, and having a smallest division of 0.005 inches.

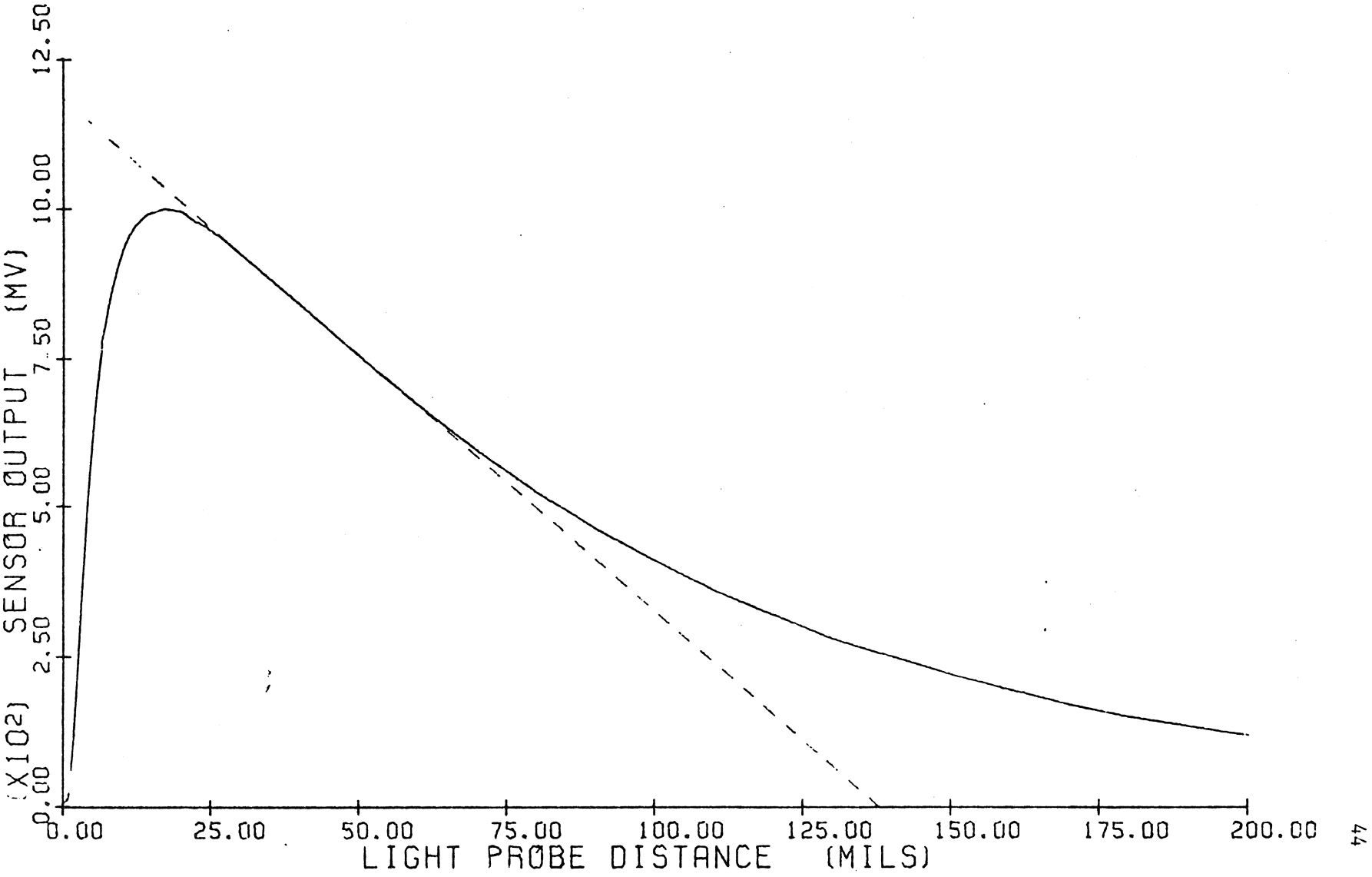

Fig. 3-1. **Fotonic sensor characteristic curve.**

Chapter 4

EXPERIMENTAL RESULTS

4.1 Types of Experiments

Three types of experiments were conducted, namely blower tests, infrasonic impedance tests, and inertia-effect tests. These experiments were carried out in three rooms in Link Hall (the main engineering building at Syracuse University), in several apartments, and in one single-family house.

4.2 Descriptions of Enclosures Tested

Link Hall is a relatively new (1970) four-story academic building of reinforced concrete construction. Interior walls are of metal lath and plaster. Room 302, the smallest enclosure tested, was designed as a photographic dark room and has a plastered ceiling. For the air-leakage tests all the openings around pipes, lights, electric outlets, etc. were carefully sealed with duct tape. Room 306C is an interior storage room. All the openings around pipes, and the junction between plastered walls and the concrete ceiling were sealed with caulking compound or duct tape. For most experiments the doors of these two rooms were sealed with duct tape also. Room 220 is an interior office or laboratory room with a false ceiling of acoustic tile. Only the air ducts were sealed during tests; the visible cracks around the edges of the ceiling were not sealed.

The second group of enclosures were all apartments in a relatively new married-student housing complex. Each two-story building has eight apartments. These buildings are made principally of precast concrete floor, wall and ceiling panels, along with some wood-frame portions. For most tests all windows were closed tightly, interior doors opened, but no special attempts were made to find and seal leaks.

Finally, one relatively small one-floor single-family house was tested. This house was built in 1960, is of conventional wood-frame construction, and has relatively large windows. The house employs hot water heating, and the floor openings around the hot water pipes were sealed, but the numerous other air leaks were left untouched. During tests the basement door was closed and sealed with duct tape so that only the main floor constituted the enclosure under test. For some tests the doors of the three bedrooms were closed and sealed with masking tape so as to reduce the enclosure volume. The outside doors and the windows were closed but not sealed during tests.

4.3 Test Procedure

For the tests on Room 302 and 306C, the infrasonic apparatus was located inside the room during the test. At some later time blower tests were carried out on the rooms, with the blower located outside the rooms, hopefully with leakage conditions identical with those for the infrasonic tests.

For all the apartments and the house the infrasonic apparatus and the blower were set up at the same time, and the tests run consecutively. The blower was connected to a special door panel by way of a 6-inch flexible hose. During infrasonic tests the blower valve was shut off. The two tests could not be performed simultaneously since the two systems interfered with each other.

4.4 Blower Tests

Figure 4-1 shows the results of a blower test made on Room 306C [Ref. 23]. In order to cover the full pressure range shown four different nozzles were employed. At the low-pressure end of the curve considerable scatter is evident, some of which may be due to the ventilating system of the building. Small leaks in the blower box can also cause errors. The solid line in the figure is a least-squared-error fit of the expression

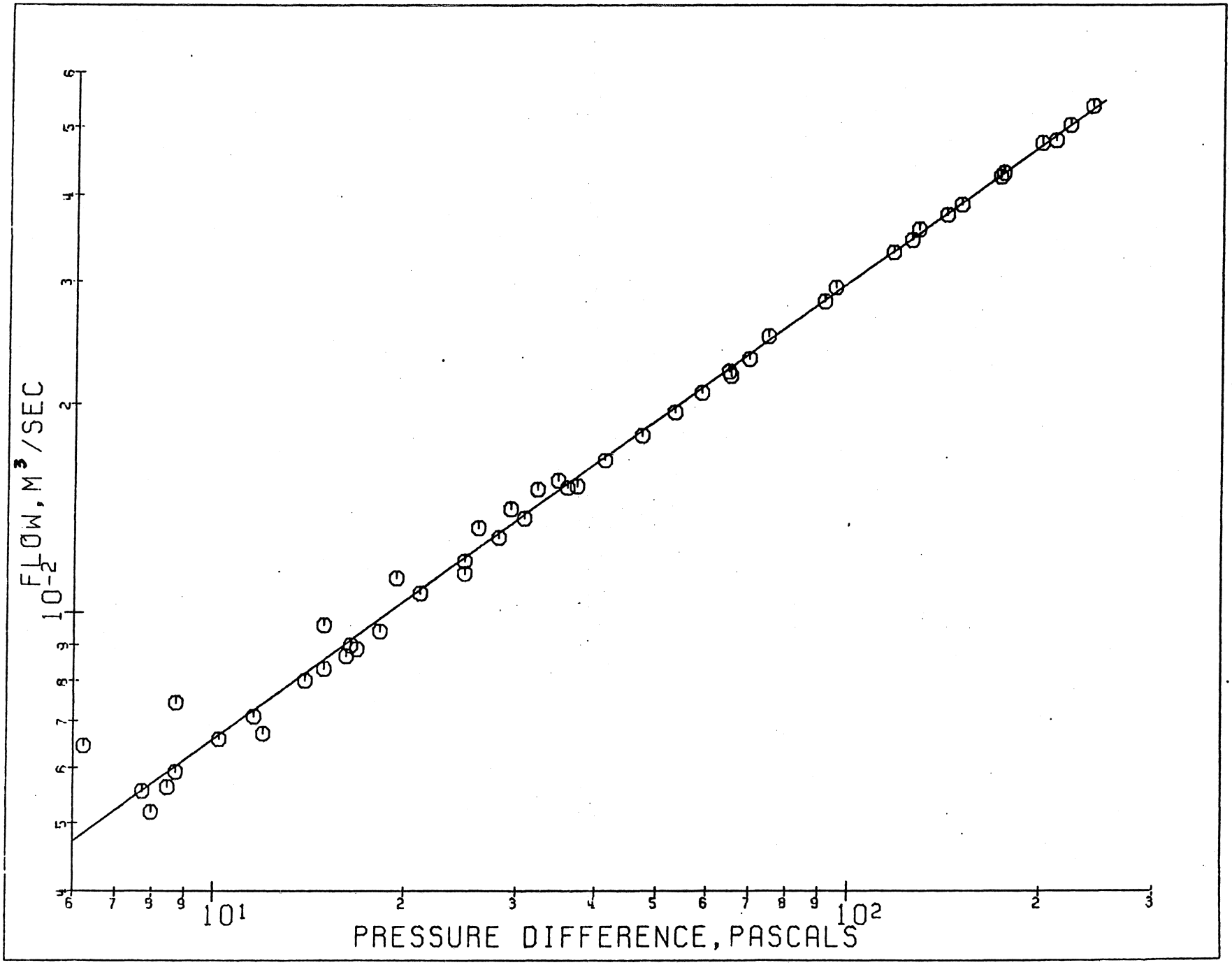

Fig. 4-1. Blower test curve for room 306C. n = 0.6566, q_o = 0.00145.

$$Q = K\ (\Delta p)^n \qquad (4\text{-}1)$$

None of our measurements is sufficiently precise to show any deviation from Eq. (4-1) for an enclosure tested.

Figure 4-2 shows the results of a blower test under less favorable conditions on the single-family house. Because the house is much leakier than Room 306C, the one hp blower can only produce a maximum pressure of about 10 Pascals (0.04 inches of water) even at a flow of 0.3 m^3/sec (640 CFM). The varying outside wind speed causes fluctuations in the indication of the manometer connected to read inside-outside pressure difference, accounting for the scattered data.

Table 4-1 shows the results of blower tests on eight different enclosures. The calculated exponent n and coefficient K are chosen to give a least-squared-error fit to Eq. (4-1). All but one of the values for n are between 0.62 and 0.70, in agreement with the experience of other experimenters. Measurement of Room 302, the one exception, will be repeated at some future time. The coefficient K is the (extrapolated) air leakage in m^3/sec at 1.0 Pascal. (0.004 in. of water). Multiplying K by 2119 would yield the flow in CFM.

4.5 Infrasonic Tests

Figure 4-3 shows a frequency response curve for Room 302 [Ref. 22]. For this small carefully-sealed room the results show the low-frequency and high-frequency asymptotes and break frequency (at 0.7 Hz) as predicted by the analysis in Chapter 2. The slope of the low-frequency asymptote yields an exponent n = 0.77, a reasonable value. (Clearly not all the leaks have been sealed!) For this small room the response signal is relatively large compared to the interference so that there is relatively little scatter in the measurement.

Figure 4-4 shows the results of two tests carried out on Room 306C [Ref. 22]. The left-hand curve, labelled "Door taped" shows again that even with a

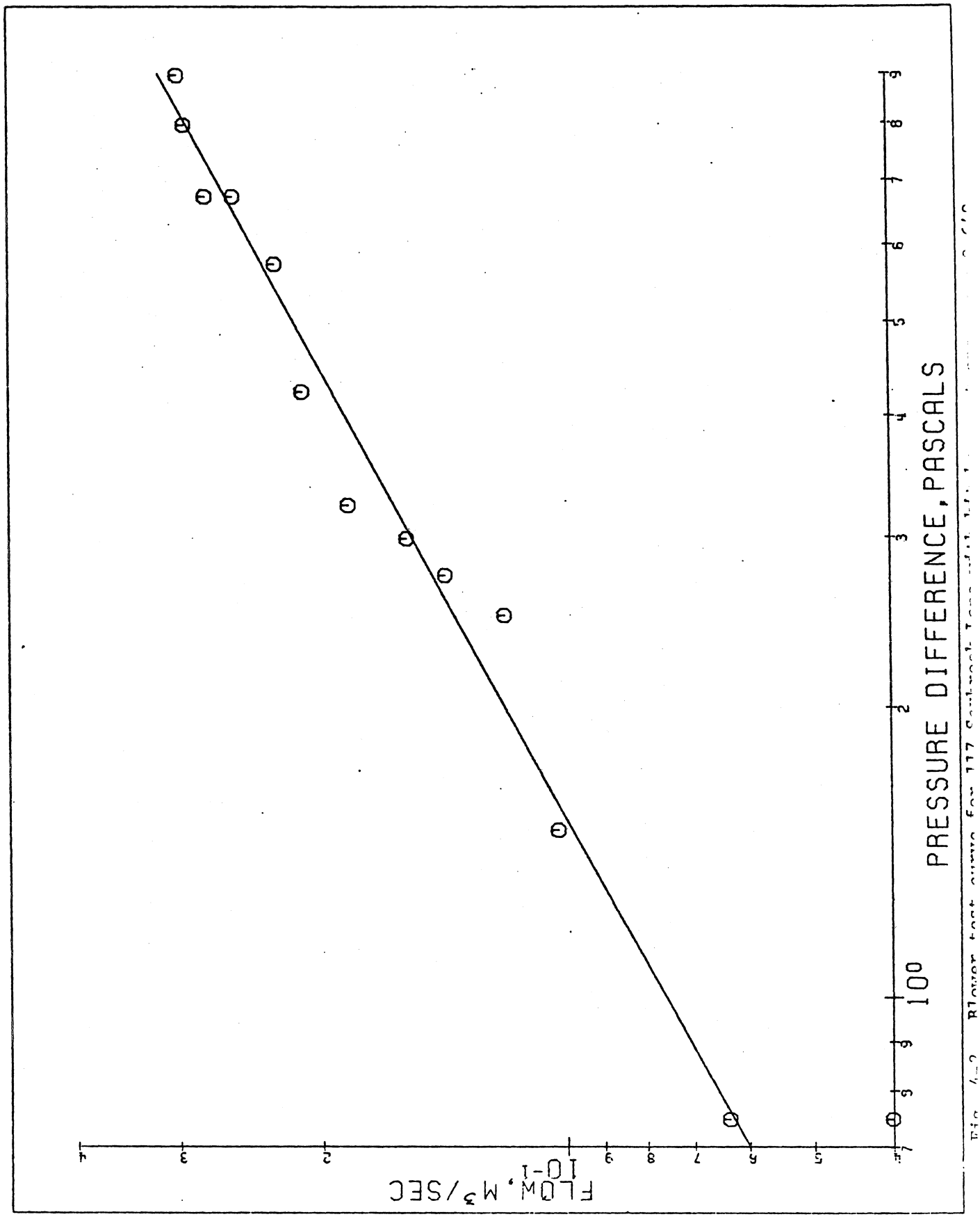
FLOW, M³/SEC
10-1
PRESSURE DIFFERENCE, PASCALS
100

TABLE 4-1

Results of Blower Tests

Location	Volume m^3 (ft^3)	Exponent n	Coefficient K (1)
306C Link	50.0 (1765.7)	0.6566	1.45×10^{-3}
220 Link	38.3 (1353.3)	0.6994	1.682×10^{-2}
Dark Room Link	20.0 (706.3)	0.4638	6.01×10^{-3}
101 Small	191.5 (6758.6)	0.6219	2.53×10^{-2}
104 Small	194.5 (6869.7)	0.6830	1.62×10^{-2}
105 Small	194.0 (6850.8)	0.6630	1.945×10^{-2}
108 Small	192.88 (6811.8)	0.653	2.16×10^{-2}
117 Saybrook	142.0 (5014.7)	0.649	7.507×10^{-2}

(1) Air leakage in m^3/sec at Δp = 1 Pascal.

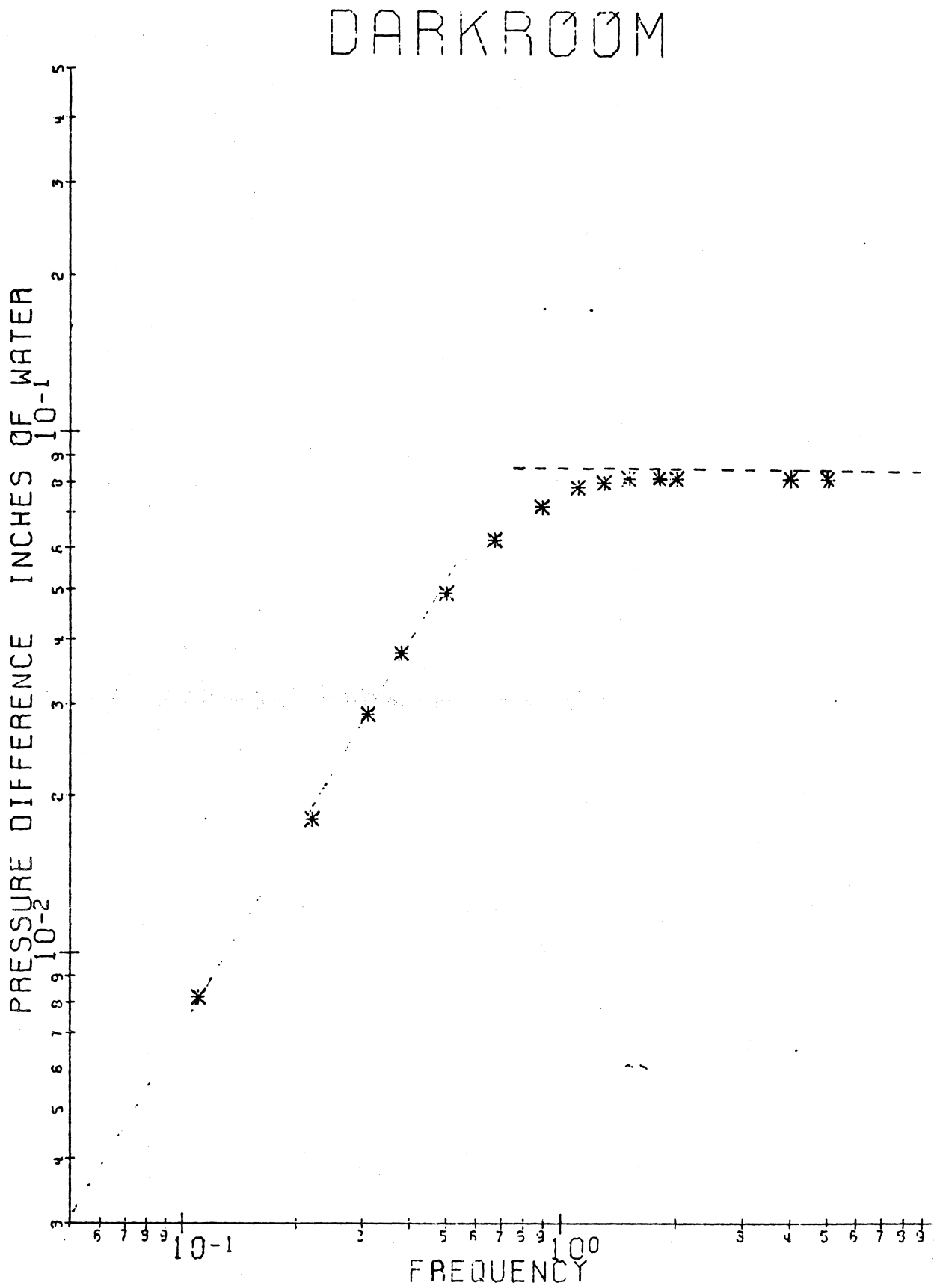

Fig. 4-3. Measured frequency response of Darkroom, Room 302.

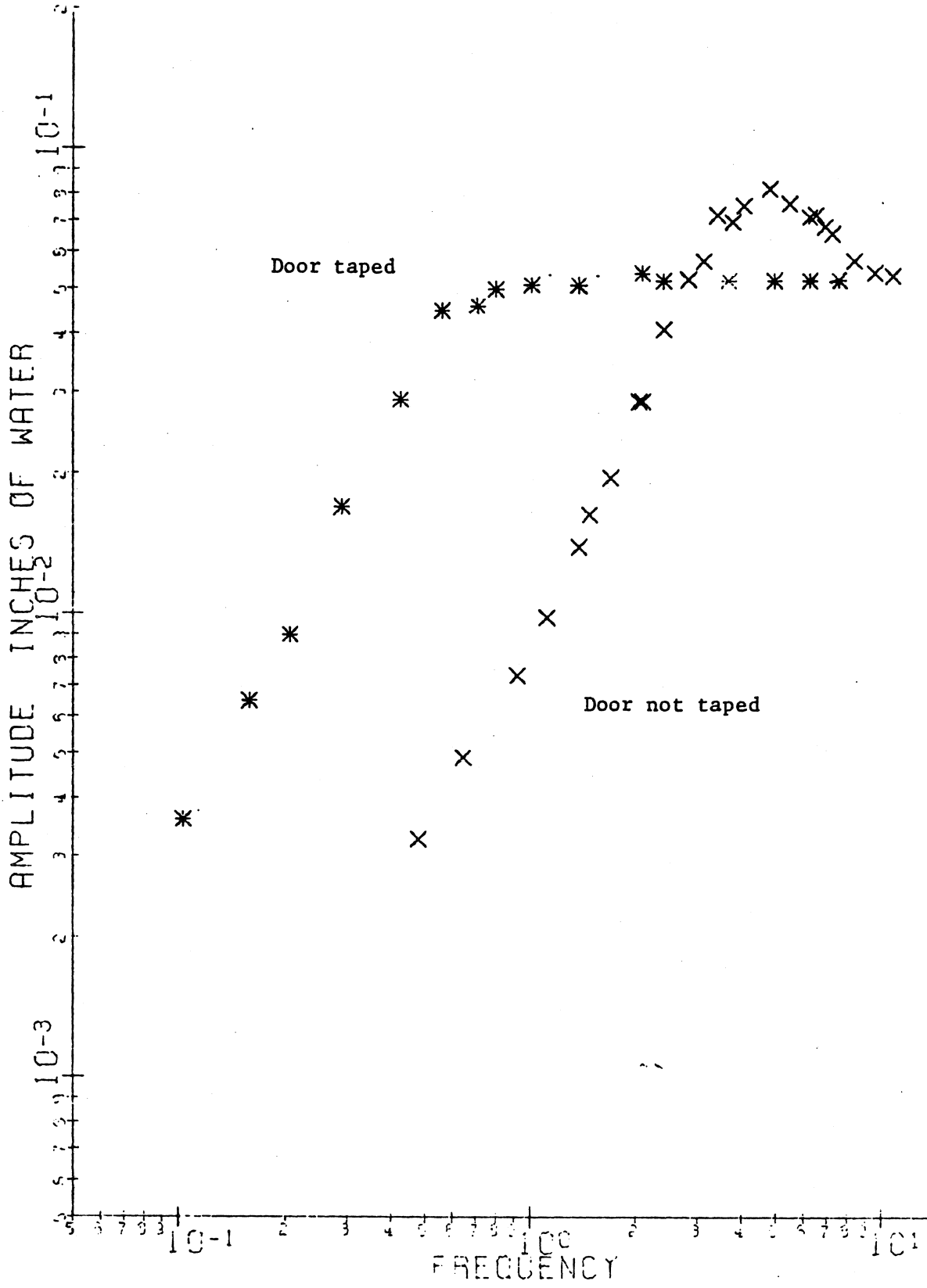

Fig. 4-4. Room 306C under different conditions.

careful sealing of a room some leaks still remain. The right-hand curve labelled "Door not taped" shows the clear overshoot resulting from a leak having inertance. Clearly the leak around the door dominates the total leakage. The coincident high-frequency asymptotes are in accordance with predictions. Figure 4-4 should be compared with Fig. 2-7 where the predicted curve for a simple inertance is shown.

Figure 4-5 [Ref. 23] shows the frequency response curve for one apartment, 101 Small Road. A least-square-error curve has been fitted to the data and shows n = 0.2107 which is an unreasonably small value, since n is usually about 0.6 to 0.7. Moreover, the calculated value of leakage from the infrasonic test is much smaller than that calculated by the blower test. Clearly the infrasonic test on 101 Small Road has not yielded a useful result.

Figure 4-6 shows the frequency response curve for another quite similar apartment, 104 Small Road. Here the least-square-error curve shows n = 0.673 a very reasonable value -- and q_o = 0.007. In this case leakage predicted by the infrasonic method and blower method agree within a factor of three.*

Figure 4-7 shows the frequency response curve for the single-family house. Here the exponent n = 0.978 is higher than would be expected, and there is a lot of scatter because of the small signal-to-interference ratio.

Table 4-2 shows the results of tests on ten enclosures. Note that in all these calculations any inertance effect is neglected. Moreover, all the measurements that were made were used in the least-squared-error curve fit program, so that no judgement was involved.

Table 4-3 compares the air leakage predicted by the blower method and by the infrasonic method at the pressure of 25 Pascals (0.1 inch of water). For all except the house 25 Pascals is within the range spanned by the blower test. However, for all the infrasonic tests, 25 Pascals represented an extrapolation

* q_o from the infrasonic test should equal K from the blower test.

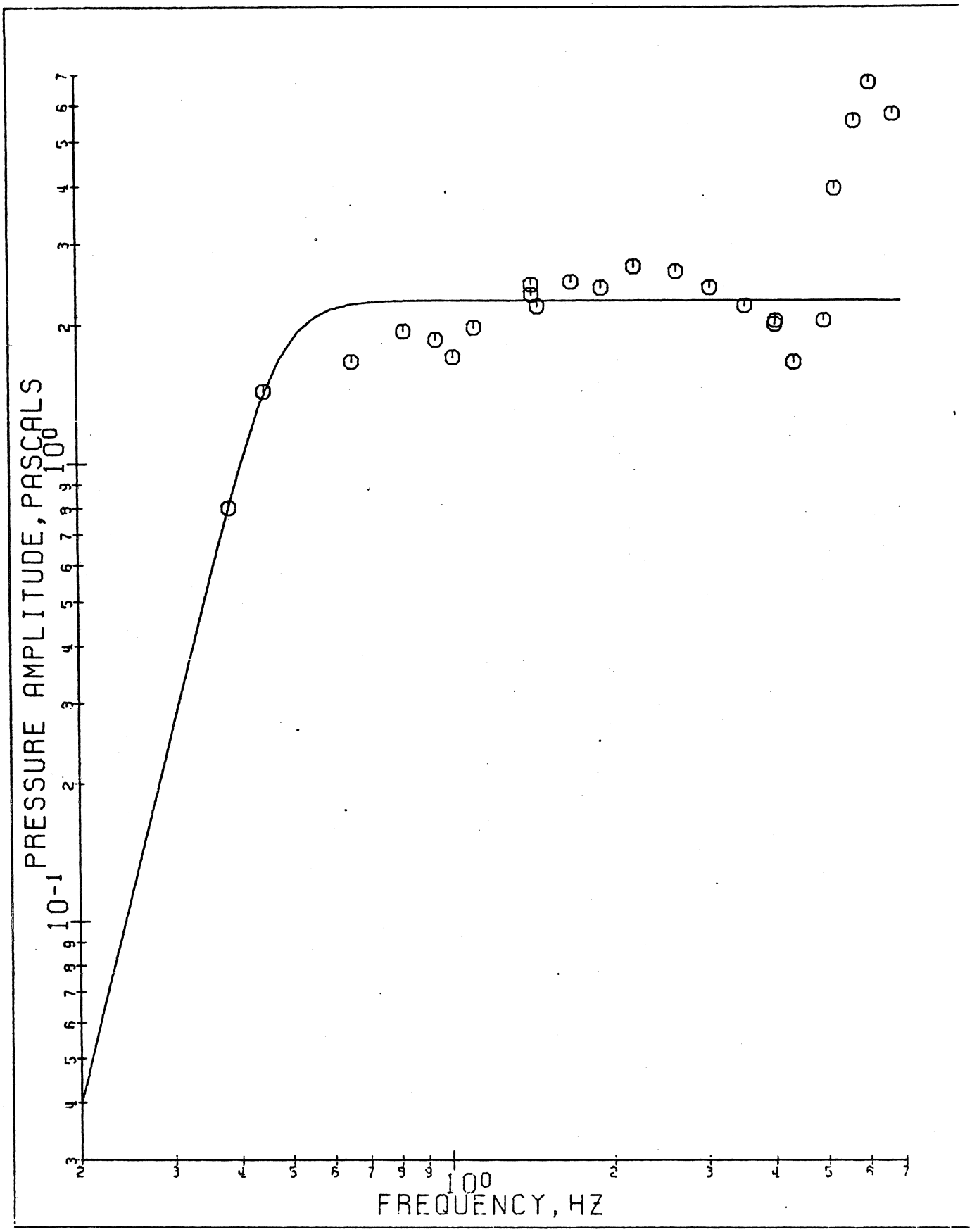

Fig. 4-5. Frequency response curve for 101 Small Road Apt. n = 0.2107, q_o = 0.00775, C = 0.00138 m^5/N.

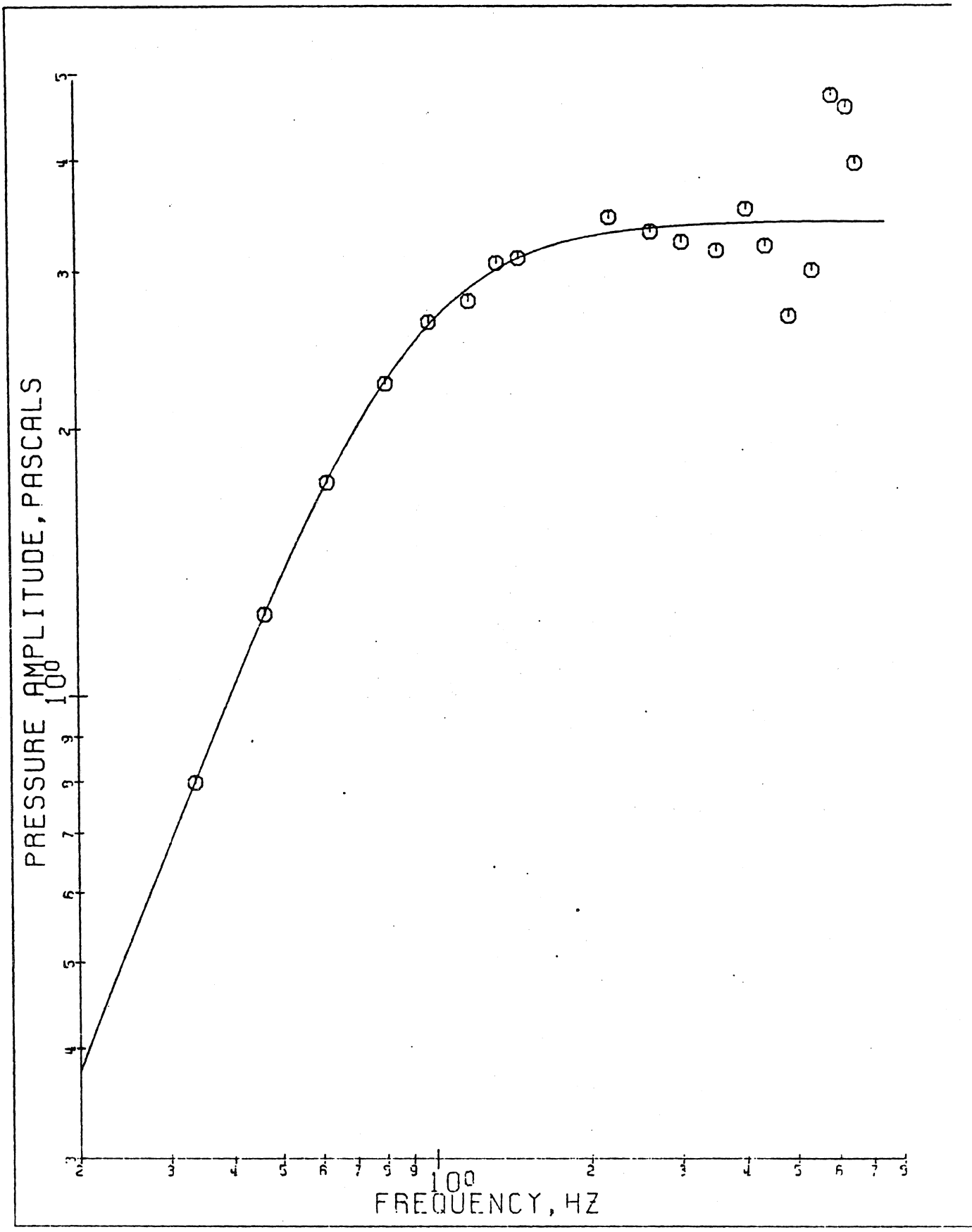

Fig. 4-6. Frequency response curve for 104 Small Road Apt. n = 0.673, q_o = 0.007, C = 0.0009149 m^5/N.

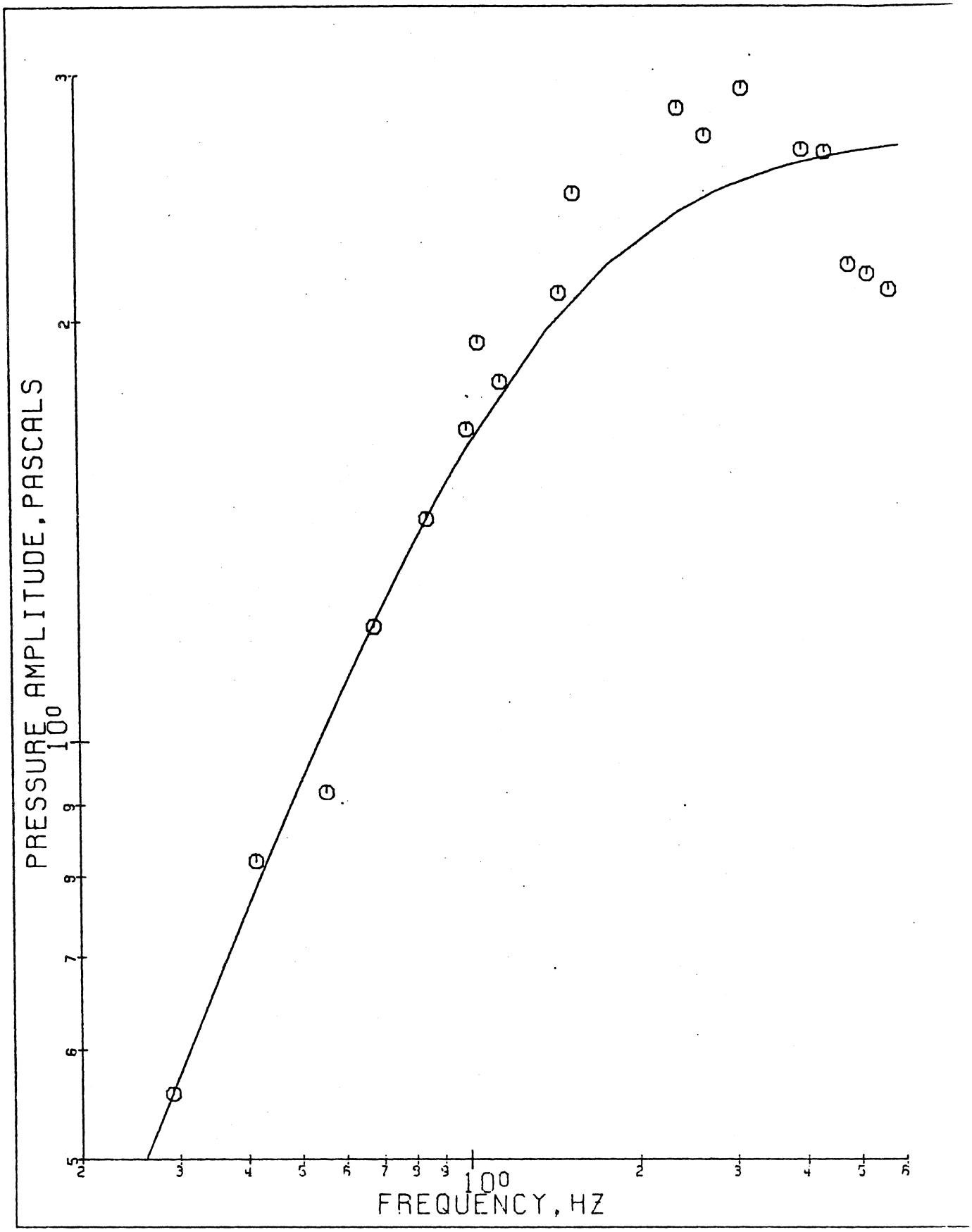

Fig. 4-7. Frequency response curve for 117 Saybrook Lane - one family house with kitchen vent closed. n = 0.978, q_o = 0.0098, C = 0.00114 m^5/N.

TABLE 4-2

Results of Infrasonic Tests on Ten Enclosures

Location	Volume m^3 (ft^3)	Calculated Capacitance $C^{(1)}$ (m^5/n)	Results			
			Capacitance $C(m^5/N)$	Exponent n	Coefficient q_o (2)	Break freq. f_2(Hz)
306C Link	50 (1765.7)	3.59×10^{-4}	--	0.64	3.1×10^{-3}	0.65
220 Link	38.3 (1353.3)	2.69×10^{-4}	4.95×10^{-4}	1.846	5.98×10^{-4}	--
Dark Room Link	20.0	1.4×10^{-4}	--	0.77	1.2×10^{-3}	0.7
101 Small	191.4 (6758.6)	1.350×10^{-3}	1.57×10^{-3}	0.2107	7.75×10^{-3}	0.46
102 Small	192.0 (6780.4)	1.353×10^{-3}	1.678×10^{-3}	1.309	1.38×10^{-2}	--
103 Small	192.5 (6798.1)	1.357×10^{-3}	0.915×10^{-3}	1.11	7.0×10^{-3}	1.65
104 Small	194.5 (6869.7)	1.371×10^{-3}	1.652×10^{-3}	0.673	6.47×10^{-3}	0.88
105 Small	194.0 (6850.8)	1.367×10^{-3}	1.080×10^{-3}	0.549	8.9×10^{-3}	0.46
108 Small	192.88 (6811.8)	1.14×10^{-3}	1.14×10^{-3}	0.773	9.8×10^{-3}	1.10
117 Saybrook	142.0 (5014.7)	1.00×10^{-3}	1.255×10^{-3}	0.978	1.14×10^{-2}	1.65

(1) Capacitance C calculated from $C = \frac{V_o}{\gamma p_o}$

(2) Air leakage in m^3/sec at $\Delta p = 1$ Pascal.

TABLE 4-3

Comparison of Air Leakage by Two Methods at 25 Pascals

Location	Blower Method $q_B(m^3/sec)$	Infrasonic Method $q_I(m^3/sec)$	Ratio q_I/q_B
306C Link	0.012	0.024	2.00
220 Link	0.159	0.227	1.42
Dark Room Link	0.026	0.014	0.538
101 Small	0.187	0.0031	0.0165
104 Small	0.146	0.0564	0.386
105 Small	0.164	0.052	0.317
108 Small	0.176	0.1180	0.670
117 Saybrook	0.611	0.265	0.433

outside the pressure range spanned in the test. The final column in Table 4-3 shows the ratio of the two predictions. Clearly there is substantial disagreement between the two predictions. However, except for 101 Small, where the exponent is not reasonable, the two methods agree within a factor of three. A comparison at other pressure levels has not yet been made.

4-6 Inertance Experiments

In order to establish both qualitatively and quantitatively that inertia effects account for the overshoots observed in the frequency response curves, experiments were designed and carried out to enhance the inertia effect [Ref. 23]. These experiments were also intended to illustrate the behavior to be expected in a housing unit having an open chimney or ventilator flue.

For the inertance experiments a 0.254 m (10 inch) diameter pipe was mounted through the door of Room 306C. Two different lengths of pipe -- 0.6096 m (2 feet) and 2.336 m (7 feet 8 inches) -- were employed. Using such large-diameter pipe meant that the air leakage due to the pipe was very large compared to the combined effect of all the other leaks, so the other leaks can be neglected. Thus Fig. 2-6 represents the experimental situation.

For each length of pipe the system parameters were calculated using the analysis of Appendix B; the results are shown in the Calculated columns of Table 4-4. Also, a least-squared-error computation was used to determine the parameters of the equation

$$\Delta p_m = V_s \frac{R^2 + \omega^2 L^2}{(1 - \omega^2 LC)^2 + (\omega RC)^2} \tag{4-2}$$

where

$$R = R_\ell + S\omega^2 \tag{4-3}$$

which gave a best fit to the experimental results. (Equation (4-3) includes

TABLE 4-4

Results of Inertance Experiments

	Short Pipe		Long Pipe	
	Calc	Meas	Calc	Meas
Pipe inertance $N\text{-}sec^2/m^5$	21.7	16.9	78	44
Room capacitance m^5/N	3.59×10^{-4}	5.23×10^{-4}	3.59×10^{-4}	5.82×10^{-4}
Resonant frequency Hz	1.80	1.69	0.95	0.99
Resistance at ω_o $N\text{-}sec/m^5$	0.18	49.2	0.43	54
Quality factor Q_o	1365	3.65	1090	3.18

a radiation term, $S\omega^2$, which theoretically is very small.) The results of this processing of the experimental results is shown in the Measured columns of Table 4-4.

Figure 4-5 shows the measured results for the 2.336 m long pipe, along with the solid line obtained from the best fit to Eq. (4-2). A similar result was obtained for the shorter pipe.

Table 4-4 summarizes the results. As can be seen, the resonant frequencies ($f_o = \omega_o/2\pi$) agree fairly closely, but the values for C and L show somewhat larger discrepancies. The resistance terms and the resonant Q_o ($Q_o = \omega_o L/R$) have large disagreements. Evidently, energy losses are very much larger than predicted. Some of the excess energy loss may have resulted because the pipes and door panel were not completely rigid. The theory itself is based on laminar flow, hence underestimates the energy loss. Many other causes for the excessive dissipation can also be suggested. Eliminating the excessive energy dissipation might also bring the values of L and C into closer accord. In spite of the substantial disagreement between theory and experiment the experiment did establish that inertance effects can result in an overshoot in the frequency response curve, as predicted.

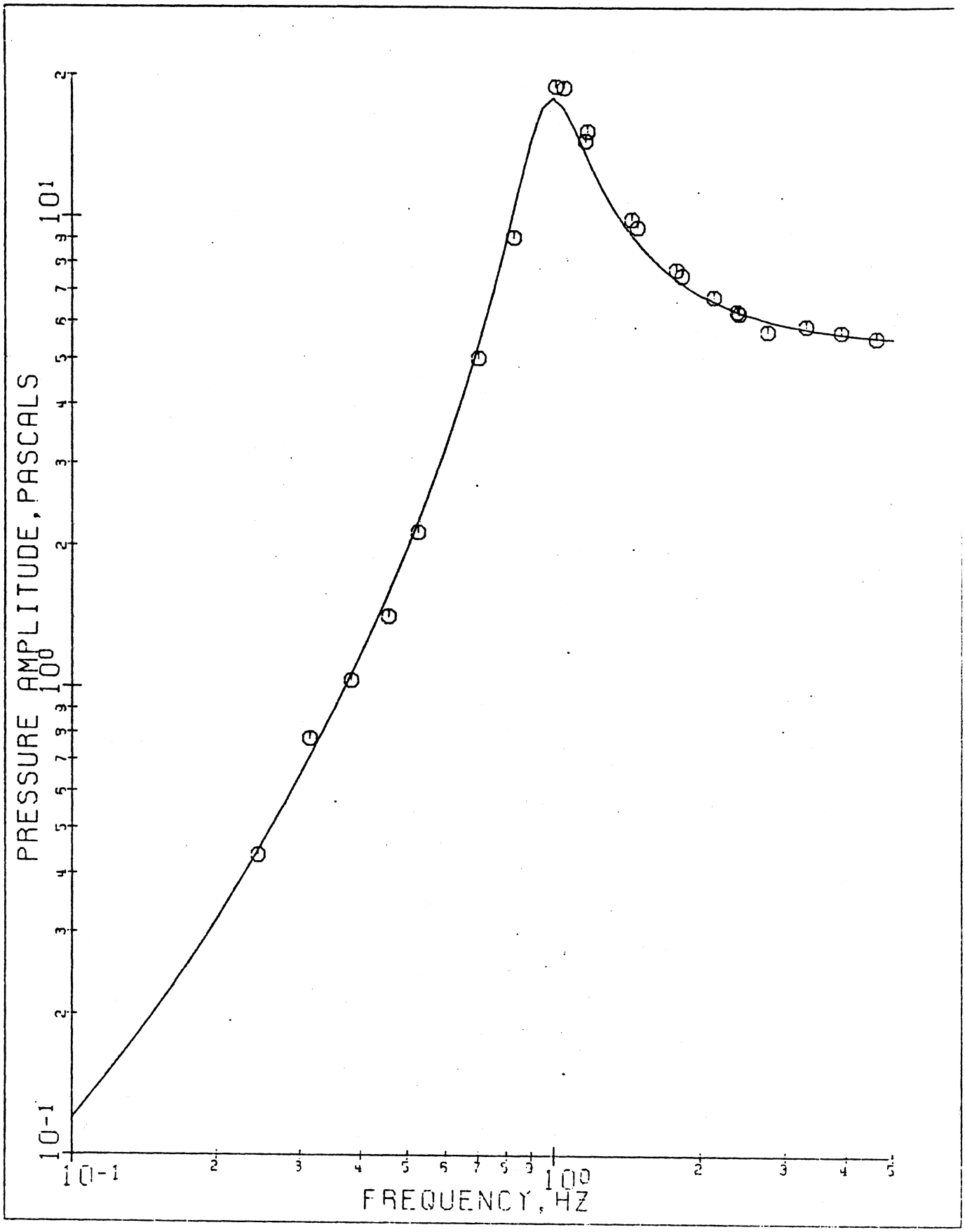

Figure 4-5. Results of inertance experiment on room 306C with 0.254 m (10 in) diameter and 2.336 m (7 ft 8 in) long pipe.

Chapter 5

EVALUATION AND CONCLUSIONS

The purpose of the research reported on here was to evaluate the proposed infrasonic measuring system, and compare it with the conventional blower system for measuring the air leakage of buildings. On the basis of the work done up to now the following evaluation can be made and conclusions drawn:

1. Accuracy: Up to this time the accuracy of the infrasonic measurements has not been very good. In most cases the blower results and the infrasonic results agree to within a factor of three. It is believed that improved equipment and procedures can reduce these discrepancies. An estimate of the accuracies that can be achieved ultimately can not yet be made.

2. Blower Test Accuracies: The results from the blower tests showed considerable scatter, so that at the low values of Δp sometimes used (1 Pascal) error of ± 25 per cent may have occurred. The worst scatter occurred on windy days.

3. Ease of Interpretation: The blower test results are easily and directly interpreted, whereas at present, interpretation of the infrasonic test results is more difficult. However, a more refined instrument could be designed to make the results more easily interpreted.

4. Limited Building Size: Because of the requirement that the building dimensions be small compared to the acoustic wavelength, the infrasonic method appears likely to be limited to use on buildings having linear dimensions of 30 meters (100 feet) or less. Larger buildings might be tested if they are relatively tight.

5. Equipment Size and Weight: At present the infrasonic equipment and the blower equipment are comparable in size. The infrasonic pump, weighing approximately 90 kg, can be reduced in weight by better design.

6. Ease of Use: One very important advantage of the infrasonic apparatus is that it is easier to use than a blower, since no through-the-wall blower vent or pressure taps are required. The set-up time of the infrasonic system is therefore much less than that of the blower system.

7. Equipment Cost: At present the infrasonic system is more costly than the blower system, and is likely to remain so. Accurate cost estimates have not been attempted.

8. Inertance Effects: The research has shown that wide cracks and open chimney or ventilator flues may have appreciable inertance. Inertance effects limit the use of the infrasonic apparatus to relatively low frequencies (a few Hertz). The presence of an overshoot in the frequency response curve due to inertance, however, may also indicate that the enclosure (house) under test has a large leak or an open flue. An important contribution of the research is the detailed theoretical analysis of the inertia effect of air flow through cracks.

9. Radiation: Analysis shows that the acoustic (infrasonic) power radiated during the infrasonic testing is negligible compared to the power dissipated by friction in the leaks.

10. Wall Movement: During an infrasonic test, slight wall movement is sometimes sensed. But there is no indication that wall movement adversely affects the infrasonic measurement for typical buildings.

11. Enclosure Contents: No experiments were conducted to determine if enclosure contents (furniture inside a house) has any effect on the infrasonic impedance. Effects, if any, are expected to be small.

12. Leakage Flow-versus-Δp Characteristics: The experiments were not sufficiently refined to show any deviation from the empirical relation $Q = K(\Delta p)^n$ for static pressure differences.

13. Man-made and Natural Interference: For both the blower tests and the infrasonic tests the predominant interference seemed to be due primarily to wind "noise" in the frequency range of interest (0.1 to 5 Hz). Barometric pressure fluctuations seemed to dominate the "d-c" interference. Our equipment was not sufficiently refined and our signal processing equipment was not sufficiently elaborate to detect infrasonic effects due to earth quakes, distant man-made events (rocket launches), or distant storms.

14. Synchronous Detector: An important contribution of the research was the development of an synchronous detector. Further analysis and development on it are required.

Appendix A

SYNCHRONOUS DETECTOR

A-1 Basic Principles

The output of the Fotonic Sensor may be regarded as a sinusoidal pressure signal mixed with noise. Because of the presence of noise along with the pressure signal and because of the small amplitude of the pressure signal an estimate of the magnitude of the pressure signal involves an unsatisfactorily large amount of guesswork when it is obtained from the strip-chart recorder readings. A much better way to obtain the pressure signal size would be to have a single instrument reading which in some way relates to the pressure signal amplitude.

It is not possible, however, simply to use an RMS voltmeter or a rectifier followed by a d-c voltmeter to obtain a meaningful reading. Although the noise has an average value of zero, it contributes a positive component to both the RMS and rectified values and thus distorts the readings. The synchronous detector, on the other hand, preserves the randomness of the noise by feeding the pressure signal through a double-pole double-throw (DPDT) switch which is controlled by another signal (called the control or carrier signal) of the same frequency as the pressure signal. The state of the control signal determines whether the switch output is the same as the input or is reversed in polarity. Ideally the average of the switch output depends only upon the pressure signal size and the phase difference between the pressure signal and the control.

When two detector circuits are used, having control signals phased 90° apart, both the amplitude and the phase shift in the pressure signal can be determined. If the phase shift of the pressure signal with respect to the control

is equal to ϕ, the pressure signal can be denoted as $V_r \sin(\omega_r t + \phi)$. The d-c average of the switch output voltage from the circuit having a control signal in phase with the pressure signal is then

$$V_a = \frac{1}{\pi} \int_o^{\pi} V_r \sin(\omega_r t + \phi)\, d(\omega_r t) = \frac{1}{\pi} (2V_r \cos\phi) \qquad \text{(A-1)}$$

while the average output of the circuit having a control shifted by 90° is

$$V_b = \frac{1}{\pi} \int_{\pi/2}^{3\pi/2} V_r \sin(\omega_r t + \phi)\, d(\omega_r t) = \frac{1}{\pi} (-2V_r \sin\phi) \qquad \text{(A-2)}$$

In both circuits, the noise, since it is assumed to be random, does not affect the average value provided that averaging over a long time is used. The readings obtained from the two circuits can then be used to find the amplitude of the pressure response, and also the phase shift of the pressure response with respect to the control. Combining Eqs. (A-1) and (A-2) yields

$$V_r = \frac{\pi}{2} \sqrt{V_a^2 + V_b^2} \qquad \text{(A-3)}$$

and

$$\phi = \tan^{-1} \left| \frac{V_b}{V_a} \right| \qquad \text{(A-4)}$$

Such a system was constructed and used.

A-2 Circuit Design

The analog electronic switch used for the synchronous detector is the National AH0014CD. A symbolic representation of this integrated circuit switch, along with the connections necessary to use it as a DPDT switch with a single control are shown in Fig. A-1. When the switch is used in the manner shown in Fig. A-1(c) the ground terminal at the output changes with each change in the

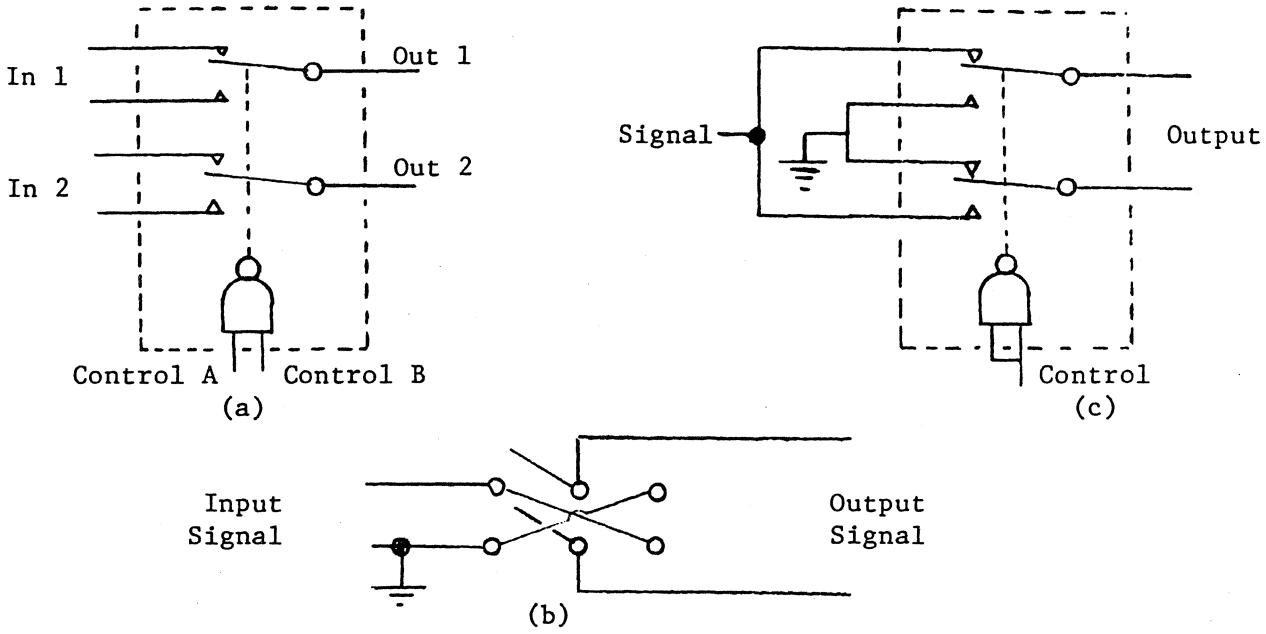

Figure A-1. National AH001HCD analog switch. (a) Simplified schematic. (b) Equivalent DPDT representation. (c) Connections to achieve DPDT bechaviors.

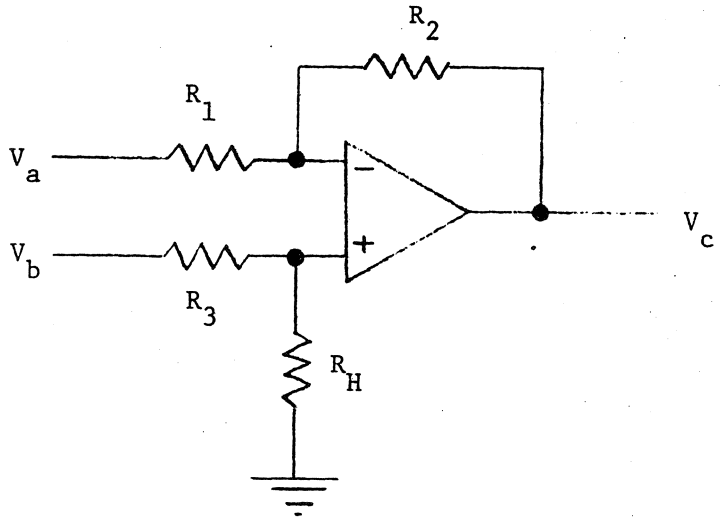

Fig. A-2. Differential amplifier circuit

control state, leaving no one output which can be read with respect to ground. This difficulty is overcome by following the switch with a differential amplifier, shown in Fig. A-2. When $R_1 = R_2$ and $R_3 = R_4$ in the DIFF AMP, the output is equal to the input at the amplifier's positive terminal minus the input at the negative terminal. That is, $V_c = V_a - V_b$; thus the output of the DIFF AMP, with respect to ground, is the required output voltage.

The square-wave control for the switches is obtained from photo detectors connected across the rim of a modified pulley on the pump shaft, made into a light chopper as shown in Fig. A-3. One half of the pulley's rim is high enough to block light transmission through the photo detectors, and the other half is low enough to allow the photo diodes to conduct. Detector A is positioned so that light transmission becomes blocked halfway through the piston's upstroke, while detector B is blocked beginning at bottom dead center. Since the output voltage of a photodetector when transmission is blocked is the higher voltage, the outputs of the detectors are square waves with the signal from detector A in phase with the piston, and the signal from detector B leading by 90°, as is shown in Fig. A-4.

Unfortunately, the signals from the photodetectors are not suitable for switching controls, since the low-voltage portions of the square waves are not at a low enough voltage level to control the AH001HCD electronic switch. To remedy this the photodetector outputs are fed into the positive inputs of operational amplifiers, having a fixed +2.1 volts d-c bias applied to the negative inputs. Using this arrangement the amplifier outputs are two sharply changing, symmetrical square waves which can be used as switch controls. The photodetector outputs, the signals from the OP AMPS, and the switching levels are shown in Fig. A-4 also

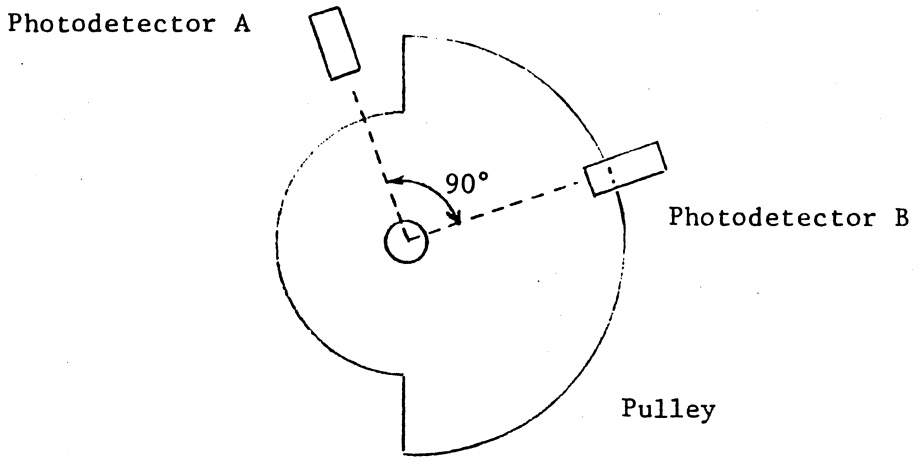

Figure A-3. Photodetector and light chopper made from the rim of a V-pulley.

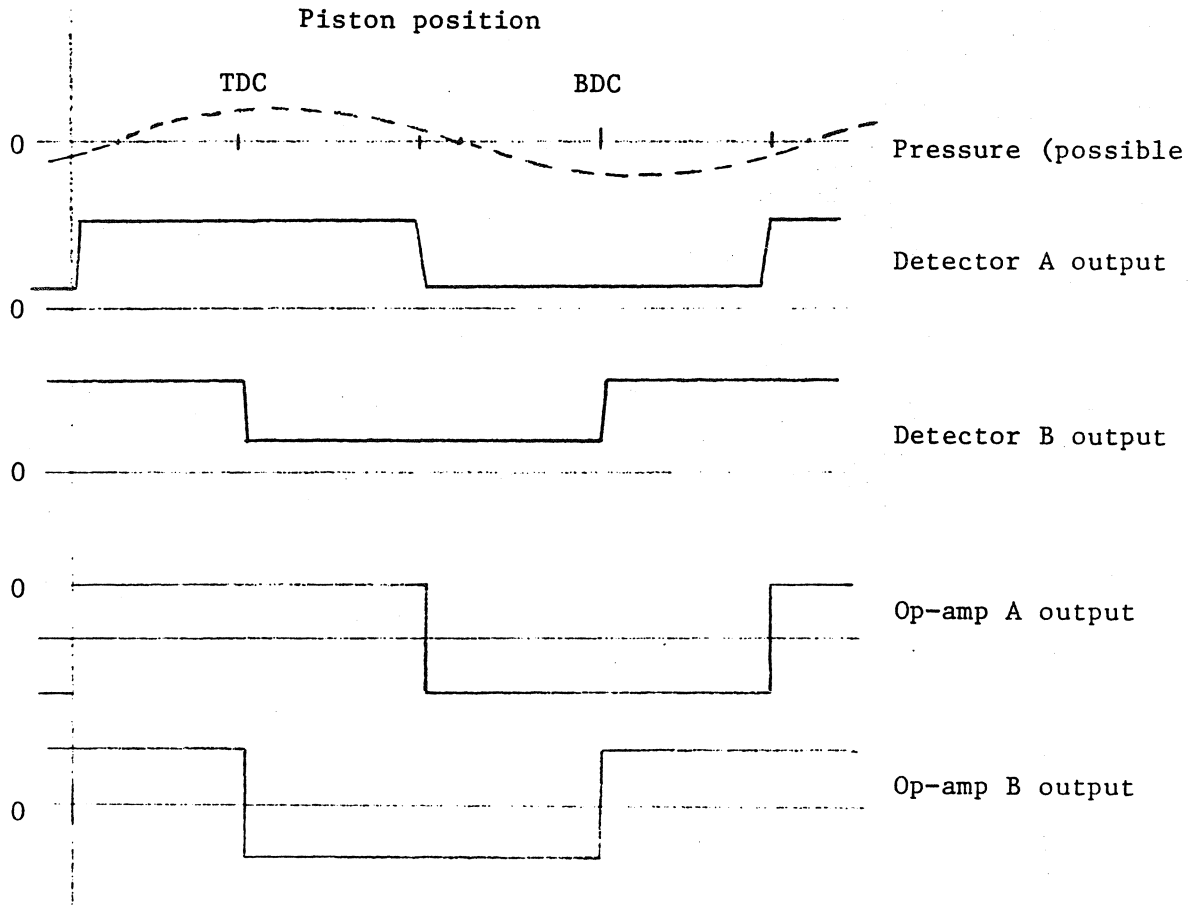

Figure A-4. Piston position, photodetector outpus, and control waveforms.

The final component of the synchronous detector is an RC low-pass filter, shown in Fig. A-5. This filter is necessary to stop voltmeter needls fluctuations when the signals from the DIFF AMPS are read. There are two main courses of the fluctuations: (1) For very-low-frequency test signals, below about 0.5 Hz, the needle is to some extent free to follow the sinusoidal variation in the signal. (2) The presence of electrical noise on the DIFF AMP output which, while leaving the signal average the same, can produce irregular movements about that average.

A-3 Response to Noise

To illustrate how the synchronous detector suppresses noise consider a system having a carrier frequency $f_c = \omega_c/2\pi$, and a sinusoidal signal of amplitude V_m in phase with the carrier.

$$v_s = V_m \cos \omega_c t$$

Clearly the average output is

$$v_o = \frac{2}{\pi} V_m$$

Now consider a representative noise voltage having the same amplitude as v_s but having a frequency

$$\omega_n = m\, \omega_c$$

where initially we assume m is an integer. For m = 2 the average output due to the noise is zero, and similarly for m = 4, 6, ...; that is, for all even integer values of m the output due to the noise is zero. By contrast, for m = 3 the average output due to the noise is one third of the output due to the signal, and similarly for m = 5, 7, ... etc the output due to the noise is 1/m of the output due to the signal. For non-integer values of m such as 5/2, 7/2,

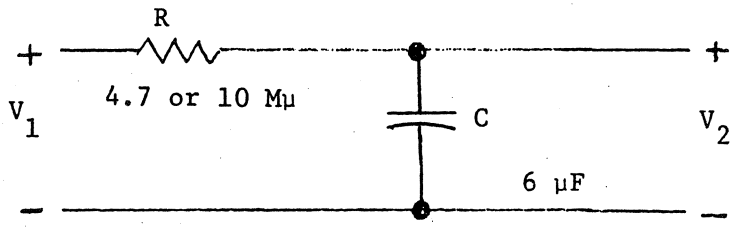

Fig. A-5. Low-pass filter. Since the Hewlett Packard 412A electronic voltmeter has an impedance of 200 MΩ the loading effect is very small.

etc intermediate values of output due to the noise are obtained. Thus, it appears that the average output due to noise voltages are attenuated by some characteristic which is bounded by $K\,|\omega_c/\omega_n|$ for $\omega_c < \omega_n$. A similar but more complicated argument shows that for noise lower in frequency than the carrier a corresponding result obtains, viz, that the lower the noise frequency the better the noise rejection. These results have been demonstrated experimentally also.

In summary, the synchronous detector as described provides at least two advantages over the strip-chart recorder as an output indicator: (1) the readings are obtained directly from indicating instruments (2) interfering signals are suppressed.

Appendix B

GENERAL ANALYSIS INCLUDING INERTANCE EFFECT [Ref.23]

B.1 Source Properties

The acoustical system associated with the infrasonic impedance method for air leakage measurement may be represented by a lumped-parameter acoustic network comprising capacitance, resistances, inertances and an excitation source. The excitation source, representing the pump, may be regarded as a constant-displacement variable-frequency volumetric current source. It provides a sinusoidally varying volumetric current in an enclosure by displacing the volume according to

$$\Delta V(t) = \Delta V_o \sin \omega t \tag{B.1}$$

so that the volumetric current q(t) is defined by

$$q(t) = \frac{d}{dt}(\Delta V) = \omega \Delta V_o \cos \omega t \tag{B.2}$$

where ΔV_o is the amplitude of volume displacement

ω is the operating frequency in radians/sec

and t is the time in seconds.

Notice that since the coefficient of cos ωt in Eq. (B.2) includes ω, the source amplitude varies linearly with frequency.

In the following sections the network representation is developed and the governing differential equation is derived, for an enclosure with a single leak. The network is generalized for a system with

several leaks. A rectangular geometry is chosen for the single leak because the natural cracks in the building can often be modeled by rectangular slits having large width-to-height ratios. The analysis will be restricted with respect to frequency range so that the lumped-parameter network representation is valid.

B.2 Volumetric Current Relationship

Consider an enclosure having a single leak to be a control volume in which the source provides a volumetric displacement according to Eq. (B.1). If a mass of air mdt (m being the instantaneous mass flow rate through the leak) is expelled through the leak in a small dt, then conservation of mass requires

$$(\rho + d\rho)(V + dV) + mdt = \rho V \tag{B.3}$$

where V and ρ are the instantaneous values of the enclosure volume and the density of the air in the enclosure respectively. Expanding the left side of Eq. (B.3), rearranging and neglecting the second order term, we get

$$\frac{V}{\rho}\frac{d\rho}{dt} + \frac{m}{\rho} = -\frac{dV}{dt} \tag{B.4}$$

In Eq. (B-4) the first term accounts for compressibility, the second for the leakage, and the right side for the source.

Next, assume that the air within the control volume behaves isentropically so that p/ρ^{γ} = constant. Taking the derivative with respect to time results in

$$\frac{d\rho}{dt} = \frac{\rho}{\gamma p}\frac{dp}{dt} \tag{B.5}$$

combining Eqs. (B.5) and (B.4) yields

$$\frac{V}{\gamma p}\frac{dp}{dt} + \frac{m}{\rho} = -\frac{dV}{dt} \tag{B.6}$$

Equation (B.6) is more convenient than Eq. (B.4) because pressure rather than density is the dependent variable.

In all cases of interest in the air leakage measurement of buildings, the source brings about very small changes (of the order of $1:10^4$) in the volume and pressure as compared to their mean values. Thus we can assume that the quantity $V/\gamma p$ is essentially constant at the value $V_o/\gamma p_o$, where V_o and p_o are the mean values of V and p. Thus, using

$$\frac{V_o}{\gamma p_o} = C$$

Eq. (B.6) becomes

$$C\frac{dp}{dt} + \frac{m}{\rho} = -\frac{dV}{dt} \tag{B.7}$$

Now, according to EFP (voltage-force-pressure) or impedence analogy [Ref.24 and 25] the acoustic capacitance of an enclosure is defined to relate changes in pressure to flow according to

$$\Delta p = \frac{1}{C}\int q_1(t)dt$$

or

$$q_1(t) = C\frac{d}{dt}\Delta p \tag{B.8}$$

where

$$\Delta p \equiv p - p_o.$$

Comparison of Eqs. (B.7) and (B.8) shows that the first term on left side is the volumetric current $q_1(t)$ through the capacitance C. Denoting m/ρ by $q_2(t)$, (the volumetric current through the leak) and knowing that

$$\frac{d}{dt}(V_o - V) = -\frac{dV}{dt} = \frac{d}{dt}\Delta V = \omega \Delta V_o \cos \omega t = q(t),$$

we can write Eq. (B.6) as

$$q_1(t) + q_2(t) = q(t) \qquad (B.9)$$

Eq. (B.9) implies that a source is connected across a two-branch network, one branch of which contains the enclosure capacitance, and the other branch carries a current $q_2(t)$ due to the presence of a leak impedance which is yet to be determined.

B.3 Impedance Parameters of the Leak Passage

In order to establish the individual elements in the leakage impedance branch, we will consider the special case of a rectangular cross section leak having its width across the flow large compared to thickness across the flow. We assume laminar flow inside the leak. The volume current through such a leak (Fig. B.1) assuming imcompressible flow, is given by

$$q_2(t) = 2 \int_o^h \frac{A}{2h} u(y,t) dy \qquad (B.10)$$

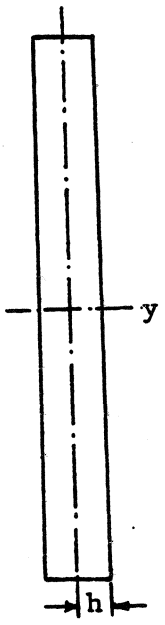

Fig. B-1. Leakage passage of rectangular geometry. Here w = 2h and A = wb = 2hb. The x-direction is into the page.

where h is the half of the slit thickness, A is the cross sectional area of the slit, y is the coordinate along the thickness, and u is the axial velocity.

The general equation of motion for one-dimensional imcompressible flow in the x direction, including the inertia effect due only to unsteadiness can be expressed as

$$\rho_o \frac{du(y,t)}{dt} = -\frac{dp}{dx} + \mu \frac{d^2u(y,t)}{dy^2} \tag{B.11}$$

where μ is the absolute viscosity of air and $\frac{dp}{dx}$ is the pressure gradient along the axial coordinate x.

We will seek a complex frequency response solution for Eq. (B.11) of the form

$$u(y,t) = U(y) \exp(j\omega t) \tag{B.12}$$

where ω is the frequency of oscillation and $U(y)$ is a function that may be a complex function of ω and y. It is understood that for calculation we would have to use

$$u(y,t) = \text{Real part of } [U(y) \exp.(j\omega t)]$$

Substituting the trial solution Eq. (B.12) into Eq. (B.11) yields

$$\rho_o j\omega U \exp(j\omega t) = -\frac{dp}{dx} + \mu \frac{d^2U}{dy^2} \cdot \exp(j\omega t)$$

Dividing both sides by $\mu \exp.(j\omega t)$, introducing kinematic voscosity $\nu \equiv \mu/\rho_o$ and transposing terms gives

$$\frac{d^2U}{dy^2} - \frac{j\omega}{\nu} U = \frac{\exp.(-j\omega t)}{\nu\rho_o} \frac{dp}{dx} \qquad \text{(B.13)}$$

The complete solution of Eq. (.13) is given by

$$U(y) = C_1 \exp(\sqrt{\frac{j\omega}{\nu}}\, y) + C_2 \exp(-\sqrt{\frac{j\omega}{\nu}}\, y) - \frac{\exp(-j\omega t)}{j\omega\rho_o} \frac{dp}{dx} \qquad \text{(B.14)}$$

where C_1 and C_2 are constants. Substituting U(y) in Eq. (B.12) yields

$$u(y,t) = \exp(j\omega t)\, [C_1 \exp(\sqrt{\frac{j\omega}{\nu}}\, y) + C_2 \exp(-\sqrt{\frac{j\omega}{\nu}}\, y) - \frac{1}{j\omega\rho_o} \frac{dp}{dx}] \qquad \text{(B.15)}$$

The boundary conditions to be satisfied by Eq. (B.15) are

$$u(h,t) = 0$$

and $$u(-h,t) = 0$$

Substituting these conditions in Eq. (B.15) we get the following values of C_1 and C_2,

$$C_1 = C_2 = \frac{1}{j\omega\rho_o} \frac{dp}{dx} \frac{\exp(-j\omega t)}{\exp(\sqrt{\frac{j\omega}{\nu}}\, h) + \exp(-\sqrt{\frac{j\omega}{\nu}}\, h)}$$

Substituting C_1 and C_2 in Eq. (B.15) and dividing both sides by

$-1/j\omega\rho_o$, we get

$$\frac{j\omega\, u(y,t)}{-\frac{1}{\rho_o}\frac{dp}{dx}} = 1 - \frac{\exp(\sqrt{\frac{j\omega}{\nu}}\, y) + \exp(-\sqrt{\frac{j\omega}{\nu}}\, y)}{\exp(\sqrt{\frac{j\omega}{\nu}}\, h) + \exp(-\sqrt{\frac{j\omega}{\nu}}\, h)} \tag{B.16}$$

It would be convenient to take

$$k \equiv h\sqrt{\frac{\omega}{\nu}}$$

So that

$$\frac{j\omega\, u(y,t)}{-\frac{1}{\rho_o}\frac{dp}{dx}} = 1 - \frac{\exp(\frac{ky}{h}\, j^{\frac{1}{2}}) + \exp(-\frac{ky}{h}\, j^{\frac{1}{2}})}{\exp(kj^{\frac{1}{2}}) + \exp(-kj^{\frac{1}{2}})} \tag{B.17}$$

Eq. (B.17) is interesting because it provides an expression for the velocity profile for any frequency of sinusoidal operation for the assumed leakage passage, which is a thin slit having thickness $2h$, in terms of the pressure gradient $\frac{dp}{dx}$. Note that the shape of the velocity profile depends on the frequency.

Eq. (B.17) is excessively complicated for most practical calculations, since the arguments of the exponential function are square roots of pure imaginary numbers. Let us examine the low frequency behavior of the right hand side of Eq. (B.17).

Expanding the exponential terms of Eq. (B.17) in series form and cancelling out terms, gives

$$\frac{j\omega\, u(y,t)}{-\frac{1}{\rho_o}\frac{dp}{dx}} = 1 - \frac{j(\frac{ky}{h})^2\frac{1}{2!} + j^2(\frac{ky}{h})^4\frac{1}{4!} + j^3(\frac{ky}{h})^6\frac{1}{6!} + \ldots}{1 + j\frac{k^2}{2!} + j^2\frac{k^4}{4!} + j^3\frac{k^6}{6!} + \ldots}$$

or

$$\frac{j\omega\, u(y,t)}{-\frac{1}{\rho_o}\frac{dp}{dx}} = \frac{j\frac{k^2}{2!}(1 - \frac{y^2}{h^2}) + j^2\frac{k^4}{4!}(1 - \frac{y^4}{h^4}) + j^3\frac{k^6}{6}(1 - \frac{y^6}{h^6}) + \ldots}{1 + j\frac{k^2}{2!} + j^2\frac{k^4}{4!} + j^3\frac{k^6}{6!} + \ldots}$$

Dividing both sides by j knowing that $j = \sqrt{-1}$, we get

$$\frac{\omega u(y,t)}{-\frac{1}{\rho_o}\frac{dp}{dx}} = \frac{N}{D} \qquad \text{(B.18)}$$

where $N \equiv [\frac{k^2}{2!}(1 - \frac{y^2}{h^2}) - \frac{k^6}{6!}(1 - \frac{y^6}{h^6}) + \frac{k^{10}}{10!}(1 - \frac{y^{10}}{h^{10}}) + \ldots.]$

$$+ j[\frac{k^4}{4!}(1 - \frac{y^4}{h^4}) - \frac{k^8}{8!}(1 - \frac{y^8}{h^8}) + \frac{k^{12}}{12!}(1 - \frac{y^{12}}{h^{12}}) - \ldots.]$$

and $D \equiv (1 - \frac{k^4}{4!} + \frac{k^8}{8!} - \ldots.) + j(\frac{k^2}{2!} - \frac{k^6}{6!} + \frac{k^{10}}{10!} - \ldots.)$

For very low frequencies i.e., 10 Hz and below, we will neglect k with fourth and higher powers. We can justify this approximation with the help of the following example:

Example:

The maximum value of frequency of the sinusoidal volumetric current used is about 10 Hz. So let us take $f = 10$ Hz, so that $\omega = 62.83$ radians/

sec. A typical crack of width .02" will have

$$h = .01 \text{ in.} = 2.54 \times 10^{-4}$$

Now $k \equiv h\sqrt{\frac{\omega}{\nu}}$

For air $\nu = 1.074 \times 10^{-5}$

Therefore $k = 2.54 \times 10^{-4} \times \sqrt{\frac{62.83}{1.074 \times 10^{-5}}}$

$$= 0.0142$$

so that we have $k^2 = 0.372 \times 10^{-4}$, $k^4 = 0.1423 \times 10^{-7}$, $k^6 = 0.537$

We therefore find that k^6, k^{10} and higher powers of k may be neglected as compared to k^2 in the real part of N and also k^4, k^8 etc., may be neglected as compared to 1 in the real part of D. Also, in the imaginary parts of N and D, the first terms will be retained and the rest of them would be neglected. Therefore, the expressions of N and D become

$$N = \frac{k^2}{2!}\left(1 - \frac{y^2}{h^2}\right) + j\,\frac{k^4}{4!}\left(1 - \frac{y^4}{h^4}\right)$$

and $$D = 1 + j\,\frac{k^2}{2!}\,.$$

Substituting N and D back in Eq. (B.18) gives

$$u(y,t) = -\frac{k^2}{2\omega\rho_o}\frac{dp}{dx}\,\frac{\left(1 - \frac{y^2}{h^2}\right) + j\frac{k^2}{12}\left(1 - \frac{y^4}{h^4}\right)}{1 + j\frac{k^2}{2}} \qquad \text{(B.19)}$$

To evaluate volumetric current $q_2(t)$, we substitute $u(y,t)$ from Eq.

(B.19) in (B.10),

$$q_2(t) = -\frac{A}{h}\frac{k^2}{2\omega\rho_o}\frac{dp}{dx}\int_o^h \frac{(1-\frac{y^2}{h^2}) + j\frac{k^2}{12}(1-\frac{y^4}{h^4})}{1+\frac{k^2}{2}}\,dy$$

or, $$q_2(t) = -\frac{Ak^2}{2\omega h\rho_o}\frac{dp}{dx}\,\frac{\frac{2}{3}h + j\frac{k^2}{12}\cdot\frac{4}{5}h}{1+j\frac{k^2}{2}} \qquad (B.20)$$

Eq. (B.20) therefore gives the complex volumetric current through the leak passage.

In order to establish the impedance, let us consider ℓ to be the length of leak. Then dp/dx can be replaced by $\Delta p/\ell$. Thus for a pressure drop along the slit varying sinusoidally with time,

$$\Delta p = \Delta p_o\, e^{j\omega t}$$

the resulting flow will be

$$q_2(t) = -\frac{Ah^2}{3\rho_o\nu}\,\frac{1+j\frac{k2}{10}}{1+j\frac{k2}{2}}\,\frac{\Delta p_o}{\ell}\,e^{j\omega t} \qquad (B.21)$$

According to EFP analogy

$$\text{Real part of } [q_2(t)] = \text{Real part of } [\frac{\Delta p_o}{Z_\ell}\, e^{j\omega t}]$$

Consequently,

$$Z_\ell = \frac{3\rho_o\nu\ell}{Ah^2}\,\frac{1+j\frac{k^2}{2}}{1+j\frac{k^2}{10}}$$

Multiplying and dividing the right side by the complex conjugate of $1 + j\frac{k^2}{10}$ gives

$$Z_\ell = \frac{3\rho_o \nu \ell}{Ah^2} \frac{(1 + \frac{k^4}{20}) + j\frac{2k^2}{5}}{1 + \frac{k^4}{100}}$$

Now, since $k^4/20$ and $k^4/100$ are very small as compared to 1 for thin slits, we have

$$Z_\ell = \frac{3\mu\ell}{Ah^2} + j\omega(\frac{6}{5}\frac{\rho_o \ell}{A}) \qquad (B.22)$$

Now, we already know that the real part of Z_ℓ is the leak resistance R_ℓ and that its imaginary part is the acoustical reactance X_ℓ

Therefore, $R_\ell = \frac{3\mu\ell}{Ah^2}$ (B.22a)

and $X_\ell = \omega(\frac{6}{5}\frac{\rho_o \ell}{A}) = \omega L_\ell$

So that, $L_\ell = \frac{6}{5}\frac{\rho_o \ell}{A}$ (B.22b)

L_ℓ is known as the acoustical inertance of the leak, there being no capacit in the reactance part X_ℓ. Eqs. (B.22), (B.22a and (B.226), therefore imply that the impedance offered by the slit in a series combination of the resistance R_ℓ and the inertance L_ℓ.

The reason for deriving expressions for R_ℓ and X_ℓ for a narrow slit (h very small) is to demonstrate that within the operating range of frequencies, the inertance is very small as compared to the resistance.

To show this let us consider the slit dimension as in the previous example and evaluate the ratio X_ℓ/R_ℓ at $\omega = 62.83$ radians/sec (10 Hz). From Eq. (B.2a) and (B.2b) we have,

$$\frac{X_\ell}{R_\ell} = \frac{2\omega h^2}{5\nu}$$

$$= \frac{2 \times 62.83 \times (2.54 \times 10^{-4})^2}{5 \times 1.074 \times 10^{-5}}$$

$$= 1.74 \times 0.151$$

Therefore we may neglect the leak inertance for the cracks (0.02 in. thick) within the operating range of frequencies of interest in this investigation.

A similar analysis for a circular leak (a pipe) gives the same impedance elements, i.e., R_ℓ and X_ℓ, whose expression are given in Ref. 2.4 by

$$Z_\ell = \frac{32\mu\ell}{Ad^2} + j\omega\left(\frac{4}{3}\frac{\rho_o \ell}{A}\right) \tag{3.23}$$

so that

$$R_\ell \equiv \frac{32\mu\ell}{Ad^2} \tag{3.23a}$$

$$L_\ell = \frac{4}{3}\frac{\rho_o \ell}{A} \tag{3.23b}$$

For the inertance experiments carried out (See Chapter 40) with a 0.254 m (10 in) diameter pipe, the ratio X_ℓ/R_ℓ at frequency of 10 Hz is given by

$$\frac{X_\ell}{R_\ell} = \frac{\omega d^2}{24\nu}$$

$$= \frac{62.83 \times (0.254)^2}{24 \times 1.074 \times 10^{-5}}$$

$$= 0.15723$$

Since X_ℓ is about 11 percent of R_ℓ and therefore it cannot be neglected as compared to R_ℓ.

On the basis of the examples given above, we therefore conclude that for ordinary cracks in buildings, the acoustical inertance would have negligible effect on the frequency-response curve, whereas for a large diameter pipe functioning as a leak, it should have a very significant effect on the response curve.

B.4 Radiation Impedance

Energy loss in the acoustical system can also occur due to radiation impedance at the leak opening. The inside excess pressure alternately goes positive and negative in a sinusoidal fashion, while the outside excess pressure will not be constantly zero because of radiation of energy at the opening.

Expressions and computed curves for radiation impedance for circular and rectangular pistons are provided in Ref. 26 and 27. These results can also be used for a vibrating layer of air if all its parts remain in phase. The radiation resistance R_r for a circular piston mounted in an infinite baffle is given by

$$R_r = \frac{\rho_o}{\pi a^2} R_1(2k_1 a) \qquad \text{(B.24a)}$$

and radiation reactance X_r is given by

$$X_r = \frac{\rho_o c}{\pi a^2} X_1(2k_1 a) \qquad \text{(B.24b)}$$

where a is the radius of the piston, c is the velocity of sound in air, and $k_1 = \omega/c = 2\pi/\lambda$, where λ is the wave length and $R_1(2k_1 a)$

are the two impedance functions defined by

$$R_1(2k,a) = -\frac{(2k_1a)^2}{2.4} - \frac{(2k_1a)^2}{2.4^2.6} + \frac{(2k_1a)^6}{2.4^2.6^2.8} - \cdots\cdots$$

and

$$X_1(2k,a) = \frac{4}{\pi}\left[\frac{2k_1a}{3} - \frac{(2k_1a)}{3^2.5} + \frac{(2k_1a)^5}{3^2.5^2.7} - \cdots\cdots\right]$$

At very low frequencies $2k_1a \ll 1$, so that only the first term in the expression of $R_1(2k_1a)$ and $X_1(2k_1a)$ will be retained, that is they may be approximated by

$$R_r = \frac{\rho_o\omega^2}{2\pi c}$$

or $$R_r = \omega^2 S \qquad \text{(B.25a)}$$

where $$S \equiv \frac{\rho_o}{2\pi c}$$

and $$X_r = \omega \cdot \frac{8\rho_o}{3\pi^2 a}$$

or, $$X_r = \omega L_r$$

where $$L_r \equiv \frac{8\rho_o}{3\pi^2 a} \qquad \text{(B.25b)}$$

For a rectangular piston membrane, the expression for R_r and X_r are the same as given by Eq (B.24a and b), "a" being a side of the rectangle. The functions $R_1(2k_1a)$ and $X_1(2k_1a)$ are plotted in Ref.26 pp. 196, against ka with ratio of sides a/b as the parameter. It is found that these functions have very small values at the low frequencies.

The radiation of energy, therefore, adds an impedance Z_r in series with the leak passage impedance. The overall leak impedance Z is the

sum of Z_ℓ and Z_r as

$$Z = Z_\ell + Z_r$$

or $$Z = (R_\ell + j\omega L_\ell) + (R_r + j\omega L_r)$$

or $$Z = (R_\ell + R_r) + j\omega(L_\ell + L_r)$$

or $$Z = R + j\omega L$$

where R and L are the overall resistance and inertance respectively. For a circular leak, R and L may be obtained by adding Eq. (B.23a) to (B.25a), and Eq. (B.23b) to (B.25b), respectively. That is

$$R = R_\ell + S\omega^2$$

or $$R = \frac{32\mu\ell}{Ad^2} + \frac{\rho_o\omega^2}{2\pi c} \qquad \text{(B.26a)}$$

and $$L = L_\ell + L_r$$

or, $$L = \frac{4}{3}\frac{\rho_o\ell}{A} + \frac{8\rho_o}{3\pi^2 a} \qquad \text{(B.26b)}$$

B.5 Network for an Enclosure with Several Leaks

It has been shown (above) by an example for a typical size rectangular crack that the leak inertance is very small as compared to its resistance. Therefore the network for an e closure with small size cracks can be developed by finding the equivalent resistance of all the separate leaks connected in parallel. The resultant network (Fig. B.2) is therefore a capacitance in parallel with a resistance and excited by a volumetric current source in parallel.

For an enclosure with a single large leak (e.g., a pipe) and several

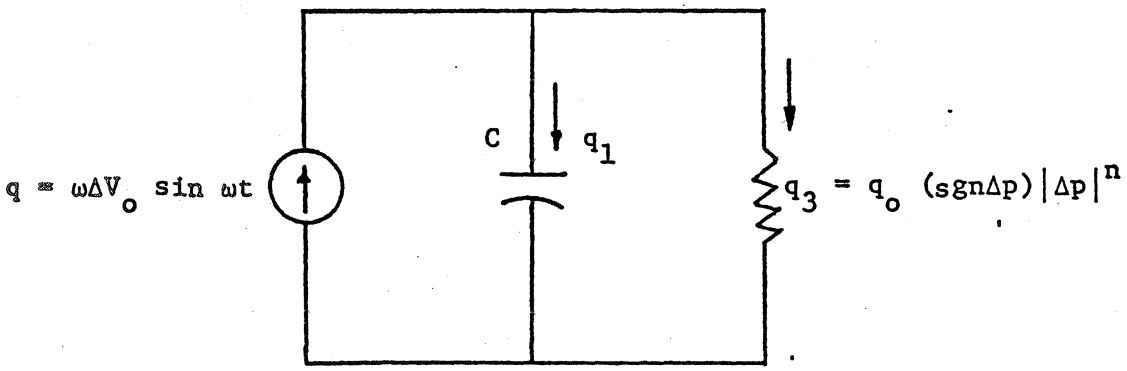

Fig. B.2. Equivalent network for an enclosure with small cracks.

small cracks, the large leak is represented by a resistance and inertance in one branch and a parallel branch of pure resistance for the small cracks. The network is shown in Fig. (B.3). If the pure resistance in this network permits a very small current as compared to that through the impedance of the large leak, we can simplify the network by eliminating this resistance. The resulting network is shown in Fig. (B.4).

B.6 Differential Equations

Let us consider first the network shown in Fig. (B.2).

The volumetric currents through different branches are given by

$$q_1(t) = C \frac{d\Delta p}{dt} \tag{B.27a}$$

where $\Delta p = p - p_o$

and $$\Delta p = L \frac{dq_2(t)}{dt} + Rq_2(t) \tag{B.27b}$$

Also, $$q_3 = q_o(\text{sgn}\Delta p)\left|\Delta p(t)\right|^n \tag{B.27c}$$

where q_o is the volumetric current at $\Delta p = 1$, $(\text{sgn}\Delta p)$ is the sign of Δp, and n is a constant for the nonlinear resistance.

The sum of instantaneous currents in different branches is equal to the instantaneous current from the source, that is,

$$q_1(t) + q_2(t) + q_3(t) = \omega\Delta V_o \sin \omega t$$

or $$q_2(t) = \omega\Delta V_o \sin \omega t - q_1(t) - q_3(t) \tag{B.28}$$

Substituting $q_2(t)$ from Eq. (B.28) in Eq. (B.27), we get

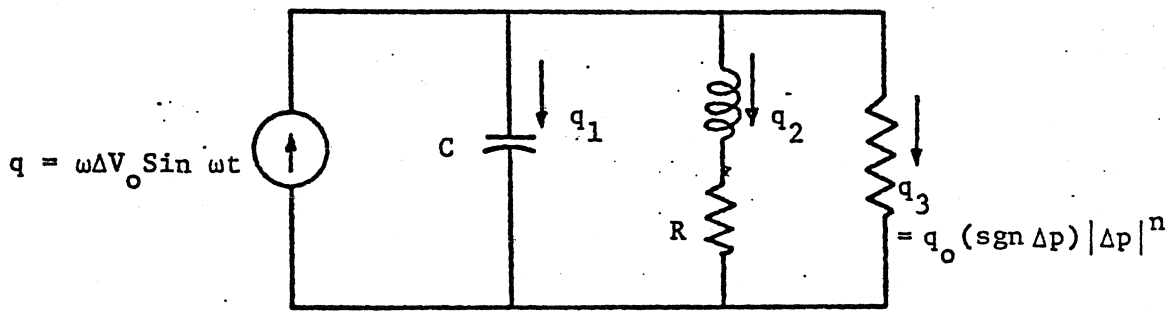

Fig. B.3. Equivalent network for an enclosure with small cracks and a single large leak.

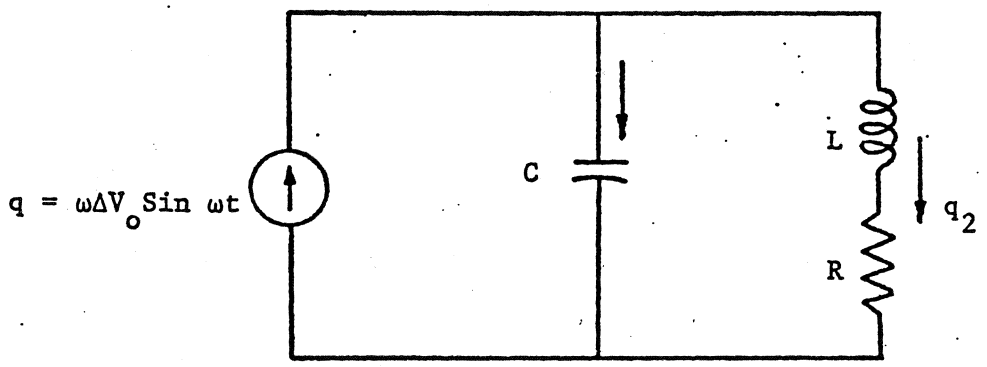

Fig. B.4. Equivalent network for an enclosure a single large leak.

$$\Delta p = L \frac{d}{dt} [\omega \Delta V_o \sin \omega t - q_1(t) - q_3(t)]$$

$$+ R[\omega \Delta V_o \sin \omega t - q_1(t) - q_3(t)]$$

Substituting $q_1(t)$ and $q_3(t)$ from Eq. (B.27a) and (B.27b), rearranging and simplifying gives

$$\frac{d^2 \Delta p}{d^2} + \left(\frac{q_o n}{C} |\Delta p|^{n-1} + \frac{R}{L}\right) \frac{d\Delta p}{dt} + \frac{R q_o}{LC} (\text{sgn} \Delta p) |\Delta p|^n$$

$$+ \frac{1}{LC} \Delta p = \frac{\omega \Delta V_o}{LC} (R \sin \omega t + \omega L \cos \omega t) \qquad \text{(B.29)}$$

Eq. (B.29) is a nonlinear differential equation for the network in Fig. (B.2). The solution for a linear resistance with $n = 1$ is given in Chapter 2.

For the network in Fig. (B.2) we can derive the differential equation by a similar procedure as above. The resulting equation is

$$\frac{d\Delta p}{dt} + \frac{q_o}{C} (\text{sgn } \Delta p) |\Delta p(t)|^n = \frac{\omega \Delta V_o}{C} \sin \omega t \qquad \text{(B.30)}$$

A numerical solution of Eq. (B.30) is given in Ref. 22. An approximate analytical expression for the particular solution of Eq. (B.30) is also given in Chapter 2.

Appendix C

SOLUTIONS OF PERTINENT DIFFERENTIAL EQUATIONS

C.1 Frequency Response Solution of Eq. (2.29) for n = 1

For n = 1, Eq. (B.29) reduces to

$$\frac{d^2\Delta p}{dt^2} + \left(\frac{q_o}{C} + \frac{R}{L}\right)\frac{d\Delta p}{dt} + \left(\frac{Rq_o}{LC} \quad \frac{1}{LC}\right)\Delta p = \frac{\omega\Delta V_o}{LC}(R \sin \omega t + \omega L \cos \omega t) \qquad (C.1)$$

To obtain a frequency response solution, we are interested in the particular solution of Eq. (C.1) which is given by

$$\Delta p_{P-I} = \Delta p_m \, \mathrm{Sin}(\omega t + \phi) \qquad (C.2)$$

where Δp_m is the pressure amplitude given by

$$\Delta p_m = V_o \left[\frac{R^2 + \omega^2 L^2}{(1 + Rq_o - \omega^2 LC)^2 + \omega^2(RC + Lq_o)^2}\right]^{\frac{1}{2}} \qquad (C.3)$$

and ϕ is the phase angle given by

$$\phi = \tan^{-1} \frac{L(1 - \omega^2 LC) - \omega R^2 C}{q_o(R^2 + \omega^2 L^2)} \qquad (C.4)$$

Eq. (C.3) is therefore the desired frequency response solution for the network in Fig. (B.3b).

C.2 Frequency Response Solution for Network in Fig. (3.1)

Fig. (B.4) shows the network representing the enclosure for inertance experiments described in Chapter 4. The differential equation is the same as Eq. (C.1) with $q_o = 0$. Therefore the frequency response solution is given by

$$\Delta p_m = \omega\Delta V_o \left[\frac{R^2 + \omega^2 L^2}{(1 - \omega^2 LC)^2 + \omega^2 R^2 C^2}\right]^{\frac{1}{2}} \qquad (C.5)$$

Eq. (C.5) is therefore the response solution for the system which does not have the non-linear leak resistance.

C.3 Numerical Solution and an Approximate Analytical Expression for the Frequency-Response Characteristics of Eq. (3.30)

Repeating Eq. (3.30) for convenience of the reader

$$\frac{d\Delta p}{dt} + \frac{q_o}{C}(\text{Sgn } \Delta p)\left|\Delta p(t)\right|^n = \frac{\omega \Delta V_o}{C}\text{Sin } \omega t \qquad (C.6)$$

Eq. (C.6) which would have a periodic steady state solution was solved as an initial-valued-problem by the fourth order Runge Kutta formula. It was found that the transient solution has almost decayed before the fifth cycle. The amplitude of the fifth cycle was therefore taken to be the steady state response at the particular frequency. The values of parameters used for solving Eq. (C.6) were n = 0.5, q_o = 1, C = 1 and ΔV_o = 0.11044. The frequency response characteristics in the frequency range of interest is shown by circled points in Fig. (C.1). The APL computer program is given in Appendix D.

An analytical expression for the frequency-response solution has been developed based on the following lines. At very low frequencies, the capacitive reactance $1/\omega C$ is very large as compared to resistance, thus allowing us to neglect the term $Cd\Delta p/dt$ as compared to $q_o(\text{sgn } \Delta p)\left|\Delta p(t)\right|^n$. Therefore at very low frequencies, the pressure response Δp_m can be taken as equal to

$$\Delta p_m^1 = \left(\frac{\omega \Delta V_o}{q_o}\right)^{1/n} \qquad (C.7)$$

In the high end of the frequency range, the capacitive reactance is very small as compared to the resistance, and therefore can be neglected. The response in this case can be taken as

$$\Delta p_m^{II} = \frac{\Delta V_o}{C} \tag{C.8}$$

The analytical expression thus has to satisfy Eq. (C.7) and (C.8) and together with that it should reduce to the exact solution at n = 1 given by

$$\Delta p_m^{III} = \frac{\omega \Delta V_o}{(q_o^2 + \omega^2 C^2)^{\frac{1}{2}}} \tag{C.9}$$

Let us consider the expression

$$\Delta p_m = \frac{P^*}{\left[\left(\frac{q_o}{\omega \Delta V_o}\right)^{2/n} + \left(\frac{CP^*}{\Delta V_o}\right)^2\right]^{\frac{1}{2}}} \tag{C.10}$$

where P* is a factor (having the same units as pressure) introduced to achieve dimensional homogeneity of Eq. (C.10). Taking the magnitude of P* as 1 we get

$$\Delta p_m = \frac{1}{\left[\left(\frac{q_o}{\omega \Delta V_o}\right)^{2/n} + \left(\frac{C}{\Delta V_o}\right)^2\right]^{\frac{1}{2}}}$$

or,

$$\Delta p_m = \frac{(\omega \Delta V_o)^{1/n}}{\left[q_o^{2/n} + \left(\frac{C}{\Delta V_o}\right)^2 (\omega \Delta V_o)^{2/n}\right]^{\frac{1}{2}}} \tag{C.11}$$

It may be noted that all the three conditions imposed by Eqs. (C.7), (C.8) and (C.9) are satisfied by Eq. (C.11). We therefore have this equation

as an approximate analytical expression for the frequency-response solution of the non-linear differential equation (C.6).

The comparison of Eq. (C.11) with a numerical solution shows that an agreement is quite close, though a deviation in the intermediate frequency range is observed.

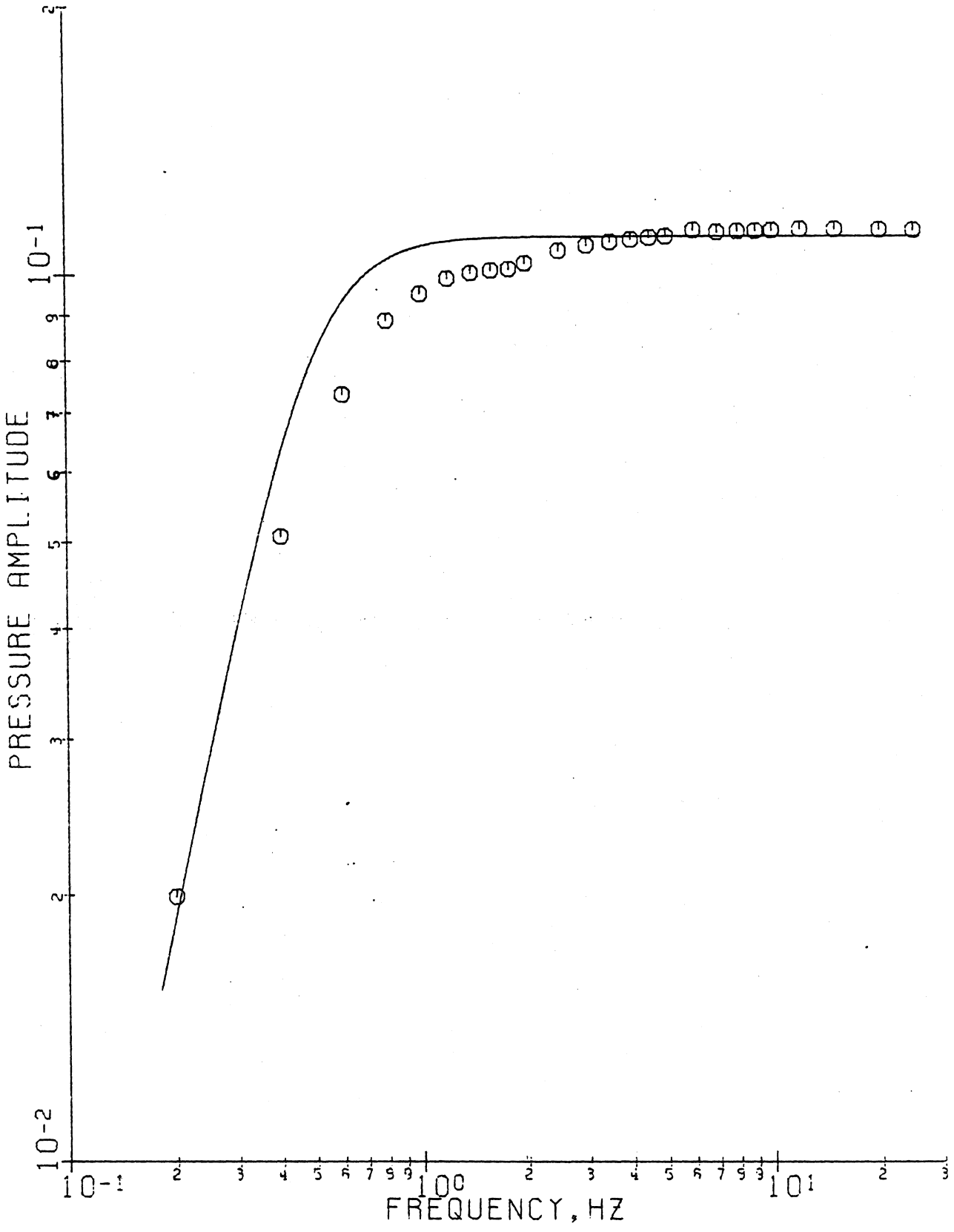

Fig. C.1. Circled points show numerical solution of Eq. C.6 and solid line represents Eq. C.11 for n = 0.5, q_o = 1. C = 1 and ΔV_o = 0.11044.

Appendix D
APL COMPUTER PROGRAMS

D.1 APL function for curve fitting of inertance experiment data.

```
      ∇LST[□]∇
    ∇ LST X;W;E;FL;FC;FR;FE;M;N;N;I;Q
[1]   CT←0
[2]   W←(○2×F)*2
[3]   T←W×(0.11044÷F)*2
[4]  L1:L←X[1]+0×C←X[2]+0×⍴R←X[3]+W×X[4]
[5]   E←((((1-W×L×C)*2)+W×(R×C)*2)÷Q←(R*2)+W×L*2)
[6]   FL←2×W×((W×L×L×C)-(R×R×C)+L)÷Q*2
[7]   FC←2×W×C-L÷Q
[8]   FR←2×R×((2×W×L×C)-1)÷Q*2
[9]   FE←W×FR
[10]  M←+/[1]((1 3 2)⍉M)×M←(3 2 1)⍉(4,4,⍴W)⍴(N⍴FL),(N⍴FC),(N⍴FR),(N←4×⍴W
[11]  N←(+/I×FL),(+/I×FC),(+/I×FR),+/FE×I←T-E
[12]  X←(X←X)+N⌹M
[13]  →L2×⍳10<CT←CT+1
[14]  →L1×⍳∨/(|(X-X)÷X)>0.0001
[15]  'INERTANCE:                '⍪X[1]⍪'
      '
[16]  'CAPACITANCE:              '⍪X[2]⍪'
      '
[17]  'RESISTANCE PARAMETERS:    '⍪X[3 4]⍪'
      '
[18]  →0
[19] L2:'FAILS TO CONVERGE AFTER 10 ITERATIONS'
    ∇
```

D.2 APL function for curve fitting of infrasonic experiment data.

```
      ∇LSS[□]∇
    ∇ LSS X;W;E;Q;FN;FK;FC;T;I;M;N;N;V
[1]   CT←0
[2]   V←(W←○2×F)×VO
[3]   T←1÷F*2
[4]  L1:E←(Q←(X[2]÷V)*2÷X[1])+(X[3]÷VO)*2
[5]   FN←-(2÷X[1]*2)×Q×⍟X[2]÷V
[6]   FK←Q×2÷×/X[1 2]
[7]   FC←2×X[3]÷VO*2
[8]   M←+/[1]((1 3 2)⍉M)×M←(3 2 1)⍉(3,3,⍴W)⍴(N⍴FN),(N⍴FK),(N←3×⍴W)⍴FC
[9]   N←(+/I×FN),(+/I×FK),+/FC×I←T-E
[10]  X←(X←X)+N⌹M
[11]  →L2×⍳10<CT←CT+1
[12]  →L1×⍳∨/(|(X-X)÷X)>0.001
[13]  'EXPONENT N:               '⍪X[1]⍪'
      '
[14]  'COEFFECIENT K:            '⍪X[2]⍪'
      '
[15]  'CAPACITANCE C:            '⍪X[3]⍪'
      '
[16]  →0
[17] L2:'FAILS TO CONVERGE AFTER 10 ITERATIONS'
    ∇
```

D.3 APL function for curve fitting of blower test data.

```
      ∇LBS[□]∇
    ∇ LBS X;E;QK;QN;M;N;T;N
[1]   CT←0
[2]  L1:E←X[2]×QK←P*X[1]
[3]   QN←E×⍟P
[4]   M←+/[1]((1 3 2)⍉M)×M←(3 2 1)⍉(2,2,⍴P)⍴(N⍴QN),(N←2×⍴P)⍴QK
[5]   N←(+/T×QN),+/QK×T←Q-E
[6]   X←(X←X)+N⌹M
[7]   →L2×ι10<CT←CT+1
[8]   →L1×ι∨/(|(X-X)÷X)>0.001
[9]   'EXPONENT N           ';X[1];'
      '
[10]  'COEFFECIENT K        ';X[2];'
      '
[11]  →0
[12] L2:'FAILS TO CONVERGE AFTER 10 ITERATIONS'
    ∇
```

D.4 APL function for finding frequency-response solution of Eq. (C.6) by Runge-Kutta method.

```
      ∇RUNK[□]∇
    ∇ Z←A RUNK X;K1;K2;K3;K4
[1]   A←(N←A[1]),(L←A[2]),H←A[3]
[2]   Z←X1←X
[3]  L1:K4←H×FUNC X+H,K3←H×FUNC X+0.5×H,K2←H×FUNC X+0.5×H,K1←H×FUNC X
[4]   Z←Z,X←X+H,(K1+K4+2×K2+K3)÷6
[5]   →L1×ι(L)>X[1]
[6]   Z←((1+(L-X1[1])÷H),N+1)⍴Z
    ∇


      ∇FUNC[□]∇
    ∇ Z←FUNC X;W
[1]   Z←(W×0.11044×1⊙X[1])×W←⊙2×F)-(X[2]÷|X[2])×(|X[2])*0.5
    ∇


      ∇DD[□]∇
    ∇ Z←DD F;A
[1]   A←1,(5÷F),1÷12×F
[2]   Z←(⌈/Z)-L/Z←¯11↑,⍉A RUNK 0 0
    ∇
```

Appendix E

EQUIPMENT LIST

1. Fotonic Sensor MTI Model KD-38
   Mechanical Technology Incorporated
   968 Albany-Shaker Rd. Latham, NY 12110

2. Two channel high speed recorder
   Bulton techni-rite electronics Model TR-722

3. DC Generator (used as shunt motor)
   Westinghouse type FK Frame D185
   style 1172247-B 40 Volts 2000 RPM 15 A

4. Speed reduction gearbox
   Ohio Gear Co. #8HU- 5 1/6 C
   reduction ratio 5 1/6 to 1

5. Crank mechanism
   3 H.P. lawnmower engine
   stroke 1.5 inches T.D.C. to B.D.C.

6. Pump diaphragm
   1/32 inch gum rubber or 1/16 inch gum rubber

7. Pickup diaphragm
   Saran wrap plastic film thickness = 1×10^{-5} m (.4 mils)

8. Belt ratios- variable by pulley changes in series with 5 1/6 to 1 gear reduction, 1.3 to 1, 2.8 to 1, 4.1 to 1, 5.4 to 1

9. Manometers: Dwyer
   model 115 -0.05 to 0 to 0.25 inches (0.005 inch div)
   " 100/5 -0.1 to 0 to 1.0 inches (0.01 inch div)
   " 109 -0.2 to 0 to 3.0 inches (0.02 inch div)

10. Nozzles
    Go-Power Systems
    1880 Embarcadero Rd
    Palo Alto, CA 94303
    Model 46108 nozzles
    Sizes 4.5 inch, 2.75 inch, 1.75 inch, 1.183 inch, 0.75 inch

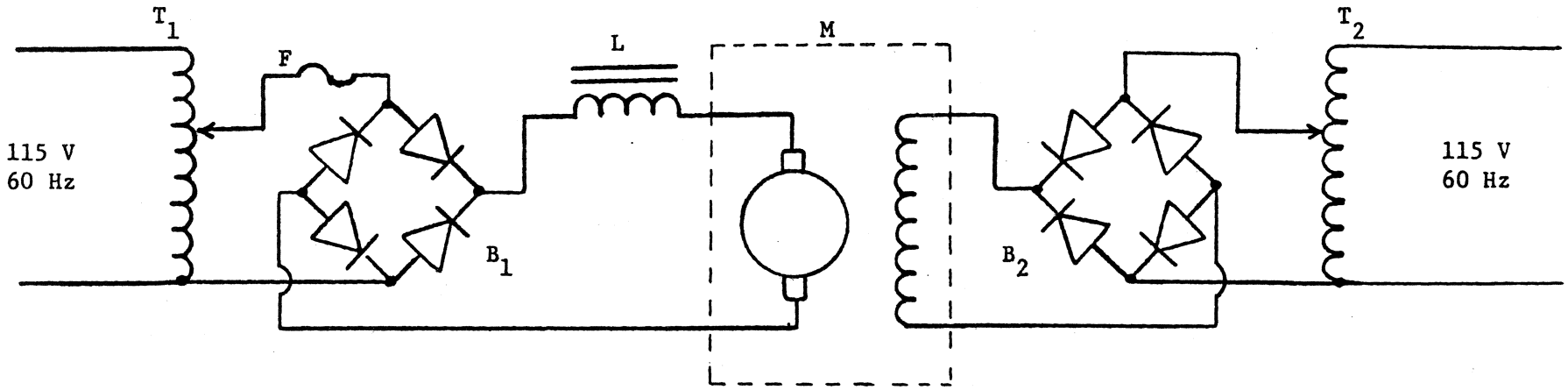

T_1 10 Amp Variac

T_2 5 Amp Variac

F 10 Amp Fuse

B_1 10 Amp diode bridge

B_2 4 Amp diode bridge

L 25 mH, 0.425 ohm d-c Res.

M D-C Shunt Motor

Fig. E-1 Motor Control Circuit

Appendix F

ELECTRONIC AMPLIFIER AND BANDPASS FILTER

Figure F-1 shows the circuit of the electronic amplifier and filter used to process the signal form the Fotonic Sensor [Ref. 22]. Connection is made from the Fotonic Sensor pickup by a shielded lead to the input buffer. Included in the buffer is a high-pass filter with a break frequency (pole) at 0.018 Hz. The high-pass filter attenuates interference and noise at frequencies below the range of interest and also provides d-c blocking. The d-c blocking is needed because, as shown in Fig. 3-1, the linear range of the Fotonic Sensor has a d-c offset of about 0.8 volts.

The second section of the electronic circuit is an adjustable-break-frequency two-pole low-pass filter. Switch S_1 allows this stage to be bypassed completely for calibration or if filtering is not desired. Rotary switch R_1 allows different resistances to be used in order to shift the break frequency as desired.

The next section is a four-pole, low-pass filter with break frequency at 7.2 Hz. Switch S_2 can bypass this filter if, for example, frequencies higher than 7.2 Hz are used. Both low-pass filter sections are Butterworth designs and provide no overshoot and a maximally-flat frequency response. Figure F-2 shows the frequency response of the entire electronic system with the adjustable two-pole filter pole at 7.2 Hertz and a gain of one.

Following the filter stages are the amplifier and output buffer. An operational-amplifier (op-amp) voltage follower prevents loading on the filter and feeds an inverting amplifier. The high-pass filter on the amplifier output provides blocking of the accumulated d-c offsets of the type 741 op-amps used while the voltage follower prevents loading and acts as a chart-recorder driver.

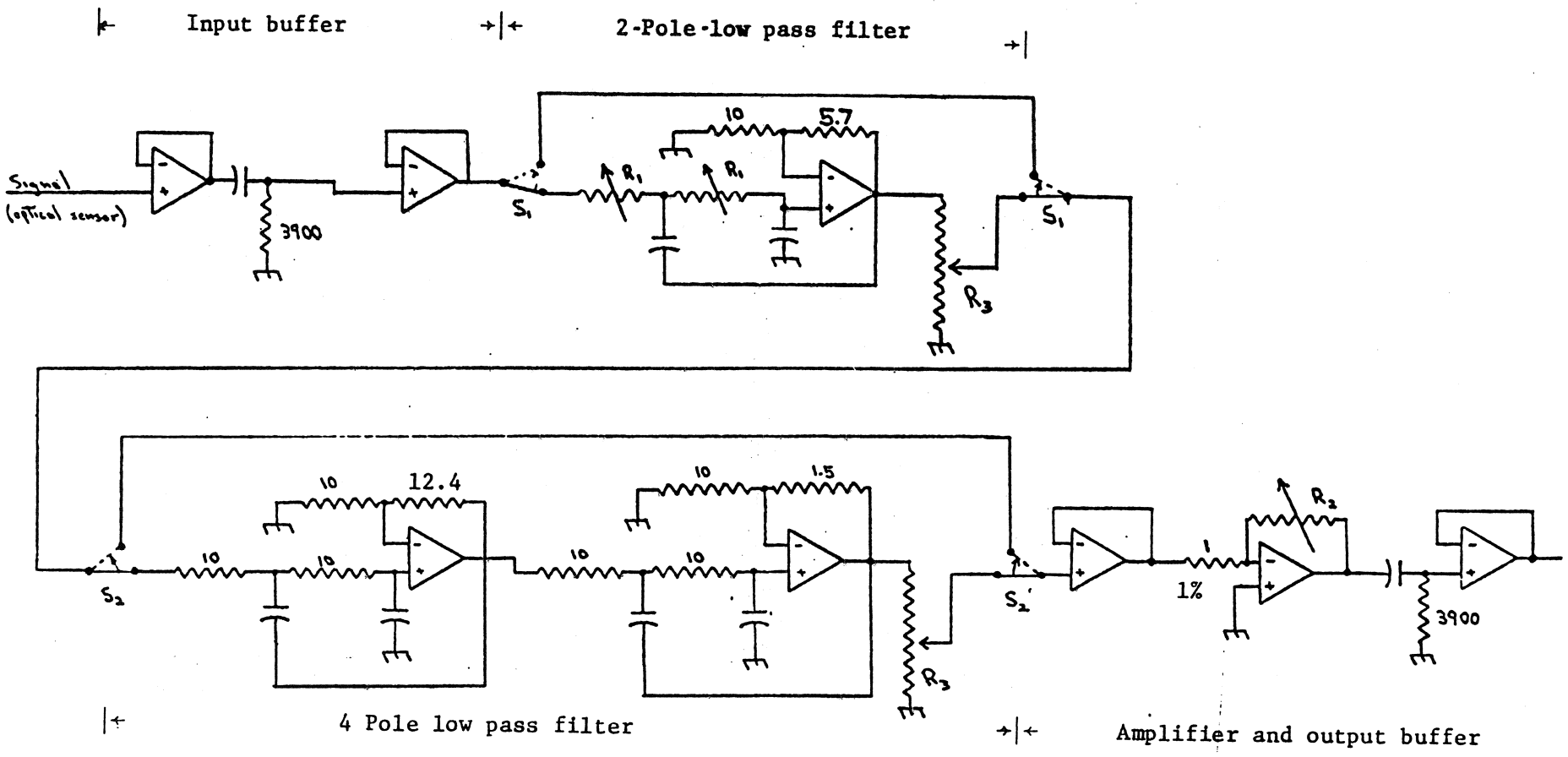

S_1 - 2 pole filter switch DPDT

S_2 - 4 pole filter switch DPDT

R_1 - 3 pole rotory switch
R = 2.2, 10

R_2 - 2 pole rotory switch
R = 1,2,4,10,15,20,30,50 (1%)

R_3 - 10K Trimpots

All resistances in kohms

All capacitors are 2.2 μF

All operational amplifiers are MC1741CP

Fig. F-1. Signal Processing Circuit.

The amplifier section provides gain selectable in discrete steps by means of a rotary switch which switches in different valued feedback resistors.

The entire electronic circuit was designed with flexibility and expansion in mind. The buffers are included so as to assure negligible loading on preceding stages and thereby reduce errors. The circuit works quite well although the high-pass filter sections require about 10 seconds to stabilize to steady-state values.

Figure F-3 shows a schematic of the electronic power supply. The design uses a simple full-wave-rectified, integrated-circuit regulated supply. The circuit is fuse-protected and designed for 1 A at plus and minus 15 V d-c.

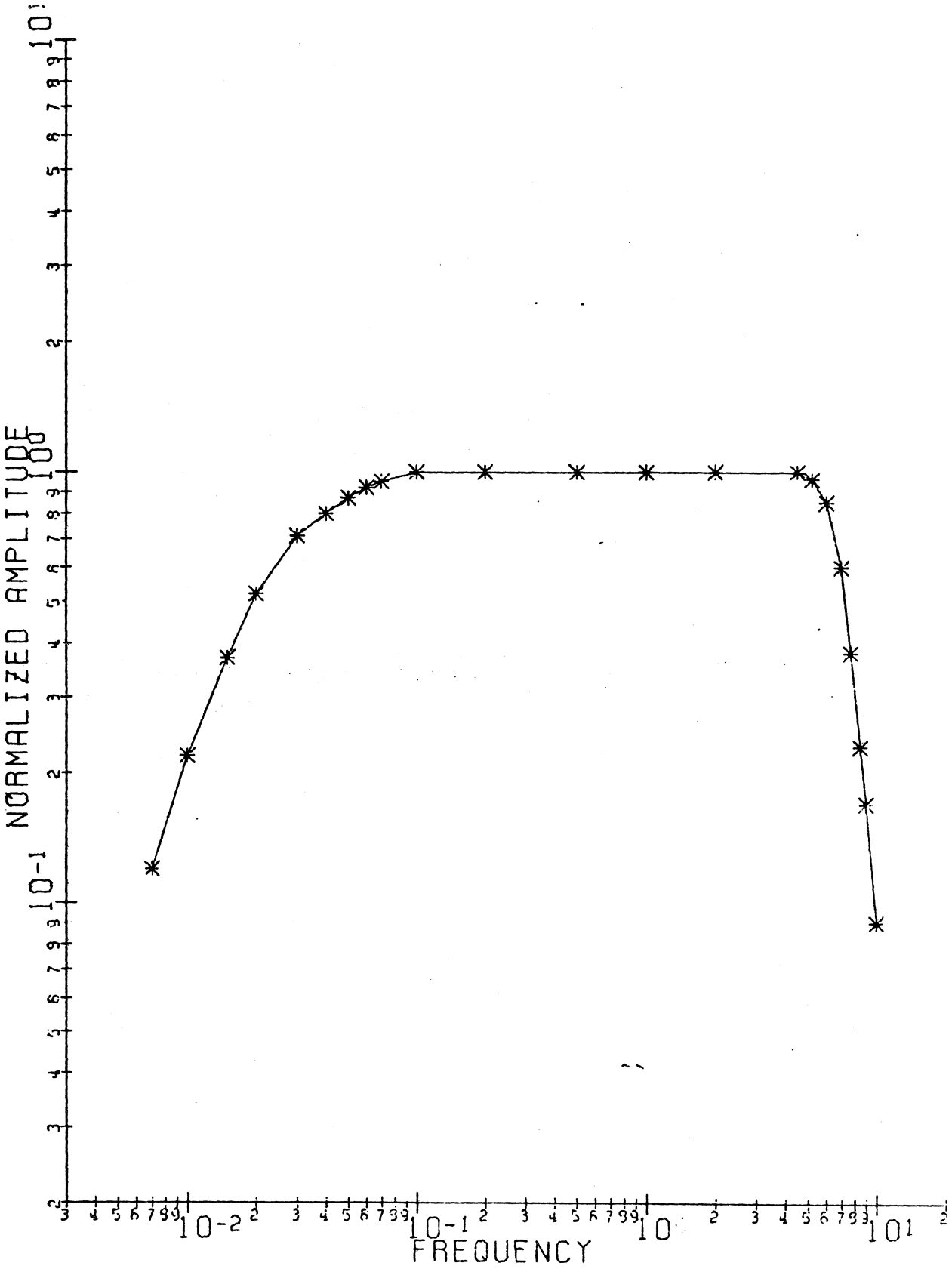

Figure F-2. Frequency response of total electronic package.

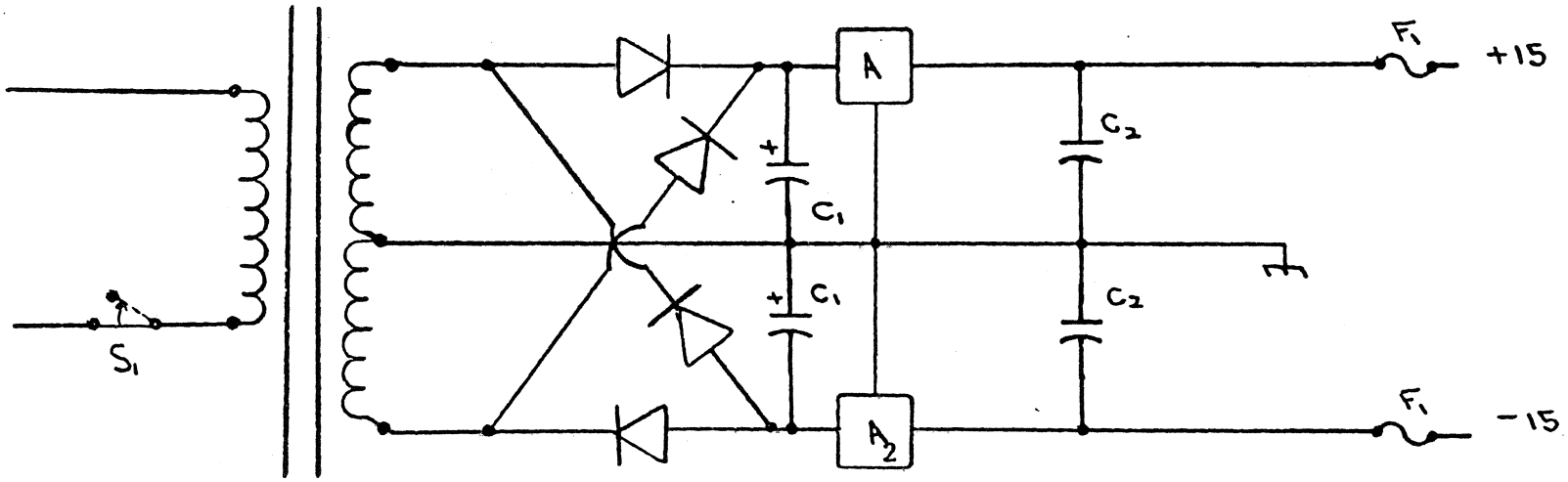

All diodes are 1N4004

C_1 - 6500 µF 25VDC

C_2 - 2.2 µF

S_1 - SPST

F_1 - amp fuse

A_1 - LM 340-15

A_2 - LM 320-15

T_1 - Stancor 36 v CT 1 amp Transformer

Fig. F-3. Power supply.

REFERENCES

1. Stanford Research Institute Patterns of Energy Consumption in the United States Superintendent of Documents, U.S. Government Printing Office, Washington, D.C., Jan. 1972, p. 6.

2. ASHRAE Handbook of Fundamentals American Society of Heating, Refrigerating and Air-Conditioning Engineers, 345 East 47th Street, New York, N.Y., 10017, 1972, pp. 381-383.

3. John M. Fox, Energy Consumption for Residential Space Heating--A Case Study, Princeton University, School of Engineering and Applied Science Center for Environmental Studies, Princeton, N.J. 08540, Report No. 4, Sept. 1, 1973, p. 29.

4. G. T. Tamura and A. G. Wilson, Air Leakage and Pressure Measurements on Two Occupied Houses, ASHRAE Transactions, Vol. 70, 1964, pp. 110-119.

5. J. R. Sasaki and A. G. Wilson, Air Leakage Values for Residential Windows ASHRAE Transactions, Vol. 71, part II, 1965, pp. 81-88.

6. R. C. Jordan, G. A. Erickson, and R. R. Leonard, Infiltration Measurements in Two Research Houses, ASHRAE Transactions, Vol. 69, 1963, pp. 344-350.

7. R. R. Laschober and J. H. Healy, Statistical Analysis of Air Leakage in Split-level Residences, ASHRAE Transaction, Vol. 70, 1964, pp. 364-374.

8. C. W. Coblentz and P. R. Achenbach, Field Measurement of Air Infiltration in Ten Electrically-Heated Houses, ASHRAE Transactions, Vol. 69, 1963, pp. 358-365.

9. C. W. Coblentz and P. R. Achenback, Design and Performance of a Portable Infiltration Meter, ASHRAE Transactions, Vol. 63, 1957, pp. 477-482.

10. John M. Fox, op.cit., p. 27.

11. James E. Hill and Tamami Kusada, Dynamic Characteristics of Air Infiltration, ASHRAE Meeting, Atlantic City, New Jersey, January 28, 1975.

12. Charles M. Hunt and Douglas M. Burch, Air Infiltration Measurements in a Four-Bedroom Townhouse Using Sulphur Hexaflouride as a Tracer Gas, ASHRAE Meeting Atlantic City, New Jersey, January 28, 1975.

13. George T. Tamura, Measurement of Air Leakage Characteristics of House Enclosures, ASHRAE Meeting, Atlantic City, New Jersey, January 28, 1975.

14. G. T. Tamura and A. G. Wilson, Pressure Differences Casued by Chimney Effect in Three High Buildings, ASHRAE Transactions, Vol. 73, part II, 1967, pp. II.1.1-II.1.10.

15. G. T. Tamura and A. G. Wilson, Building Pressures Caused by Chimney Action and Mechanical Ventilation, ASHRAE Transactions, Vol. 73, part II, 1967, pp. II.2.1-II.2.12.

16. C. Y. Shaw, D. M. Sander, and G. T. Tamura, Air Leakage Measurements of the Exterior Walls of Tall Buildings, ASHRAE Transactions, Vol. 79, 1973, pp. 40-48.

17. Saul Stricker, Measurements of Air-Tightness of Houses, ASHRAE Meeting, Atlantic City, New Jersey, January 28, 1975.

18. ASHRAE Handbook of Fundamentals, 1971 Edition, p. 334.

19. ibid, p. 333.

20. ibid, p. 337

21. K. Kreith and R. Eisenstadt, Pressure Drop and Flow Characteristics of Short Capillary Tubes at Low Reynolds Number, ASME Transactions, Vol. 79, 1957, pp. 1070-1078.

22. Richard W. Graham, Infrasonic Impedance Measurements of Buildings for Air Leakage Determination, Master's Thesis, Department of Electrical and Computer Engineering, Syracuse University, May, 1977.

23. Ahsan Sallman, Investigation of the Air Leakage Properties of Buildings by an Infrasonic Impedance Method, Master's Thesis, Department of Mechanical and Aerospace Engineering, Syracuse University, January, 1978.

24. C. P. Rohmann and E. C. Grogan, On the Dynamics of Pneumatic Transmission Lines, ASME Transactions, Vol. 79, May, 1957, pp. 853-874.

25. B. B. Bauer, Equivalent Circuit Analysis of Mechano-Acoustic Structures, Journal of the Audio Engineering Society, Vol. 24, No. 8, Oct. 1976, pp. 644-655.

26. I. Malecki, Physical Foundations of Technical Acoustics, PWN - Polish Scientific Publishers Warszawa, 1969.

27. L. E. Kinsler and A. R. Frey, Fundamentals of Acoustics, John Wiley and Sons, Inc., New York, 1950.

28. J. Kortschinski, R. C. Murtz and M. C. Curry, Microbarograph for Meteorological Studies, Journal of Physics E: Scientific Instruments 19, Vol. 4, (1971), pp. 307-310).